



8-1993

Depositional History, Sequence Stratigraphy and Diagenesis of the Maryville Limestone (Middle Cambrian) Southern Appalachians

Krishnan Srinivasan
University of Tennessee - Knoxville

Follow this and additional works at: https://trace.tennessee.edu/utk_graddiss



Part of the [Geology Commons](#)

Recommended Citation

Srinivasan, Krishnan, "Depositional History, Sequence Stratigraphy and Diagenesis of the Maryville Limestone (Middle Cambrian) Southern Appalachians. " PhD diss., University of Tennessee, 1993.
https://trace.tennessee.edu/utk_graddiss/2640

This Dissertation is brought to you for free and open access by the Graduate School at TRACE: Tennessee Research and Creative Exchange. It has been accepted for inclusion in Doctoral Dissertations by an authorized administrator of TRACE: Tennessee Research and Creative Exchange. For more information, please contact trace@utk.edu.

To the Graduate Council:

I am submitting herewith a dissertation written by Krishnan Srinivasan entitled "Depositional History, Sequence Stratigraphy and Diagenesis of the Maryville Limestone (Middle Cambrian) Southern Appalachians." I have examined the final electronic copy of this dissertation for form and content and recommend that it be accepted in partial fulfillment of the requirements for the degree of Doctor of Philosophy, with a major in Geology.

Kenneth R. Walker, Major Professor

We have read this dissertation and recommend its acceptance:

Kula Misra, Craig Barnes, Gary Jacobs, Steve Driese

Accepted for the Council:

Carolyn R. Hodges

Vice Provost and Dean of the Graduate School

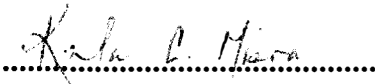
(Original signatures are on file with official student records.)

To the Graduate Council

I am ~~submit~~ submitting herewith a dissertation written by Krishnan Srinivasan entitled "Depositional History, Sequence Stratigraphy and Diagenesis of the Maryville Limestone (Middle Cambrian) Southern Appalachians". I have examined the final copy of this dissertation for form and content and recommend that it be accepted for the degree of Doctor of Philosophy, with a major in Geology.

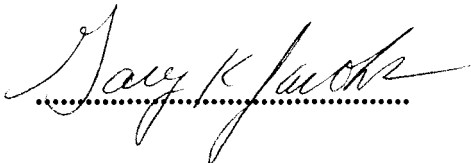

.....
Kenneth R. Walker, Major Professor

We have read this dissertation and recommend its acceptance

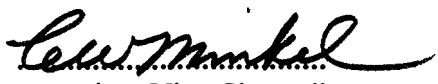

.....


.....


.....


.....

Accepted for the council


.....
Associate Vice Chancellor
and Dean of the Graduate
School

DEPOSITIONAL HISTORY, SEQUENCE STRATIGRAPHY AND DIAGENESIS OF
MARYVILLE LIMESTONE (MIDDLE CAMBRIAN), SOUTHERN APPALACHIANS

A Dissertation
Presented for the
Doctor of Philosophy
Degree
The University of Tennessee, Knoxville

Krishnan Srinivasan
August, 1993

ACKNOWLEDGMENTS

My sincere thanks to Dr. Kenneth R. Walker, Carden Professor of the Department of Geological Sciences, for his help and support in all aspects of this dissertation. Ken's constant moral and financial support and his concern for my well being throughout my graduate career is greatly appreciated.

I would like to thank other members of my committee who are Drs. Kula Misra and Steve Driese from the Department of Geological Sciences at the University of Tennessee, Dr. Gary Jacobs from Oak Ridge National Laboratory, and Dr. Craig Barnes from the Chemistry Department at the University of Tennessee for their critical reviews and guidance. Dr. Claudia Mora's generosity with the stable isotope facility at the Department of Geological Sciences, University of Tennessee is much appreciated.

Mike Doty and Allan Patchen at the Department of Geological Sciences, University of Tennessee provided valuable help with stable isotope and microprobe analyses. Interest in this work of present and past members of the Carbonate Research Group at the University of Tennessee, Lincoln Foreman, Keith Roberson, Mark Steinhaff, Mike Kozar, Ken Tobin, Gene Rankey, and Bosiljka Glumac are greatly appreciated.

Special thanks to Fred Read, Noel James, J.F. Sarg, Bob Shaver, and Jay Gregg for providing critical reviews for my manuscripts. This research was supported by NSF under a grant to Dr. K.R. Walker. Additional support for this research was provided by the Mobil Carbonate Fund, Sigma Xi, the Geological Society of America, and the University of Tennessee Discretionary Fund. Finally, I would like to thank my parents, my brother and sister for their constant support and encouragement.

ABSTRACT

The Conasauga Group constitutes part of a thick pericratonic Cambro-Ordovician passive-margin sequence along the eastern North American continent. The Cambrian carbonate platform was flanked by a high-relief shelf margin towards the east, facing the open ocean, while to the west the carbonate platform sloped into an intrashelf basin. It is this western shelf margin that is the topic of the present study. Detailed lithofacies analysis of the Middle Cambrian Maryville Limestone along a shelf-to-basin depositional transect reveals that the shelf evolved from a gently basinward sloping ramp to a rimmed platform fringed with steeper slopes. Cyanobacterial buildups (*Renalcis-Girvanella*) dominated the platform margin environments. Progradation of the platform occurred towards the craton.

A process oriented approach is applied to define the sequences, sequence boundaries, and the stacking pattern of the Maryville Limestone. The Maryville Limestone sequence consists of two depositional subsequences. The boundary between the two subsequences is not a sequence boundary, because it does not separate rocks deposited in different environmental regimes. The two subsequences within the Maryville sequence consist of a combination of aggradational, retrogradational, and progradational units (with respect to the platform interior). The stacking pattern recognized is the result of variations in sedimentation rate, subsidence, and eustatic sea-level change. Each of the dominantly carbonate units within the Conasauga represents this gradual transition from a ramp-like platform to basin transition into a rimmed platform.

In the study area, the transition between the Maryville Limestone (Middle Cambrian) and the overlying Nolichucky Shale (Late Cambrian) is a sequence boundary. This sequence boundary is both an exposure surface and a drowning unconformity, and marks a distinct shift in the pattern of sedimentation.

The Maryville Limestone was subjected to a complex diagenetic history. A combined field, petrographic, and geochemical approach are applied to describe the diagenetic history of the Maryville Limestone. The stabilization history of the Maryville Limestone during early diagenesis was characterized by microscale dissolution and reprecipitation during shallow burial and fabric selective dissolution in response to subaerial exposure and influx of meteoric fluids. However, during deep burial dolomitization was the dominant diagenetic event.

Depositional components such as intraclasts and ooids and syndimentary fibrous (marine) cements were subjected to microscale dissolution and reprecipitation during shallow burial. Depleted oxygen isotopic composition of ooids (mean $\delta^{18}\text{O} = -8.7 \text{ ‰}$ PDB) and fibrous cements (mean $\delta^{18}\text{O} = -8.4 \text{ ‰}$ PDB) relative to Cambrian marine carbonate value ($\delta^{18}\text{O} = -5.0 \text{ ‰}$ PDB) suggests that diagenetic alteration probably occurred during burial. Preserved ultrastructures of ooids and fibrous cements suggest that stabilization involved microscale dissolution and reprecipitation. Blocky, turbid calcite in intergranular pores is interpreted to be of shallow burial origin based on the presence of inclusions and cross cutting relationships. Blocky, turbid calcite spar is characterized by depleted oxygen isotopic composition (mean $\delta^{18}\text{O} = -8.2 \text{ ‰}$ PDB). Sr isotopic composition of blocky turbid calcite spar (0.7095) which is similar to Cambrian seawater values (0.7091-0.7095) suggests that shallow burial cementation occurred within a rock dominated system.

In contrast, wholesale dissolution and cementation occurred in response to the influx of freshwater during periods of subaerial exposure. Meteoric diagenesis is restricted to parts of formation near exposure surfaces. Petrographic evidence for subaerial exposure consists of planar truncation surfaces, *in situ* brecciation, pores partly filled with vadose silt, and fabric-selective dissolution and cementation. Fabric selective dissolution yielded biomolds. Blocky, clear calcite spar commonly occludes the moldic pores. The

stable oxygen isotope composition of blocky, clear calcite spar ($\delta^{18}\text{O} = -8.0$ ‰ to -9.5 ‰ PDB) is considerably depleted when compared to Cambrian marine carbonate values (-5 ‰ PDB). Depleted $\delta^{18}\text{O}$ values are consistent with subaerial exposure and meteoric diagenesis. However, $\delta^{13}\text{C}$ values show little shift. A possible reason for this lack of negative shift in carbon isotopic values is probably the absence of land plants developed on the surface during exposure. Blocky, clear calcite spar is enriched in Fe (avg. 1600 ppm). Enriched Fe values in blocky, clear calcite spar suggest that the meteoric system was relatively stagnant promoting reducing conditions. $^{87}\text{Sr}/^{86}\text{Sr}$ values of blocky, clear calcite spar which are similar to Cambrian marine carbonate composition offers supporting evidence for meteoric origin of blocky clear calcite spar.

Detailed petrographic analyses along a depositional transect from a carbonate-platform to shale basin reveal that dolomite is the principal burial diagenetic phase. Four different types of dolomite were identified based on detailed petrographic and geochemical analyses. Dolomite occurs as replacement of precursor carbonate and as inter- and intraparticle cements.

Type I dolomite occurs as small, irregular disseminations typically within mud rich facies. Type II dolomite typically occurs as inclusions of planar-e rhombs (ferroan), 5 to 300 μm in size, in blocky, clear ferroan calcite (meteoric) spar. Type II dolomite is non-luminescent. Type I and II dolomite formed during shallow-intermediate burial diagenesis. Type III dolomite consists of subhedral to anhedral crystals approximately 10 μm to 150 μm in size. Type IV dolomite consists of baroque or saddle-shaped, 100-1500 μm crystals, and is non-luminescent. Type IV dolomite formed during maximum burial.

Types III and IV dolomite increase in volume downslope. Type III dolomite contains 1.2-2.6 wt% Fe and a maximum of 1000 ppm Mn. The distribution of these elements displays no distinct vertical or lateral trends. In contrast, Fe and Mn distributions in Type IV dolomite exhibit distinct spatial trends. Fe and Mn values

decrease from 3.5-4.5 wt% Fe, and 0.1-0.3 wt% Mn in the west (slope/basin) to 1.5-2.5 wt % Fe, and less than 600ppm Mn in the east (shelf-margin), over a distance of approximately 60 km. Type III and Type IV dolomite have a mean $\delta^{18}\text{O}$ value of -7.8 ‰ and a mean $\delta^{13}\text{C}$ value of +1.1 ‰ (relative to the PDB standard). Based on an assumed basinal fluid composition of 5 ‰ SMOW, temperatures calculated from $\delta^{18}\text{O}$ values of Type III and Type IV dolomite range between 85° C to 105° C. $^{87}\text{Sr}/^{86}\text{Sr}$ compositions of Type III and Type IV dolomite are enriched with respect to Cambrian marine values and range from 0.7111-0.7139, probably indicating that the diagenetic fluid had interacted with the siliciclastic sediments of basinal shales.

Based on the Fe and Mn distributions in Type IV saddle dolomite, a west-east fluid flow during late burial diagenesis is indicated. Calculated temperatures indicate that the fluids were warm. The distribution of Paleozoic facies in the southern Appalachians indicates a Cambrian shale source for these fluids, and burial curves suggest an early Ordovician age for burial fluid movement.

TABLE OF CONTENTS

CHAPTER	PAGE
1. INTRODUCTION.....	1
Stratigraphic Setting.....	5
Purpose and Significance.....	9
2. SEQUENCE STRATIGRAPHY OF AN INTRASHELF BASIN CARBONATE RAMP TO RIMMED-PLATFORM TRANSITION: MARYVILLE LIMESTONE (MIDDLE CAMBRIAN), SOUTHERN APPALACHIANS	11
Introduction.....	11
Geologic Setting.....	13
Methods.....	14
Description of Maryville Rock Types.....	14
Environmental Interpretation of Maryville Rock Types.....	16
Subtidal Onshelf.....	16
Shelf Margin.....	21
Slope/Basin.....	27
Depositional Sequences, Subsequences and Stacking Patterns.....	29
Lower Subsequence.....	30
Aggradational Stacking Pattern.....	33
Retrogradational Stacking Pattern.....	33
Progradational Stacking Pattern.....	34
Upper Subsequence.....	34
Rimmed Shelf Progradational Stacking Pattern.....	35
Retrogradational Stacking pattern.....	35
Sequence Bounding Surface.....	36
Summary of Evolution of Platform.....	37
Conclusions.....	42
3. MICROSCALE AND FABRIC SELECTIVE DISSOLUTION AND CEMENTATION DURING EARLY DIAGENESIS OF MARYVILLE LIMESTONE (MIDDLE CAMBRIAN), SOUTHERN APPALACHIANS.....	44
Introduction.....	44
Geologic Setting.....	46
Methods.....	47
Early Diagenesis of Maryville Limestone.....	49
Description of Depositional and Diagenetic Components.....	49
Fibrous (marine) Cements.....	49

Microcrystalline Calcite and Microspar Cement.....	53
Syntaxial Overgrowths.....	53
Blocky, Turbid Calcite Spar.....	53
Blocky, Clear Calcite Spar (intergranular pores).....	54
Blocky Clear Calcite Spar (moldic pores).....	54
Intraclasts.....	57
Dolomite.....	57
Geochemistry.....	57
Stable Isotopes.....	57
Elemental Composition.....	58
Sr Isotopes.....	62
Discussion of Stabilization Processes.....	65
Shallow Burial (microscale dissolution and reprecipitation).....	65
Subaerial Exposure and Meteoric Diagenesis (fabric selective dissolution and cementation).....	66
Conclusions.....	68
4. PETROGRAPHIC AND GEOCHEMICAL CONSTRAINTS FOR FLUID SOURCE AND POSSIBLE PATHWAYS DURING BURIAL DIAGENESIS OF MARYVILLE LIMESTONE (MIDDLE CAMBRIAN), SOUTHERN APPALACHIANS.....	70
Introduction.....	70
Geologic Setting.....	71
Methods.....	72
Burial Diagenesis and Dolomitization.....	73
Petrographic and Cathodoluminescence Characteristics.....	73
Type I Dolomite.....	73
Type II Dolomite.....	77
Type III Dolomite.....	77
Type IV Dolomite.....	78
Stratigraphic Distribution.....	78
Geochemistry.....	79
Major Element Chemistry.....	79
Minor and Trace Elements.....	81
Stable isotopes.....	84
Strontium Isotopes.....	87
Burial History.....	89
Discussion of Fluid Source and Diagenetic Pathways.....	89
Early Dolomitization.....	91
Late Burial Dolomitization.....	93
Constraints on Fluid Source from Carbon, Oxygen and strontium Isotope Ratios.....	94

Fluid-Rock Ratios, Variations in $\delta^{18}\text{O}$, $^{87}\text{Sr}/^{86}\text{Sr}$ Isotope Compositions.....	97
Conclusions.....	98
5. CONCLUSIONS.....	99
LIST OF REFERENCES.....	102
APPENDICES.....	121
A. STANDARD MEASUREMENT CONVENTIONS.....	122
B. DESCRIPTION OF STRATIGRAPHIC SECTIONS.....	124
C. ELECTRON MICROPROBE DATA.....	146
D. STABLE ISOTOPE DATA.....	160
VITA.....	166

LIST OF TABLES

TABLE	PAGE
2.1. Description of Lithofacies.....	17
3.1. Summary of all geochemical data.....	60

LIST OF FIGURES

FIGURE	PAGE
1.1. Palinspastic base map showing the three major phases of Middle and Upper Cambrian sedimentation.....	2
1.2. Map of study area in eastern Tennessee.....	3
1.3. General sequence stratigraphy of Middle and Upper Cambrian Conasauga Group in eastern Tennessee.....	7
1.4. A Cross section showing Conasauga stratigraphy in eastern Tennessee.....	8
2.1. Cross section of the Maryville Limestone along the depositional transect from shelf-to-basin illustrating the sequence and subsequences with correlated facies.....	15
2.2. Photomicrographs (cross polarized light) of different types of lithofacies of Maryville Limestone.....	19
2.3. Photographs of polished slabs and photomicrographs of Maryville lithologies from Woods gap section.....	23
2.4. Photographs and photomicrographs of Maryville lithologies.....	25
2.5. An idealized model for the development of the ramp to rimmed-platform sequences of the Conasauga Group developed from the study of Maryville Limestone.....	31
2.6. Map showing Middle Cambrian paleogeography in eastern Tennessee and southwest Virginia.....	38
2.9. Block diagrams summarizing the evolution of the platform during the deposition of the Maryville Limestone.....	40
3.1. Paragenetic sequence of the Maryville Limestone.....	50
3.2. Photomicrographs of different diagenetic phases of the Maryville Limestone.....	51
3.3. Photomicrographs and photograph of a polished slab of Maryville Limestone showing different diagenetic features	55

3.4.	$\delta^{18}\text{O}$ versus $\delta^{13}\text{C}$ crossplot showing isotopic composition of depositional components and early diagenetic phases	59
3.5.	MgCO_3 and CaCO_3 content of blocky, clear calcite spar in moldic pores and unaltered oncoids.....	61
3.6.	Fe and Mg content of blocky, clear calcite spar in moldic pores and unaltered oncoids of Maryville Limestone.....	63
3.7.	$\delta^{18}\text{O}$ versus $^{87}\text{Sr}/^{86}\text{Sr}$ crossplot of early and late burial diagenetic phases	64
4.1.	Paragenetic sequence of the Maryville Limestone.....	74
4.2.	Photomicrographs of different dolomite types of Maryville Limestone in the study area.....	75
4.3.	Electron microprobe data of Maryville dolomite types.....	80
4.4.	$\delta^{18}\text{O}$ versus $\delta^{13}\text{C}$ crossplot of replacement stylolite dolomite (Type III) and void filling saddle dolomite (Type IV).....	86
4.5.	$\delta^{18}\text{O}$ versus $^{87}\text{Sr}/^{86}\text{Sr}$ of saddle dolomite (Type IV), stylolite dolomite (Type III) and other associated cement phases.....	88
4.6.	Burial history plot for Maryville Limestone.....	90

CHAPTER 1

INTRODUCTION

The Conasauga Group (Middle and Upper Cambrian) consists of a sequence of six alternating limestone and shale formations. It constitutes part of a thick pericratonic Cambro-Ordovician passive-margin sequence along the eastern edge of the North American continent. The Conasauga sequence consists of three distinct phases of sedimentation during the Middle and Late Cambrian (Rodgers, 1953): (1) an area dominated by carbonate lithologies to the east, (2) a western and northwestern area dominated by shale, and (3) a central zone of interbedded carbonate formations and shale formations (Fig. 1.1). A detailed regional stratigraphic framework for the Conasauga has been established by several workers in the past (Rodgers, 1968; Harris, 1964; Erwin, 1981; Markello and Read, 1981, 1982; Simmons, 1984; Kozar, 1986; Hasson and Haase, 1988; Weber, 1988; Foreman, 1991). This research is focused on the central phase which consists of a succession of interbedded carbonate and shale formations. This dissertation concerns the detailed sedimentology, sequence stratigraphy and diagenesis of the Maryville Limestone (Middle Cambrian). The outcrops of interest for this study are exposed within the Copper Creek fault block (Fig. 1.2).

The dissertation is organized into five chapters. In Chapter I, regional stratigraphic setting, and purpose and significance of the dissertation are described. Beginning with chapter 2, the dissertation examines depositional history, sequence stratigraphy and diagenesis. A brief description of the salient features of chapters 2, 3 and 4 are given below. The major conclusions of the dissertation are summarized in chapter 5.

Chapter 2: Sequence Stratigraphy of an Intrashelf Basin Carbonate Ramp to Rimmed Platform Transition: Maryville Limestone (Middle Cambrian), Southern Appalachians.

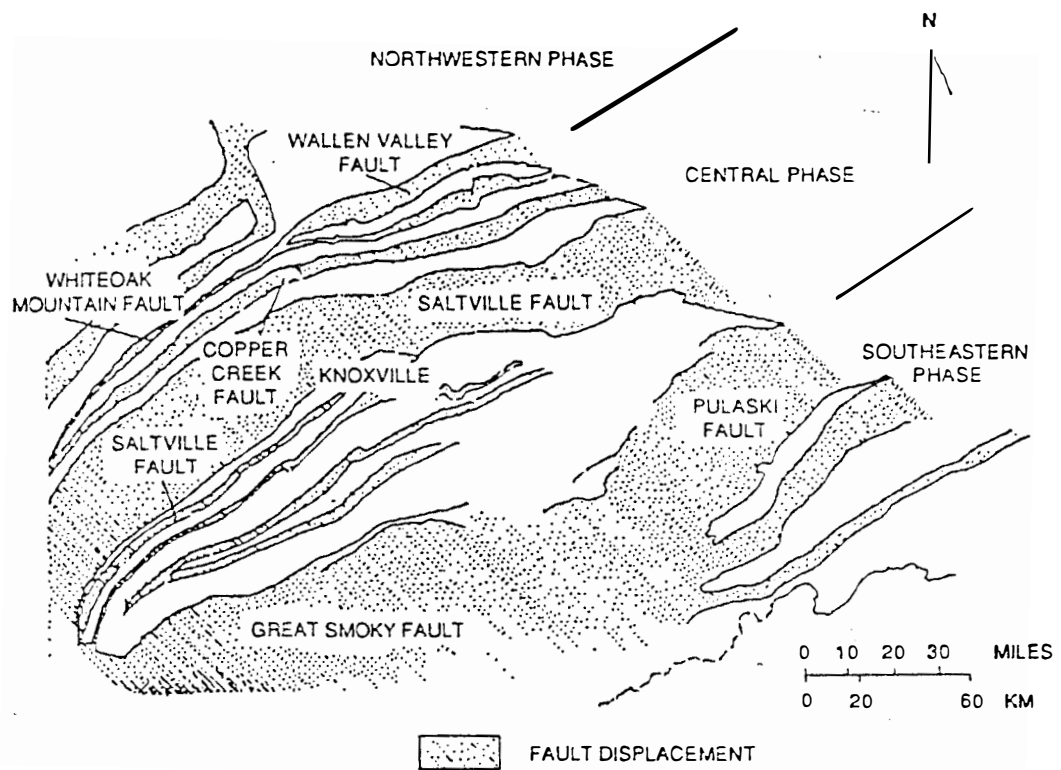


Figure 1.1 Palinspastic base map of Tennessee showing the three major phases of Middle and Upper Cambrian sedimentation (from Weber, 1988, modified after Hasson and Haase, 1988).

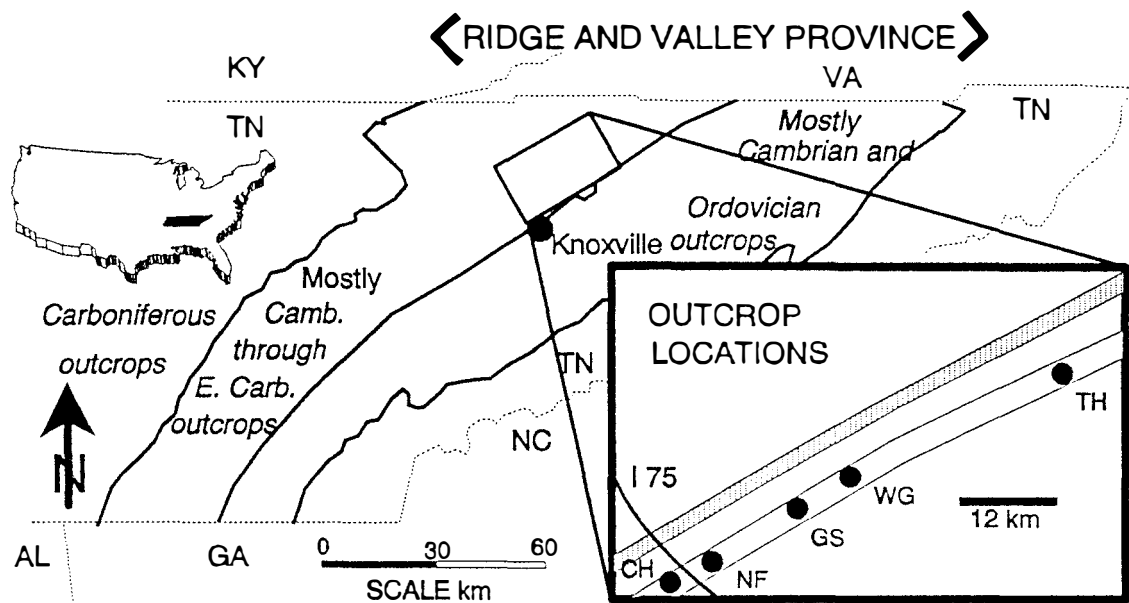


Figure 1.2. Map of study area in eastern Tennessee. Inset shows outcrop locations.

The lines with no pattern represent Copper Creek and crosshatched lines represent Whiteoak Mountain thrust sheet which is located west of Copper Creek thrust sheet. TH - Thorn Hill, WG - Woods Gap, GS - Graveston, NF - Norris Freeway, CH - Clinton Highway.

In this chapter, detailed depositional history, evolution and sequence stratigraphy of the Middle Cambrian carbonate platform is described. Detailed lithofacies analysis along a shelf-to-basin depositional transect within the Copper Creek fault block reveals that the shelf evolved from a gently basinward sloping ramp to a rimmed platform fringed with steeper slopes. Cyanobacterial buildups (*Renalcis-Girvanella*) dominated the platform margin environments.

Sequence stratigraphy has its roots, and has been most widely applied in siliciclastic systems. In contrast, applications of sequence stratigraphic concepts to carbonate rocks, both ancient and recent has been rather limited. Schlager (1991) argued for a much needed process oriented approach in carbonate systems. Such an approach was particularly useful in defining sequences, sequence boundaries, and the stacking pattern of the Maryville Limestone.

The approach here involved detailed field and petrographic analysis. Subaerial exposure surfaces were documented on the basis of field, petrographic and geochemical evidence (stable carbon and oxygen isotopic composition).

Chapter 3: Microscale and Fabric Selective Dissolution and Cementation During Early Diagenesis of Maryville Limestone (Middle Cambrian), Southern Appalachians.

Previous studies only briefly touched on the diagenesis of the Maryville Limestone (Kozar, 1986). In this study an integrated approach consisting of detailed petrography and geochemistry (trace elements, stable carbon, oxygen, and strontium isotopic ratios) was applied to describe the diagenetic history of the Maryville Limestone. The Maryville Limestone was subjected to a complex diagenetic history. In general, this history may be divided into early diagenesis consisting of marine, meteoric, and shallow burial (less than 1 km of burial) and deep burial diagenesis (maximum burial depth 4 km). The emphasis of chapter 3 is on the stabilization of the Maryville Limestone during early diagenesis. Early

diagenesis consisted of microscale dissolution and reprecipitation during shallow burial and fabric selective dissolution and cementation in response to subaerial exposure and meteoric diagenesis.

Chapter 4: Petrographic and Geochemical Constraints for Fluid Source and Possible Pathways During Burial Diagenesis of Maryville Limestone (Middle Cambrian), Southern Appalachians.

This chapter focuses on the deep burial diagenesis of the Maryville Limestone, which consisted mostly of partial dolomitization. Petrographic analyses, both conventional and cathodoluminescent microscopy, reveal that dolomite is the principal burial diagenetic phase. Four different generations of dolomite were identified along the platform-to-basin depositional transect. An integrated approach consisting of detailed petrography and geochemistry (stable carbon and oxygen isotopes, trace elements, and Sr isotopes) was applied to unravel the burial diagenetic history, trace the direction of fluid flow, and to hypothesize about possible fluid source (s) during deep burial dolomitization. Sr isotopic composition of the burial dolomite phases proved critical in identifying the fluid source and composition. Minor and trace elements were particularly useful in delineating the fluid migration pathways. Burial curves were constructed to estimate the maximum burial depth, and thus maximum burial temperatures of the Maryville Limestone in the study area.

Stratigraphic Setting

A broad regional carbonate shelf was established along the eastern North American continental margin following the Late Precambrian rifting (Bird and Dewey, 1970; Read, 1988). Initial rifting of the eastern North American continent was followed by rift-dominated sedimentation. The rift-to-drift transition and establishment of passive

margin carbonate sedimentation occurred by Late Cambrian time period according to Rankey (1993, in prep). The Conasauga sequence (Middle and Upper Cambrian) in northeast Tennessee and Virginia are part of this passive margin sequence.

General sequence stratigraphy of Conasauga (Fig. 1.3) and other Cambrian strata in east Tennessee is adopted from Kozar et al. (1990). The regional Conasauga stratigraphy is given in Figure 1.4. The Conasauga rocks in northeast Tennessee are exposed in a series of southeasterly dipping imbricate thrust sheets. It overlies the Lower Cambrian Rome Formation which is predominantly of tidal flat origin and is in turn overlain conformably by the Knox Group which consists dominantly of shallow subtidal and peritidal carbonate rocks (Rodgers and Kent, 1948; Harris, 1964). The thickness of the Conasauga Group in east Tennessee ranges between 350 m and 700 m. In the Valley and Ridge province, the carbonate parts of the Conasauga sequence are much thicker in the more eastern exposures.

The Maryville Limestone (Middle Cambrian) crops out in the southeasterly dipping thrust sheets in the Valley and Ridge Province of the southern Appalachians. It consists of a combination of peritidal and subtidal carbonates in the more eastern exposures (for example, in the Dumplin Valley thrust sheet). However, the more western and northwestern exposures (Copper Creek thrust sheet) dominantly consist of shallow and deep subtidal carbonates with an increased proportion of interbedded shale. The present research is focused on five outcrops of the Maryville Limestone (Fig. 1.2). The five outcrops represent a depositional transect from shelf (east) to basin (west). Biostratigraphy of the Maryville Limestone based on trilobite zonation reveals that the upper part of the Maryville Limestone in the study area ranges between the *Bolaspidella* zone (Middle Cambrian) and the overlying *Cedaria* zone (Dresbachian) (Derby, 1965). Within the Copper Creek fault block, deeper water environments to the west and

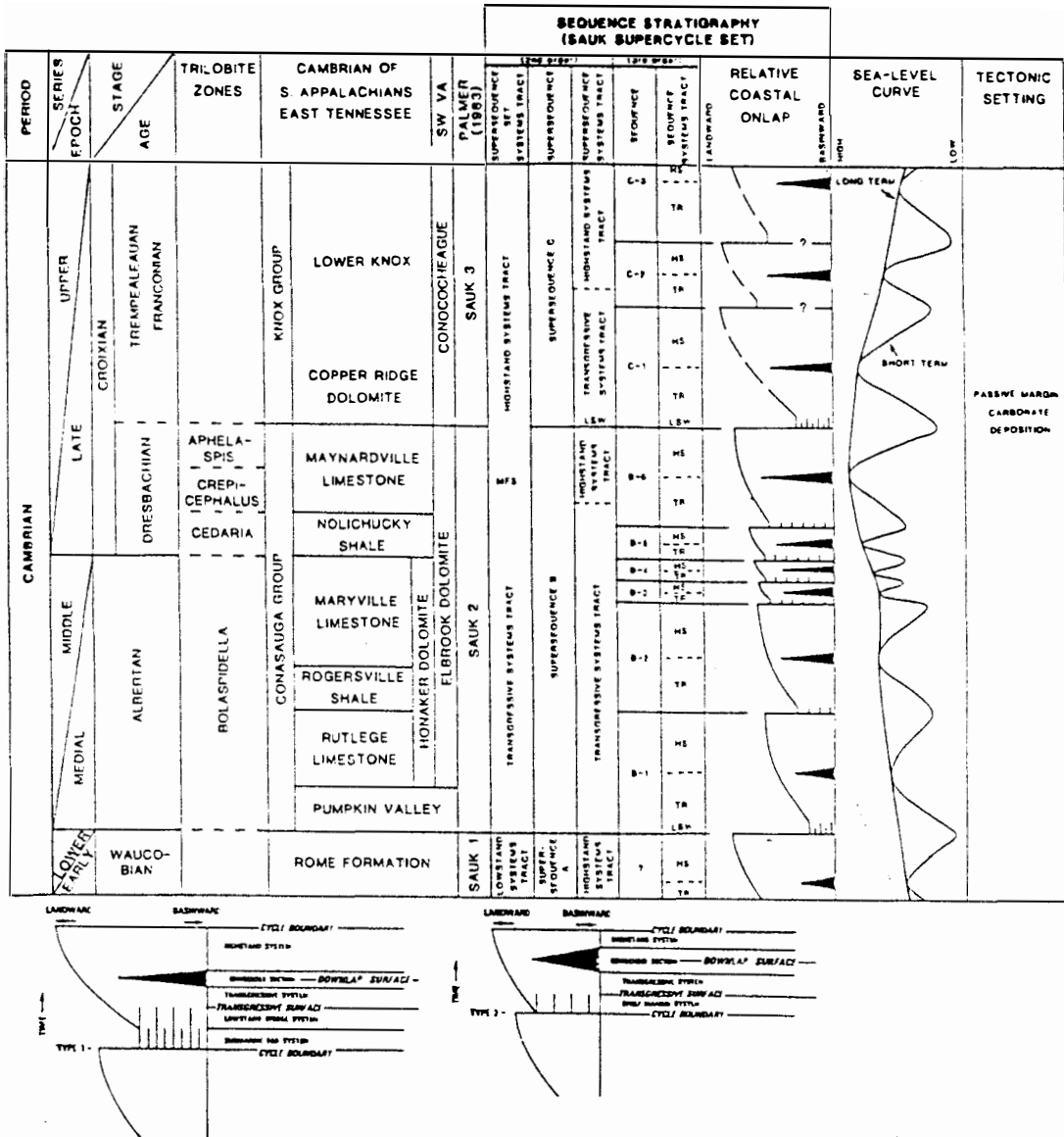


Figure 1.3 General sequence stratigraphy of Middle and Upper Cambrian Conasauga Group in eastern Tennessee (from Kozar et al., 1990).

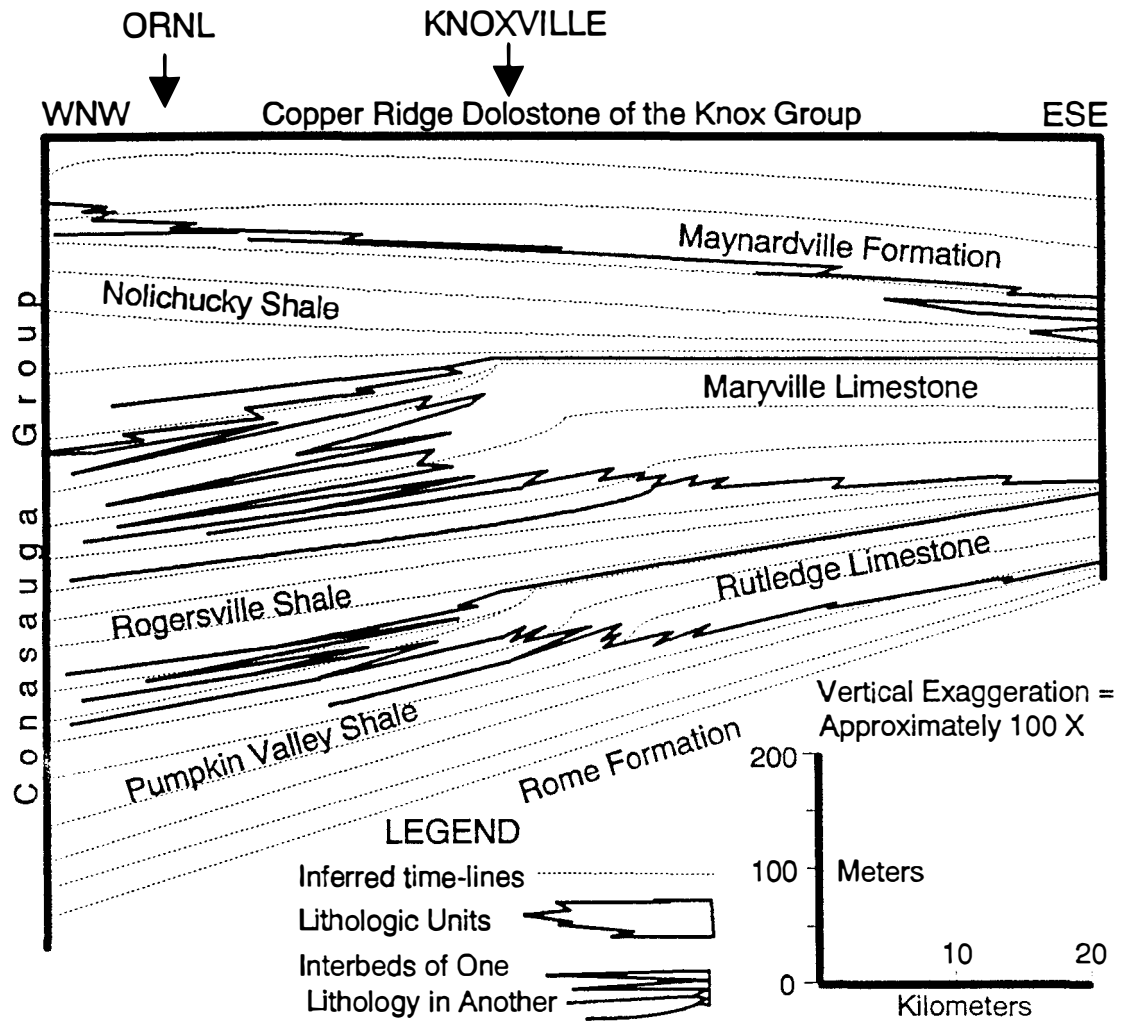


Figure 1.4 A cross section showing Conasauga stratigraphy in eastern Tennessee. Dotted lines are time-lines inferred from stratigraphic relationships; solid lines enclose formation-level units except to the left of the Maryville Formation where a more shaly (basinal) equivalent of the Maryville exists. Note gradual progradation of each carbonate unit toward the basin and the concomitant conversion of the basin-platform transition from gentle ramp to steeper slope (from Walker and others, 1990).

southwest are replaced further northeast (southwest Virginia) by peritidal areas as documented by Markello and Read (1981) and Erwin (1981).

Purpose and Significance

Few studies prior to this (Simmons, 1984; Kozar, 1986) have focused on the detailed paleoenvironmental interpretation, sequence stratigraphy, and diagenesis of the Maryville Limestone. The main objectives of this study are to: (1) establish a detailed depositional history of the Maryville Limestone along a shelf-to-basin depositional transect, (2) develop a detailed sequence stratigraphic model for the formation, and (3) finally, to use the sequence stratigraphic model thus developed as a basic framework for the interpretation of the diagenetic history of the Maryville Limestone.

Sequence stratigraphy has been most widely applied to siliciclastic successions. In contrast, application of sequence stratigraphic concepts to carbonate successions has been more limited. There is presently no entirely satisfying conceptual framework for discussing the sequence stratigraphy of carbonate successions. This is mainly due to the fact that carbonate depositional systems are fundamentally different from siliciclastic systems. The application of sequence stratigraphic concepts to the evolution of Middle Cambrian carbonate sequence can serve as a useful analog to other lower Paleozoic and possibly younger passive-margin carbonate sequences.

An integrated approach combining petrography and geochemistry facilitated a better understanding of the physical and chemical processes that operated during diagenesis of the Maryville Limestone. The diagenetic history of the Maryville Limestone demonstrates the control of sea-level changes on the early diagenetic history and the influence of shale diagenesis on the late diagenetic history of shallow platform carbonates, and provides insight into regional burial dolomitization and cementation of the Maryville

Limestone and perhaps of the entire Conasauga. In the future, research on burial dolomitization of the Maryville Limestone will be extended to the more eastern exposures where the peritidal section of the Maryville Limestone is well exposed (Rankey, in prep). Such a regional study is more likely to demonstrate the importance of early versus late burial dolomitization of platform carbonates.

CHAPTER 2

SEQUENCE STRATIGRAPHY OF AN INTRASHELF BASIN CARBONATE RAMP TO RIMMED-PLATFORM TRANSITION: MARYVILLE LIMESTONE (MIDDLE CAMBRIAN), SOUTHERN APPALACHIANS

Introduction

The Conasauga Group (Middle and Upper Cambrian) consists of a sequence of six alternating limestone and shale formations. The changes from mostly limestone to mostly shale deposition were likely caused by sea-level changes (Kozar and others, 1990; Srinivasan and others, 1991). The alternating limestone and shale formations are characteristic of Cambrian strata of the southern Canadian Rocky Mountain, the Appalachian, and the Cordilleran passive-margin sequences. These alternating limestone-shale formations from the southern Canadian Rocky Mountains were originally described as "grand cycles" by Aitken (1966).

The Conasauga Group constitutes part of a thick pericratonic Cambro-Ordovician passive-margin sequence along the eastern edge of the North American continent. Following late Precambrian crustal extension and rift dominated sedimentation during early and middle Cambrian time period, passive-margin sedimentation was initiated during late Cambrian time period along the eastern North American continent. The Conasauga sequence resulted from three distinct paleogeographic phases of sedimentation during Middle and Late Cambrian time (Rodgers, 1953): (1) a succession dominated by carbonate lithologies to the east and southeast, (2) a western and northwestern succession

Note: This chapter is a paper in press, GSA Bulletin.

Srinivasan, K., and Walker, K.R., 1993, Sequence stratigraphy of an intrashelf basin carbonate ramp to rimmed-platform transition: Maryville Limestone (Middle Cambrian)

dominated by shale, and (3) a central succession of interbedded carbonate formations and shale formations. The present study concerns a part of this central phase. Deposition of the Conasauga strata occurred within a regional intrashelf depocenter consisting of intracratonic basin and associated carbonate platform environmental arrays (Markello and Read 1981; 1982).

The Maryville Limestone (Middle Cambrian) of the Conasauga group represents deposition along a rimmed shelf edge-to-basin transition (Srinivasan and others, 1991). Shelf, shelf-margin, and slope/basin lithologies are well exposed in the Copper Creek fault block in east Tennessee (Fig. 1.2). Cyanobacterial buildups (*Renalcis* - *Girvanella*) dominated the platform-margin environments. This is the first reported occurrence of Cambrian shelf-margin cyanobacterial buildups in Tennessee. Although the Middle Cambrian platform margin-to-basin transition in the study area was marked by slope steepening, absence of large shelf-edge-derived blocks in the periplatform deposits suggests that it was not a high-relief shelf edge or a high angle slope. The platform-margin prograded basinward in a direction west to southwest (present geographic direction). The facies distribution of the Maryville Limestone reflects a change in the depositional mode through time from a gently sloping ramp (1° or perhaps less) (Erwin, 1981; Markello and Read, 1981; Simmons, 1984; Kozar, 1986) to rimmed-platform depositional mode with significant slope steepening (2° to 3°).

A high-relief shelf margin on the oceanward side (east) of the Cambrian carbonate platform has been documented from different parts of the Appalachians (Reinhardt, 1977; Pfeil and Read, 1980; James, 1981; Read and Pfeil, 1983; Demicco, 1985; James and Stevens, 1986; Barnaby and Read, 1990). The shelf margin documented in the present study faced a shallower intracratonic basin to the west.

The objectives of this paper are to: (1) outline the lithofacies types of the Maryville Limestone exposed within the Copper Creek fault block, and (2) describe the evolution

and the sequence stratigraphy of the Middle Cambrian carbonate platform. One of the interesting aspects of the Conasauga Group are the alternating limestone-shale formations (Fig. 1.4). The emphasis of the present research is on the transition between the Maryville Limestone (Middle Cambrian) and the overlying Nolichucky Shale (Late Cambrian), but the general nature of the limestone-shale transitions (exposure/drowning) in the entire group will also be discussed. The Maryville-Nolichucky transition has been identified as a third-order sequence boundary by Read (1989) and Kozar and others (1990). We employ a process-oriented approach to describe the sequence stratigraphy of the Maryville.

Geologic Setting

Late Precambrian crustal extension of the eastern North American continent was accompanied by the establishment of a broad regional carbonate shelf (Bird and Dewey, 1970; Read, 1989, among others). As mentioned earlier, the regional shelf that fringed the eastern North American continental margin experienced more or less continuous deposition from Early Cambrian through Early Ordovician time. The Middle and Upper Cambrian Conasauga rocks in northeastern Tennessee and Virginia are part of this Cambro-Ordovician sequence. In the study area, the Conasauga rocks are exposed in a series of southeasterly dipping imbricate thrust sheets. The Conasauga Group in East Tennessee conformably overlies the Rome Formation (lower Cambrian) and is in turn overlain conformably by the Knox Group (Rodgers and Kent, 1948; Harris, 1964; Palmer, 1971). During deposition of the Rome Formation the environmental pattern was influenced by linear "pull-apart" basins initially formed during the breakup of the continental margin that occurred in late Precambrian and Early Cambrian time (Read, 1989). The upper part of the Maryville Limestone in northeastern Tennessee and parts of southwestern Virginia ranges between the *Bolaspidella* zone (Middle Cambrian) and the overlying *Cedaria* zone

(Dresbachian) (Derby, 1965).

Methods

The regional stratigraphic framework presented here for the Conasauga Group was adopted from the work of Rodgers (1968), Harris (1964), Erwin (1981), Markello and Read (1981, 1982), Simmons (1984), Kozar (1986), Hasson and Haase (1988), Weber (1988), Foreman (1991). A more detailed stratigraphy of the Maryville Limestone was established by the examination of five complete or partial stratigraphic sections within the Copper Creek fault block in the study area. Detailed field work was accompanied by analysis of over 200 thin sections from the five stratigraphic sections. Definition of sequence boundaries is based on detailed field studies and petrographic analysis. Data from the latter approach were especially useful in defining sequence bounding surfaces, many of which are the result of exposure or flooding. These events (particularly exposure) are commonly more clearly reflected in the diagenetic fabrics observed by petrographic study and in the geochemical signatures of components in the affected sediments than in the characteristics visible in the field.

Description of Maryville Rock Types

The Maryville Limestone in the study area consists entirely of subtidally deposited rocks. A detailed cross-section of the Maryville Limestone is given in Figure 2.1. Thus, the cyclicity delineated by other workers in the Conasauga in Virginia and upper northeast Tennessee, where many cycles are capped by intertidal or supratidal facies (e.g., Markello and Read, 1981, 1982), is not so obviously developed in our study area. Only larger excursions of relative sea-level are evidenced in these wholly subtidal settings, and the

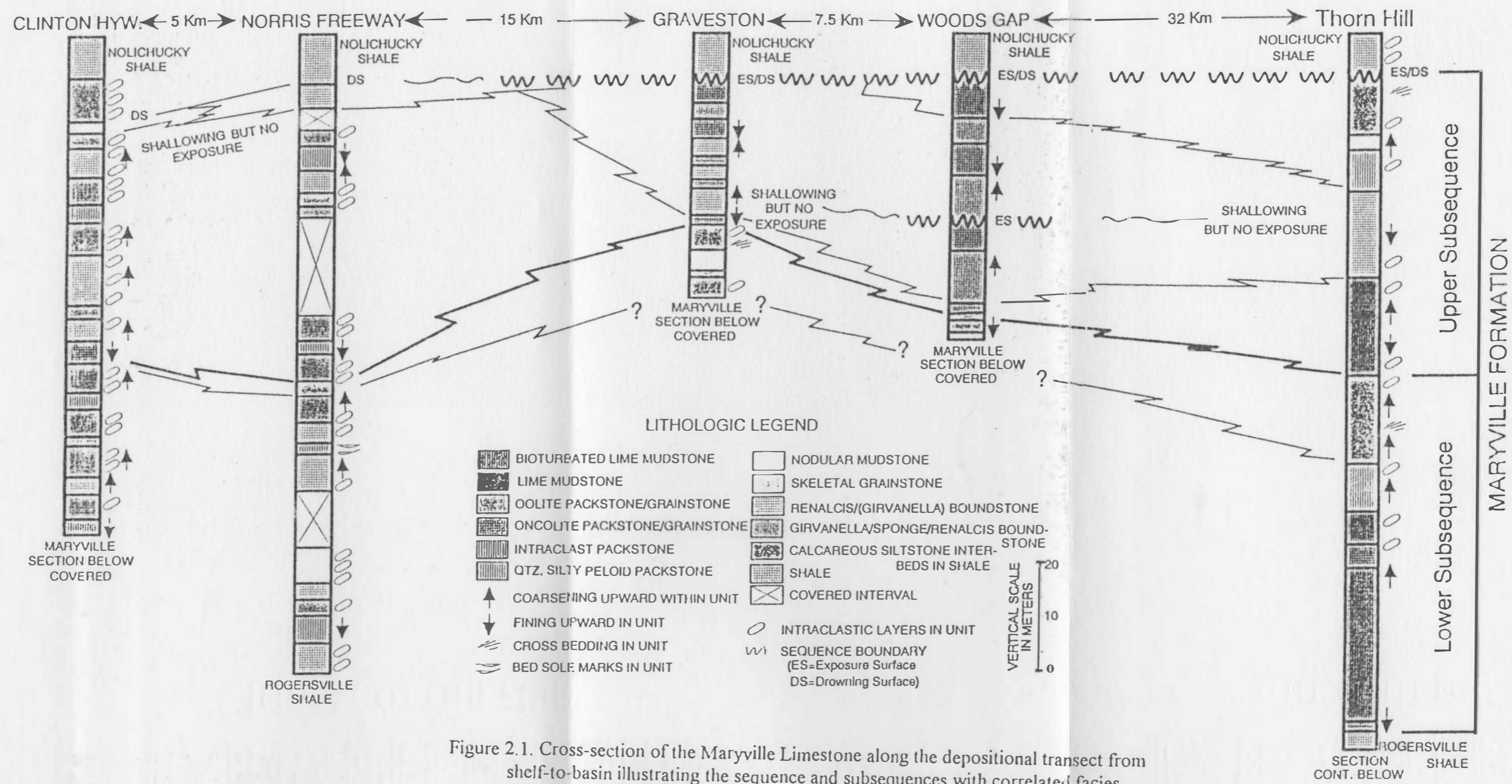


Figure 2.1. Cross-section of the Maryville Limestone along the depositional transect from shelf-to-basin illustrating the sequence and subsequences with correlated facies. See Figure 1.2 for outcrop locations.

effects of autocyclic processes such as tidal-island migration should be minimal. The Maryville Limestone exposed within the Copper Creek fault block consists of mostly shallow subtidal rocks towards the northeast and deeper subtidal towards the southwest. Along this depositional transect, shelf, shelf-margin and slope/basin are well exposed. As shown by Table 2.1, each depositional setting is characterized by a distinctive suite of rock types.

Environmental Interpretation of Maryville Rock Types

Subtidal Onshelf

Burrow mottled lime mudstone indicates subtidal open-marine conditions of deposition. The wackestone and mudstone (Fig. 2.2A) lithologies represent deposition below normal wave base, perhaps on the upslope or possibly in onshelf areas protected from current agitation by the basinward shelf-marginal cyanobacterial buildups. Packstone and grainstone lithologies indicate periodic increased agitation, perhaps during storms. Thus, deposition of burrow-mottled lime mudstone occurred below normal wave base but above storm wave base. Fining upward sequences indicate deposition during waning energy conditions (Kriesa, 1981). Burrow mottled lime mudstone possibly represents deposition in water depths ranging between 10-20 m. The ooid grainstone and packstone layers within this facies represent resedimentation of grains derived from nearby ooid producing, shoal-water environments.

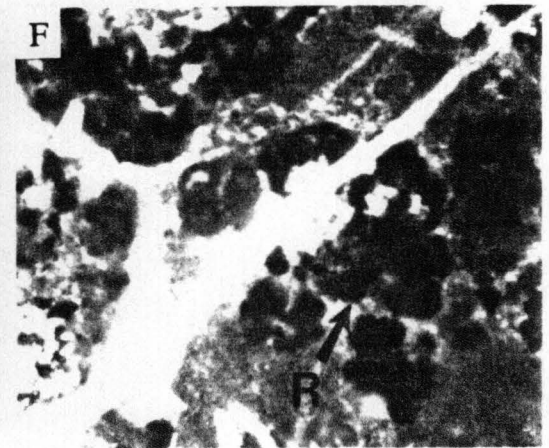
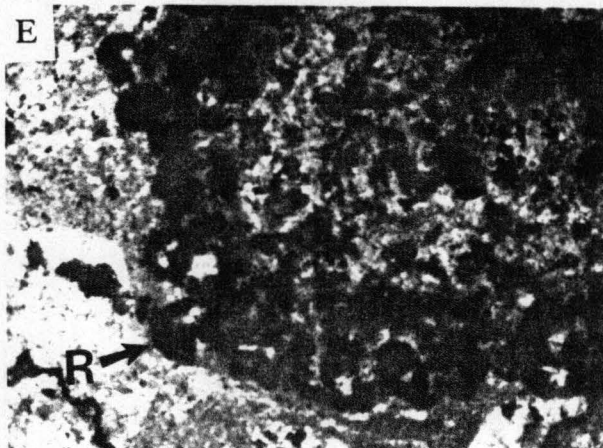
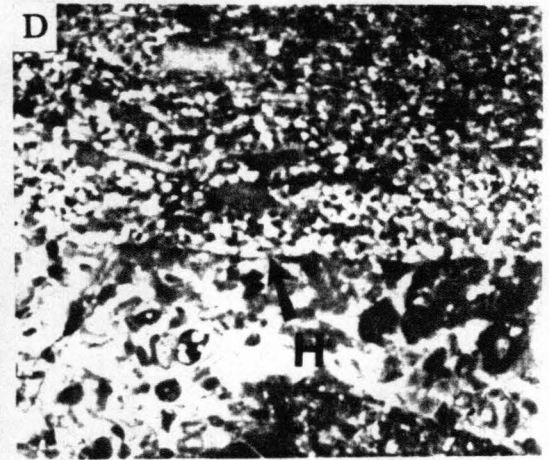
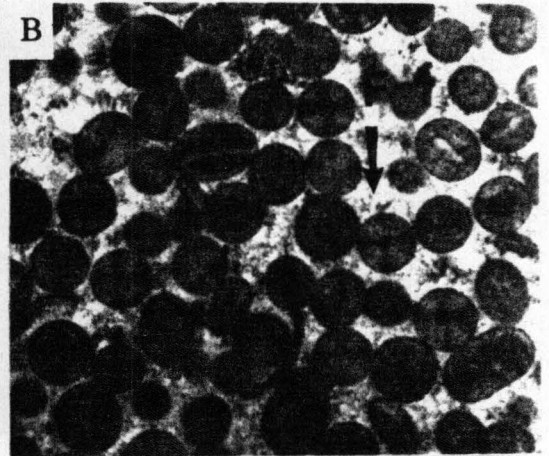
In the thicker ooid shoal (up to 13m) deposits, two subenvironments can be recognized: (1) an active oolite zone, characterized by the dominance of ooids as allochems (Fig. 2.2B), cross beds, and well washed grainstone with marine cements and (2) a stabilized oolite zone, characterized by a decrease in ooids as allochems and by the

Table 2.1. Description of lithofacies

I. Depositional Setting - Subtidal onshelf				
Lithofacies	Color and Thickness	Constituents	Sedimentary Structures	Early Diagenesis
Burrow mottled lime mudstone (wackestone with thin packstone and grainstone layers)	Dark gray to light gray. Weathers buff. Thickness 0-40m.	Micrite dominant with ooids, oncoids, trilobite fragments, echinoderms, peloids, intraclasts, and <u>Renalcis</u>	Fining upward sequences consisting of grainstone, packstone, wackestone, and mudstones. Burrows in wackestone (Fig. 4A)	Burrows dolomitized. Hardgrounds occur as planar darkened surfaces.
Oolitic/oncolitic (packstone/grainstone wackestone and thin mudstone layers)	Generally light gray. Thickness 0-13m.	Ooids, oncoids, trilobite fragments, echinoderms, <u>Renalcis</u> , peloids, silt sized angular quartz grains, and intraclasts.	Percentage of ooids, and cross laminations increase upward (Simmons, 1984), similar to those of Holocene ooid shoal deposits (Newell, et al., 1960; Ball, 1967; and Harris, 1979, 1984). Thinner oolite layers lack these trends.	Fibrous cements in grainstone and packstone layers (Fig. 4B). Blocky calcite spar is evidence for subaerial exposure.
Oncolitic packstone/grainstone (thin wackestone layers)	Light gray. Thickness 0-5m.	Oncoids (C, P, and I type of Logan et al., 1964), trilobite fragments, ooids, peloids, quartz silt, and minor sponge spicules. Oncoids range up to 5-6mm (Fig. 4c).	Lacks internal bedding and other sedimentary structures.	Fibrous, micritic, fine equant, and blocky spar. Blocky calcite spar is evidence for subaerial exposure. Hardgrounds truncate oncoids.
Quartz silty peloidal packstone	Dark gray. Thickness 0-10m.	Angular silt sized quartz grains dominant with peloids, ooids, oncoids, intraclasts, echinoderms, and phosphatic brachiopods.	Thin laminations and possible hummocky cross stratification.	Hardgrounds occur as irregular to planar blackened surfaces (Fig. 4D). Pyrite and glauconite common.
II. Depositional setting: Shelf margin				
Lithofacies	Color and Thickness	Constituents	Sedimentary Structures	Early Diagenesis
<u>Renalcis</u> - <u>Girvanella</u> boundstone (Grainstone, packstone, and wackestone)	Light to dark gray. Thickness 0-15m. Thickness decreases downslope from shelf margin.	<u>Renalcis</u> clusters and fragments, <u>Girvanella</u> crusts, oncoids, trilobite fragments, and minor sponge spicules. <u>Renalcis</u> display the chambered morphological form (Figs. 4D and E). Proportion of oncoids increases upwards.	Biohermal geometry. Growth cavities floored with geopetal sediment and fibrous cement. <u>Renalcis</u> clusters display relief of a few cm.	Hardground at base of the buildup is stylolitized in places and locally shows borings filled with sediments and spar (Fig. 5A). Subaerial exposure surface caps buildup. The surface is local, restricted to shelf margin.
<u>Girvanella</u> -sponge- <u>Renalcis</u> boundstone (packstone, and wackestone)	Dark gray to gray. Thickness 0-10m, decreases downslope.	<u>Girvanella</u> crusts and fragments, sponge spicules (Monaxon and polyaxon, (Fig. 5F), <u>Renalcis</u> , oncoids, trilobite fragments, calcispheres, peloids, and calcareous sponges(?) Proportion of oncoids increases upwards.	Biohermal in shape. Growth cavities floored with internal sediment and cement. Burrows commonly occur in mudstone lithologies.	Fibrous cement in packstone layers. Buildup capped by subaerial exposure surface. The surface is coincident with the top of Maryville Limestone. Pervasive occurrence of blocky clear calcite spar (Figs. 6A & B). Meteoric diagenesis widespread on outer shelf, shelf margin and upper slope.

III. Depositional setting: Slope/basin				
Lithofacies	Color and Thickness	Constituents	Bedding and Sedimentary Structures	Early Diagenesis
Intraclastic packstone	Dark gray. Thickness of beds 5-35 cm	Intraclasts, silt sized angular quartz grains, trilobite fragments, and peloids. Intraclasts consist of peloidal, laminated and non-laminated calcareous siltstone, micrite, and multigeneration.	Beds display crude grading. Lower contacts are irregular and erosional. Sole marks common. Beds occasionally amalgamated. Thin intervening layers of mud occur between two intraclastic layers. The clasts display subparallel to random orientation, occasionally imbricated (Fig. 6C).	Absence of peloidal flattening, stylolites, and clast breakage suggest early diagenesis (Fig. 6D).
Calcareous siltstone	Dark gray. Bed thickness 0-10cm	Silt sized angular quartz grains, peloids, and bioclasts.	Interbedded with intraclastic packstone, lime mudstone/nodular limestone, and shale. Thin laminations, small scale hummocky cross stratification, and partial Bouma sequences occur (Fig. 6E). Planar lower contacts. Sole marks occur. Grading is subtle.	Hardgrounds common, with associated pyrite and glauconite.
Lime mudstone/nodular lime mudstone (wackestone)	Thickness 0.2 m.	Lime mud, peloids, and silt-sized quartz grains. Few well preserved bioclasts.	Thin argillaceous layers intercalated with lime mud. Burrows common. Occurs as interbeds within shale.	Glauconite and pyrite.
Allochthonous oolitic/oncolitic grainstone/packstone	Thickness 0.75 cm.	Ooids, trilobite fragments, oncoids, echinoderms, intraclasts, and quartz silt. Matrix contains abundant mud. Ooid microfabrics similar to ooids of shoal water origin.	Beds lack internal primary sedimentary structures. Usually occurs as interbeds within calcareous siltstone. Lower contacts are erosional.	Hardgrounds with glauconite and pyrite.
Shale	Dark gray to black. Thicker in the lower part, and as thin beds in upper part of sequence.	Black lime mud with terrigenous clay and quartz silt. Fossils absent.	Thinly laminated.	None.

Figure 2. 2. Photomicrographs (cross-polarized light) of different types of lithofacies of the Maryville Limestone (field width = 4.5 mm). A) Burrow mottled limestone from Thorn Hill section. Note the vertical burrow is filled with spar. B) Oolitic grainstone from Thorn Hill section. Note abundant intergranular fibrous cements (F) (field width = 4.5 mm). C) Oncolitic packstone from Woods Gap section (field width = 4.5 mm). D) Quartz silty peloidal packstone from Thorn Hill section. Note the hardground (H) truncates depositional components (field width = 4.5 mm). E) and F) *Renalcis-Girvanella* limestones from Woods Gap section (field width = 1 mm). Note the chambered morphology of *Renalcis* (R).



occurrence of intraclasts and interstitial micrite. Thin bedded oolitic/oncolitic limestone (up to 2m) with fewer ooids and a higher proportion of mud, silt, and bioclastic remains was probably derived by resedimentation from nearby ooid-forming environments. They represent deposition in relatively deeper water. Oncolitic limestones in the Maryville Limestone with well-developed oncoids (Fig. 2.2C) and abundant fibrous and micritic cements represent shallow subtidal deposition in water depths of less than 5 m. Actively growing oncolites in the modern Joulter's Cay area occur in very shallow subtidal settings in water depths of less than 1 m (Gebelein, 1976). Ginsburg (1960), Logan and others (1964), and Flugel (1982) described examples of oncolites from shallow subtidal settings. In contrast, oncolitic limestones of the Maryville with quartz silt, skeletal fragments, and other constituents represent deposition in deeper subtidal settings in which the oncoids have been transported from shallower areas. Similarly Markello and Read (1981) and Kozar (1986) described oncolitic limestones with quartz silt from deeper subtidal environments.

Quartz silty peloidal packstone represents deposition in relatively deeper water below normal wave base (Fig. 2.2D). The associated layers of intraclasts, ooids, and skeletal fragments can be attributed to lowered wave base during storms, or alternatively these grain types may have been transported into deeper water (20-30 m) by grainflows and/or debris-flows triggered by storms (Kozar and others, 1986).

Shelf Margin

The dominant constituents of the shelf-margin reefal lithologies are *Renalcis*, *Girvanella*, sponge spicules, and carbonate mud. Other associated reef constituents are trilobite skeletal fragments, peloids, and calcispheres. The fossils to a large extent are in place and many (especially the cyanobacteria) are found in their growth position. Growth

cavities are filled with geopetal sediment and fibrous cements. Fibrous and micritic cements are common in the intergranular pores. Finally, the buildups had the capability of modifying conditions in surrounding environments, a characteristic of true reefs.

Renalcis and *Girvanella* are described as calcimicrobes (calcified microbial microfossils; James and Gravestock, 1990). The framework of these Maryville reefs was built by cyanobacterial calcification (*Renalcis*) and sediment binding action (*Girvanella*). The reefs at the shelf margin are biohermal in shape. On the basis of the dominant constituents, the reefal complex is subdivided into: (a.) *Renalcis-Girvanella* boundstone (Figs. 2.2E and F), this part of the reefal complex being floored by a hardground (Fig. 2.3A). (b.) *Girvanella-sponge-Renalcis* boundstone (Figs. 2.3E and F, also see Table 2.1 for description).

The increase in *Girvanella* oncoids upwards indicates that the buildups shallowed upward. The reefal complex is punctuated by two subaerial exposure surfaces caused by falls in relative sea-level. The stratigraphically lower subaerial exposure surface is restricted to the shelf margin area. Evidence for this stratigraphically lower subaerial exposure consists of a planar truncation surface, *insitu* brecciation (Fig. 2.3B), pores partly filled with laminated vadose silt (Fig. 2.3C), scalloped surface (Fig. 2.3D) and blocky clear calcite spar in inter- and intraparticle pores (Fig. 2.4A). However, the exposure surface which caps the top of the Maryville (Fig. 2.4B) is areally more extensive (see Fig. 2.1). Although the upper exposure surface itself is not easily traceable from outcrop to outcrop in the field, subaerial exposure in most places at this stratigraphic level can be confidently inferred from the diagenetic fabrics. Petrographic evidence for subaerial exposure consists of extensive dissolution and calcitization of depositional components such as *Renalcis* grains, *Girvanella* oncoids, and trilobite fragments in addition to those features described above. Blocky, clear calcite spar occludes inter- and intraparticle pores. Stable oxygen isotope composition of blocky, clear calcite spar (mean

Figure 2. 3. Photographs (A and B) of polished slabs and photomicrographs (C - F) of Maryville lithologies from Woods Gap section. A) Note a hardground separates the underlying burrowed mudstone from oncolite grainstone. The hardground (H) is stylolitized in part (S), but at places it is still well preserved. The hardground is locally bored (scale bar = 1 cm). B) Features associated with subaerial exposure which include, the exposure surface (ES) and *insitu* brecciation (IB, scale bar = 1 cm). C) Thin section plane polarized light showing laminated vadose silt (LS) associated with the exposure surface (field width = 4.5 mm). D) Thin section under cross-polarized light showing scalloped surface (SS, field width = 4.5 mm). E) Thin section under cross polarized light of *Girvanella-Renalcis* boundstone (G, R). The light colored areas are *Girvanella*. F) Under plane polarized light, thin section showing sponge spicules (field width = 4 .5 mm)

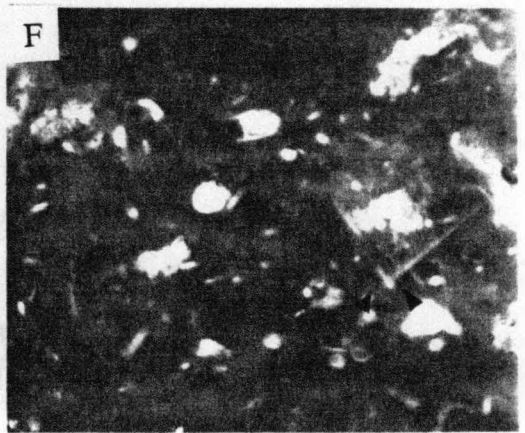
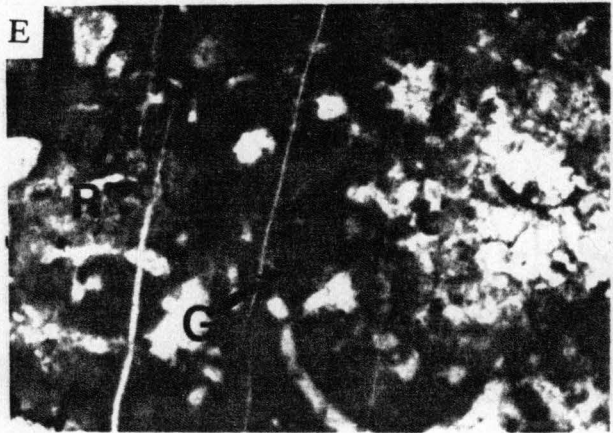
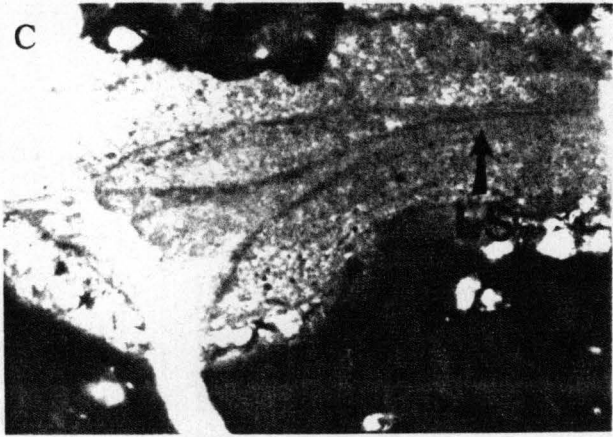
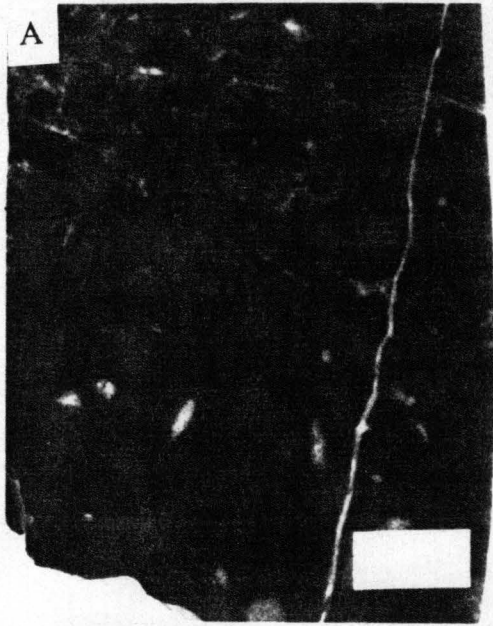
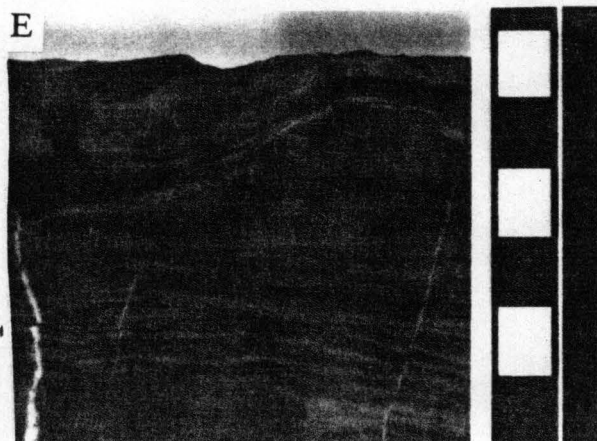
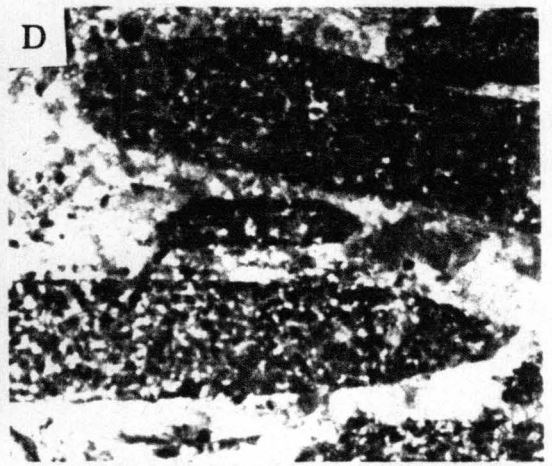
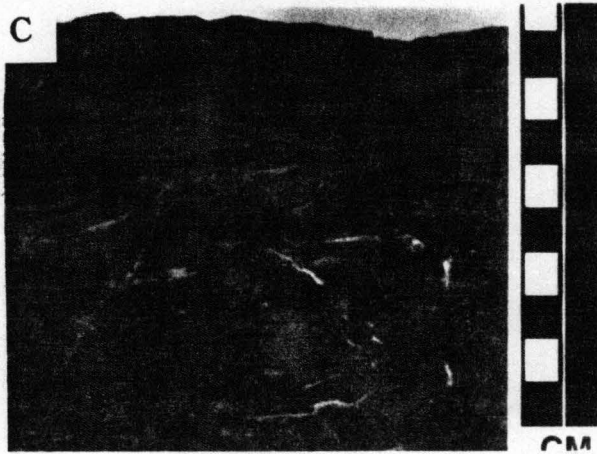
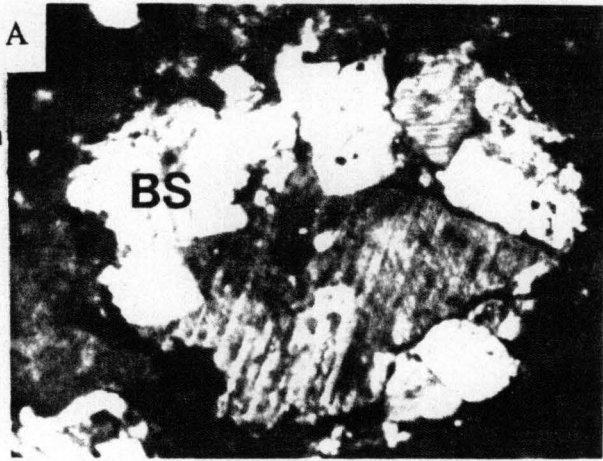


Figure 2. 4. Photographs (B, C, E and F) and photomicrographs (A and D) of Maryville lithologies. A) Thin section under cross-polarized light from Woods Gap section showing diagenetic evidence for subaerial exposure and meteoric diagenesis in the upper part of the Maryville Limestone. The evidence consists of leached fossils (in this case *Renalcis*) replaced with clear blocky spar (BS). B) Polished slab from Woods Gap section showing the contact between Maryville Limestone and the overlying Nolichucky Shale (scale bar equals 1 cm). The top of the Maryville is an exposure surface (ES) as well as a drowning surface (DS). C) Polished slab of intraclastic packstone from Clinton Highway section. Note the clasts in the upper part of the photograph are imbricated (scale bar equals 1 cm). D) Thin section of intraclastic packstone under cross-polarized light. Note the clasts are composed of peloids and silt sized quartz grains (field width = 4.5 mm). E) Polished slab of laminated calcareous siltstone from Norris Freeway section displaying partial Bouma sequence (A,B, and C). F) Field photograph of shale interbedded with thick bedded intraclastic packstone from Norris Freeway section. Hammer for scale.



$\delta^{18}\text{O} = -9.3$, range -9 to -10 ‰ PDB) is considerably depleted (at least $4-5$ ‰ PDB) compared to Cambrian marine values of -5 ‰ PDB (Lohmann and Walker, 1989; Walker and others, 1989). The depleted oxygen isotope composition is consistent with subaerial exposure and meteoric diagenesis. The lack of negative shift in carbon isotopic values is interpreted to be the result of the absence of land plants developed on the surface during exposure.

Lowering of relative sea-level at slope localities (Fig. 2.1, Norris Freeway section) during formation of the exposure surface at shelf-margin localities (Fig. 2.1, Woods gap section), allowed development of cyanobacterial reefs on the former slopes. The upper part of the Maryville Limestone indicates a possible progradation of the shelf margin toward the west or southwest (present geographic direction). The magnitude of progradation during deposition of the upper part of the Maryville is estimated to have been about 20 km. This estimation is based on three well-spaced outcrops down the depositional slope within the same thrust sheet.

Slope/basin

The slope and basinal facies in the study area represent mid- to upper-slope positions. Other localities farther west and southwest represent more basinal positions (e.g. Kozar, 1986). The majority of these lithofacies in the present study area represent deposition below normal wave base in water depths on the order of 25 to 50 meters. This interpretation is based on the general abundance of allochthonous lithologies, paucity of fossils, and abundance of lime mud and quartz silt. However, gravity slides and slumps have not been recognized, although debris flows occur. On the basis of modern analogues, these flows suggest slope angles on the order of 2° to 4° (Reading, 1986).

The characteristics of intraclastic limestones (Fig. 2.4C) which favor a relatively

deeper water origin are: (1) their association with dark colored shales, (2) abundance of fine-grained quartz silt, and (3) absence of associated tidal-flat features such as mudcracks, fenestrae, and subaerial exposure features, as well as shallow subtidal features such as ripple marks and planar cross-bedding. In addition, presence of glauconite, and framboidal (?) pyrite further support a deeper water, low oxygenated environment. Features which support an allochthonous origin for the intraclastic limestones include rafted and projecting clasts, polymictic clast associations, subparallel to random clast orientations, and fine grained lime mud in the matrix (Kozar and others, 1986). However, some of the associated beds are probably storm-derived as evidenced by the occurrence of monomictic clasts, shelter voids and well washed grainstone.

The composition of most of the individual clasts suggests initial deposition in a shallower subtidal setting. Absence of compaction features like peloidal flattening, stylolites, and clast breakage (Fig. 2.4D) suggests that early submarine cementation played an important role in the origin of intraclasts (Sepkoski, 1982; Srinivasan and others, 1990).

Thin laminated calcareous siltstone with evidence of grading is commonly interpreted to have been deposited in deep water slope/basinal settings (Wilson, 1969). Similarly the calcareous siltstone beds of the Maryville Limestone are interpreted to have been deposited in relatively deeper water slope settings (many 10 's of meters). Beds that display a partial Bouma sequence represent deposition by turbidity currents (Fig. 2.4E). These beds are analogous to facies TM and MT (originally silt turbidites/mud turbidites, see Stow and Shanmugam, 1980) described by Ghibaudo (1992).

Mud sized lime sediment is commonly generated in shallow water environments (Stockman and others, 1967). Lime mud generated in shallow shelves such as in the case of Campeche bank are later redeposited downslope from shelf margin (Logan and others, 1969). Similarly lime mudstone/nodular mudstone which occur as interbeds in shale and

calcareous siltstone in the Maryville is interpreted to have been deposited in deeper water slope/basinal settings. This interpretation is further supported by the presence of a limited fauna and the abundance of thin layers of terrigenous silt. Ooid packstone/grainstone interbeds within this facies are interpreted to be allochthonous because the matrix is composed of mud suggesting a lack of winnowing. The ooid microfabrics are similar to those of the ooids of shoal origin.

Stratigraphic association of shale (Fig. 2.4F) with the above mentioned rock types suggests deeper water slope/basin conditions of deposition. Absence of shallow water features and absence of evidence of emergence further support this interpretation.

Depositional Sequences, Subsequences and Stacking Patterns

During the deposition of the Conasauga Group, the shelf followed a cyclical pattern of evolution from a ramp depositional mode to a platform depositional mode. Gentle depositional slopes prevailed during deposition of shales such as those of the Rogersville Shale that underlies the Maryville. The deposition of pure carbonates represents a gradual change in a depositional mode to a flat topped platform fringed by relatively steeper slopes. This interpretation is based on the regional facies distribution. It is our belief that a combination of several factors including tectonics, eustasy, and sedimentation rate played an important role in shaping the Conasauga stratigraphy in the southern Appalachians.

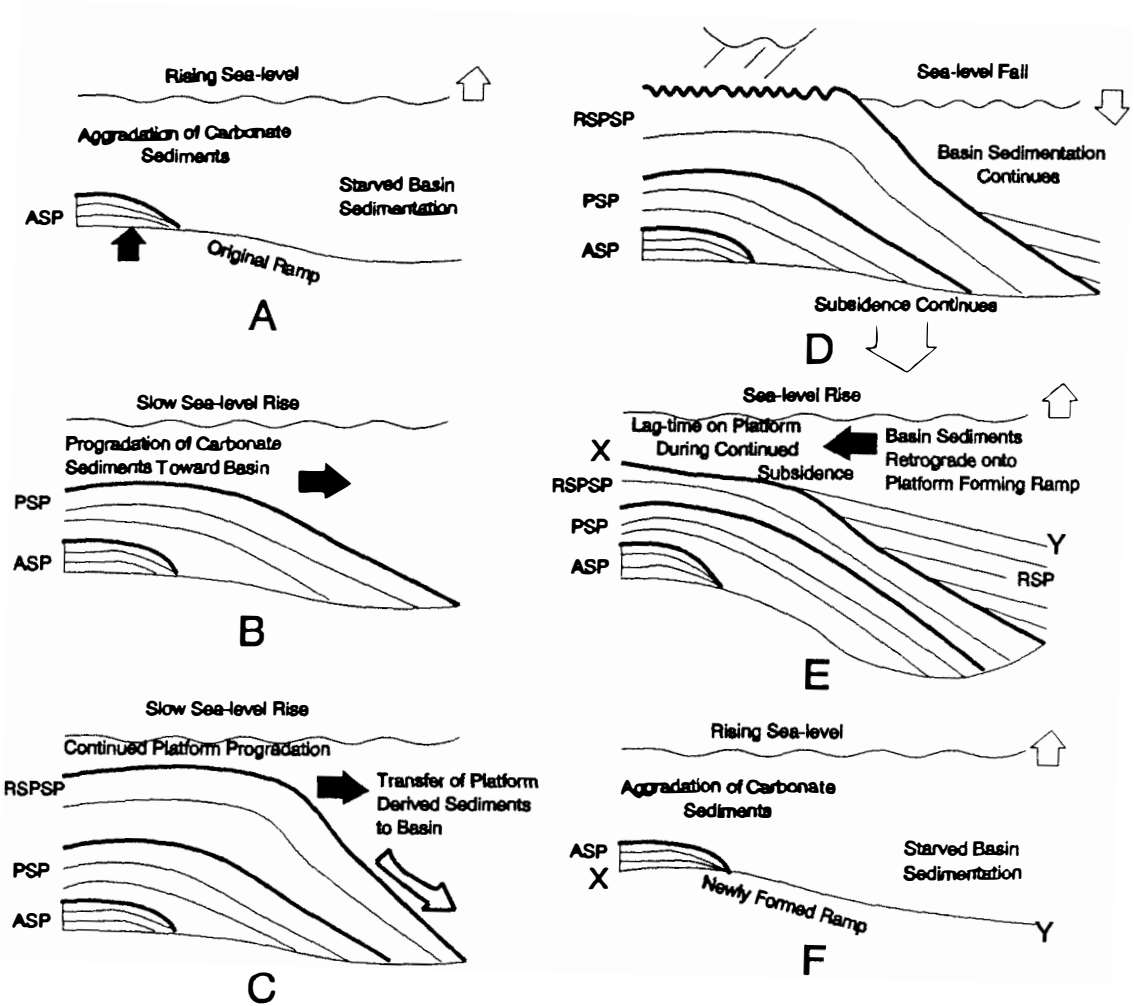
The Maryville Limestone is a third order sequence. The Maryville sequence can be subdivided into two subsequences on the basis of the stacking of lithologic units. The boundary between the subsequences is marked by a shallowing upward event, but does not separate genetically different groups of strata. This boundary is not defined as a sequence boundary since it does not represent a long break in sedimentation and there is no distinct

change in the pattern of sedimentation across the boundary. In contrast, the upper subsequence is capped by a subaerial exposure surface representing a longer break in deposition, and a consequent profound change in depositional regime. In this section we describe the subsequences, stacking patterns, and sequence boundaries. Although we are using the term sequence in the sense of Mitchum and others (1977), we have avoided terms such as transgressive systems tract (TST) because we do not feel they fit well with the development of this carbonate sequence.

Lower Subsequence

The thickness of the lower subsequence varies from about 3-60 m on the shallow platform to a maximum of 40 m further basinward (see Fig. 2.1). The general succession of lithofacies from bottom to top on the shallow platform consists of burrow mottled lime mudstone, quartz silty peloidal packstone, and oolitic/oncolitic packstone/grainstone. This succession indicates a shallowing upward event. The lower subsequence is separated from the overlying subsequence by the culmination of this shallowing upward event. Shoaling upward was in response to a decrease in accommodation space. Shoaling on the shallow platform was accompanied by the deposition of platform derived oolitic limestones further basinward. The slope/basinal part of the subsequence is dominated by shale and platform derived allochthonous lithologies but no subaerial exposure occurred. In terms of the spatial sequencing, processes involved in producing the stacking pattern of this lower subsequence consisted of a combination of aggradational, retrogradational and progradational units.

Figure 2.5. An idealized model for the development of the ramp to rimmed-platform sequences of the Conasauga Group developed from study of the Maryville Limestone. A = oldest, F= youngest. Black arrows show dominant direction of facies migration. ASP = Aggradational stacking pattern where sedimentation "keeps up" with increase in accommodation space. PSP = Progradational stacking pattern where carbonate sediment production outpaces increase in accommodation space and the platform progrades basinward. RSPSP = Rimmed shelf progradational stacking pattern in which a steepened slope results in mass movement of platform edge sediments down slope. RSP = Retrogradational stacking pattern in which basal facies are deposited onto the old platform.



Aggradational Stacking Pattern (ASP)

Burrow mottled lime mudstone of the Maryville represents the initiation of carbonate sedimentation on the shallow subtidal ramp (Fig. 2.5A). This lithofacies represents open- and normal-marine conditions of deposition. Lateral facies variations and sediment thicknesses indicate that muddy sediment deposition occurred on a gentle seaward sloping ramp. This initial accumulation of carbonate mud is similar to the start-up phase of Kendall and Schlager (1981). The stacking pattern of this unit is aggradational, that is, the depositional rate on the mid-to-upper ramp probably was about equivalent to the increase in sediment accommodation space. While deposition of muddy carbonates occurred on the shelf, further offshore starved conditions of deposition prevailed (Fig. 2.5A), represented by well developed hardgrounds in downslope sections. Thus, down-ramp deposition rate did not keep pace with increase in accommodation space. These differences in up-ramp versus down-ramp rates of sediment deposition versus accommodation space lead to aggradation in up-ramp areas and the beginning of change in the ramp profile.

Retrogradational Stacking Pattern (RSP)

In the Maryville Limestone, deposition of quartz silty peloidal packstone and shale intervals represent periods of apparent deepening of the platform. These lithofacies are characterized by a high amount of quartz silt and terrigenous clay and carbonate mud. The stacking pattern is retrogradational and is caused by migration of deeper-water environments bankward. This apparent deepening can be attributed to an increase in the rate of sea-level rise, decrease in carbonate productivity, and a consequent decrease in sedimentation rate.

Progradational Stacking Pattern (PSP)

Oolitic/oncolitic limestone in the Maryville represent deposition during a period when carbonate deposition kept pace with or outpaced sea-level rise (decreasing accommodation space) on the platform leading to transportation of sediment off the platform. The oolitic/oncolitic lithologies characterize the shallow subtidal shelf and the shelf-margin, forming shoals and also occurring as subtidal sand sheets derived from active ooid-forming environments. The succession of lithologies consisting of wackestone, packstone, and grainstone in the oolitic/oncolitic limestone indicates a decrease in accommodation space (shoaling upward). The stacking pattern is typically aggradational to progradational (Fig. 2.5B). Increased proportion of ooids upwards, coupled with presence of planar, trough, and ripple-drift crossbeds suggests increased wave activity in response to shoaling. Lateral transport (progradation) was the dominant process in response to a decrease in accommodation space.

Upper Subsequence

The total thickness of this subsequence which comprises the upper part of the Maryville (Fig. 2.3), ranges up to a maximum of 55 m on the shallow platform. It decreases in thickness farther basinward. The development of the upper subsequence accompanied the establishment and migration of reefal environments basinward. The shelf-margin reefs prograde basinward and downlap slope/basinal deposits. The succession of lithofacies consisting of burrow mottled limestone, *Renalcis-Girvanella* boundstone, oolitic and oncolitic limestones suggests shallowing upward. Development of the upper subsequence was terminated by subaerial exposure. Subaerial exposure of the shallow platform and platform margin was accompanied by the development of reefs

(upper part of Norris Freeway section) on top of platform derived allochthonous deposits on the former slope.

Rimmed Shelf Progradational Stacking Pattern (PSP)

Studies of several outcrops along the depositional transect of the study area provide critical evidence for the basinward progradation of a shelf-margin reefal complex (Fig. 2.5C). This lateral expansion of the platform was in response to a relative rise in sea-level because carbonate production requires flooding of the bank margin (Harris and others, 1986). The boundstone deposits downlap the underlying deeper water lithologies. Progradation of Northwest Bahama Bank toward the Straits of Florida indicates that lateral expansion of platforms are facilitated by low depositional slopes, increase in carbonate productivity, and the ability of currents to transport sediments (Eberli and Ginsburg, 1989). Progradation during late Maryville depositional time may have been facilitated by a combination of slow relative rise in sea-level and fairly gentle depositional slopes, allowing carbonate deposition to keep pace with the rising sea-level (Kendall and Schlager, 1981). The basinward progradation of the *Renalcis* boundstone occurred for a distance of about 20 kilometers. This estimate is based on three well-spaced outcrops down the depositional slope. Deposition of reefal lithologies downslope of the shelf-margin occurred during a period of relative sea-level lowstand when the bank-margin was subaerially exposed (top of Maryville).

Retrogradational Stacking Pattern (RSP)

The close of Maryville deposition in the area of the platform was marked by a fall in sea-level and the consequent development of an exposure surface. As mentioned earlier

the exposure interval is not recorded in the down-slope localities (e.g. Norris Freeway) but shallowing did occur there leading to the development of cyanobacterial buildups on the former slope. The rise in sea level following the exposure event led to deepening again on the slope, and a flooding of the old Maryville platform. During the carbonate "lag time" in the area of the old exposure surface, continued subsidence led to gradual deepening and establishment of slope/basin depths, and a change in the profile to a ramp. Deposition of the Lower Nolichucky formation shales began, marking the first stages of the next ramp to platform transition and the next Conasauga sequence.

To summarize, the Maryville Limestone sequence consists of two depositional subsequences. The stacking pattern within the subsequences consists of a combination of aggradational, retrogradational and progradational units, as a consequence of variations in sedimentation rate, subsidence, and absolute sea-level change. The sea-level change may have been eustatic in nature (Osleger and Read, 1991) or only of regional extent. If the latter, it may have ultimately been caused by regional or subregional tectonism. The intrashelf basin may have developed and been maintained by repeated subsidence in relict normal faulted basins which existed during early Cambrian deposition of the Rome Formation (Rankey in prep)

Sequence Bounding Surface

As originally recognized by Mitchum and others (1977) some sequence-bounding surfaces developed subaerially; others developed as submarine surfaces. According to Van Wagoner and others (1988), a sequence-bounding surface is a surface of subaerial truncation. As proposed by Schlager (1991) sequence boundaries, particularly in carbonate successions, should have a more process-oriented definition, and they should represent a significant change in the pattern of sedimentation. Subaerial truncation and

drowning unconformities are ubiquitous in the Phanerozoic rock record. Drowning can occur with or without subaerial exposure (Schlager, 1981, 1989). Drowning unconformities represent a significant change in the depositional pattern in which shallow water carbonate deposition is terminated, accompanied by onlap of deep water sediments over the shallow carbonate deposits (Schlager, 1991).

As described earlier, the upper part of the Maryville Limestone is punctuated by two stratigraphic discontinuities caused by minor relative sea-level falls. The stratigraphically lower discontinuity is restricted to the bank-margin. The upper discontinuity which is coincident with the top of the Maryville Limestone in the study area is areally extensive (Fig. 2.5D). In terms of duration of the sea-level fall, that which formed the upper surface probably lasted longer as evidenced by extensive meteoric diagenesis in the upper part of the Maryville Limestone. Subsequently, a rapid relative sea-level rise drowned the platform (Fig. 2.5E). This drowning unconformity is recognized on the basis of an abrupt shift in facies (deep water shale superposed upon shallow platform limestone), indicating a significant change in the pattern of sediment input. Deposition of shallow platform carbonates was suppressed and siliciclastics derived from the west and northwest (craton) were deposited on the platform. This transition between the Maryville Limestone and the overlying Nolichucky Shale is interpreted here as a sequence boundary. Suppression of carbonate deposition, slow deposition of fine siliciclastics, and continued subsidence lead to gradual deepening and finally to re-establishment of a ramp-like profile (Fig. 2.5F).

Summary of Evolution of The Platform

This Middle Cambrian carbonate platform was flanked by an intrashelf basin to the west and northwest and open, deeper ocean to the east (Fig. 2.6). The complex pattern of

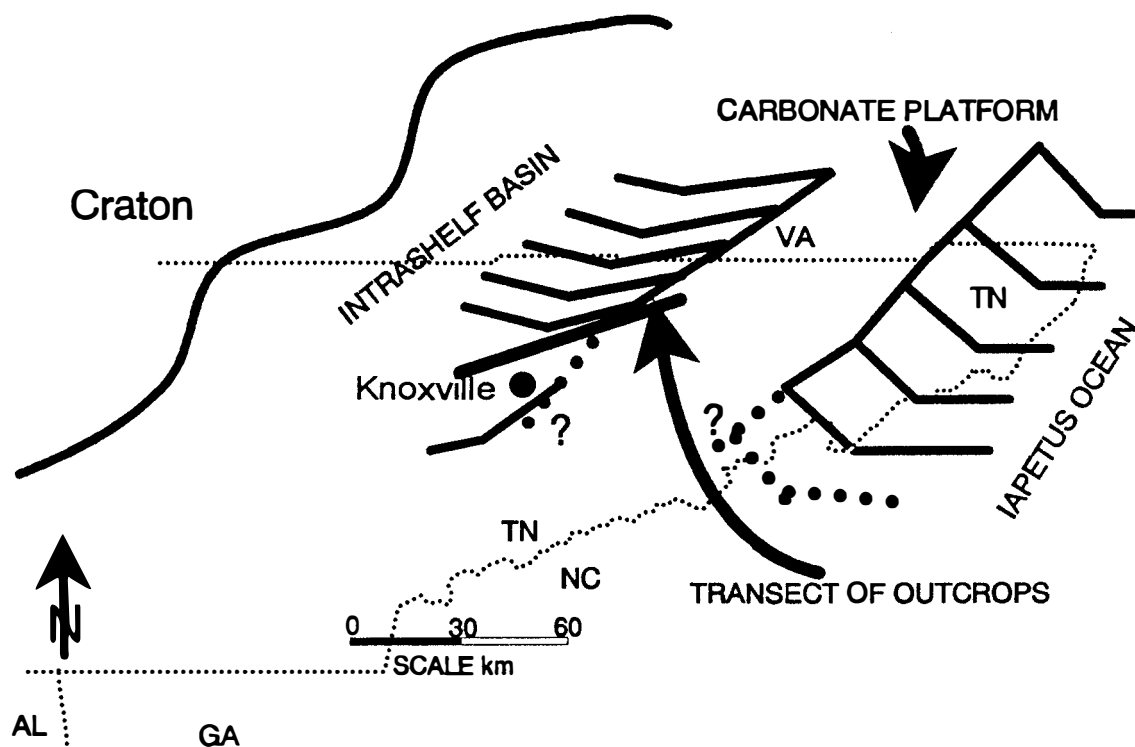


Figure 2. 6. Map showing Middle Cambrian paleogeography in eastern Tennessee and southwest Virginia. The angled lines on the western side of the platform mark the transition to the intrashelf basin.

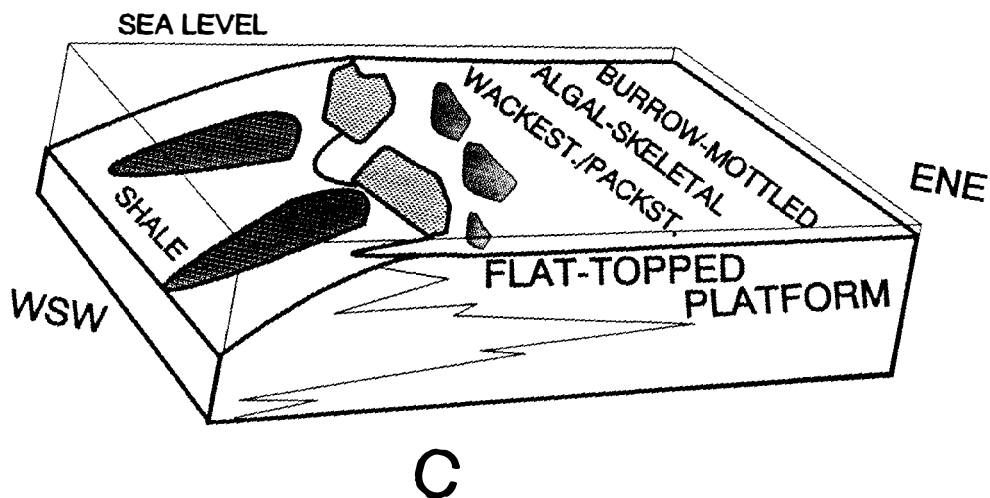
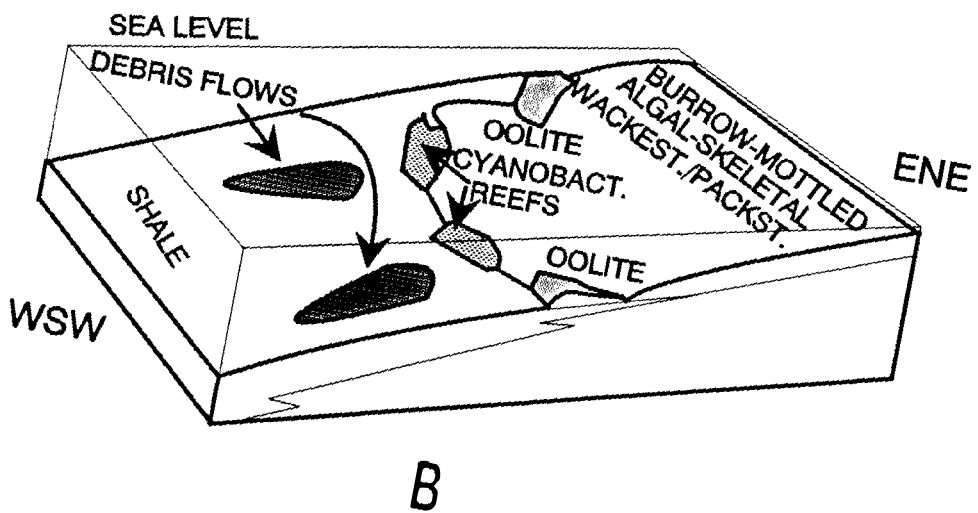
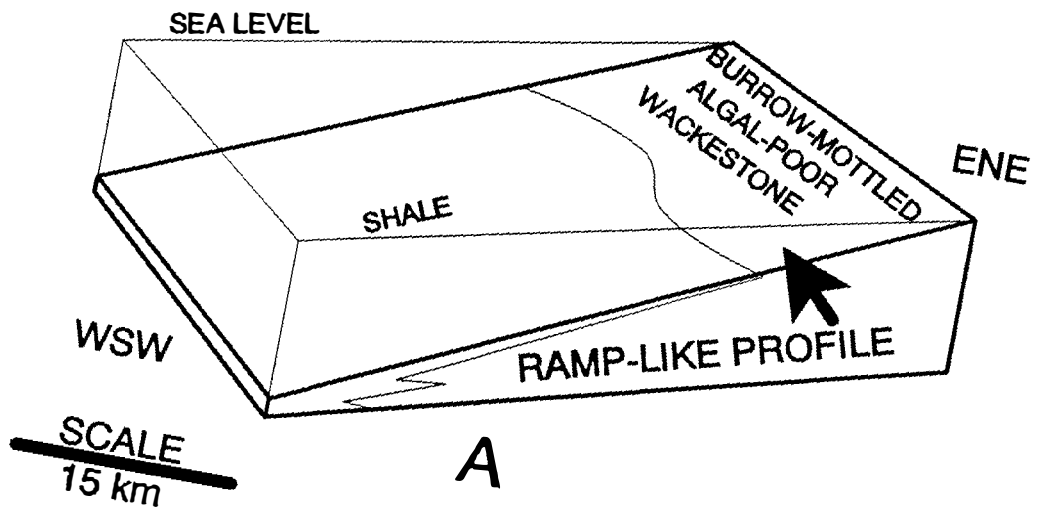
evolution of the shelf from ramp to a platform and vice versa involved a strong interplay between siliciclastic basinal environments located to the northwest and carbonate dominated environments which were located to the southeast. Deep-water subtidal environments to the west and southwest are replaced farther northeast (southwestern Virginia) by peritidal areas and shallow intrashelf basin documented by Erwin (1981) and Markello and Read (1981).

Carbonate sedimentation on the shallow subtidal shelf was initiated in response to widespread flooding of the shelf. Burrow mottled limestone and quartz silty peloidal packstone represent the initial establishment of carbonate mud-forming environments. They characterize deposition on a gentle basinward-sloping ramp (Fig. 2.7A) during deposition of the lower part of the Maryville Limestone. The recognition of ramp depositional mode is based on the vertical and lateral facies relationships. A relative decrease in the rate of sea-level rise, accompanied by increased carbonate productivity, caused widespread deposition of oolitic/oncolitic and *Renalcis* limestone and progradation of shallower subtidal environments westward across the ramp. Shoaling by this process eventually converted the ramp into a flat-topped platform. Oolitic/oncolitic limestone deposits seaward of the shallow shelf, shoal upward into cyanobacterial buildups, which eventually formed a barrier (Fig. 2.7B). During a period of slow relative sea-level rise, the shelf-margin buildups prograded basinward. Establishment and migration of this seaward barrier accompanied the change in the depositional mode from a ramp to a flat-topped platform fringed by relatively steeper slopes. Abundance of mass flows and turbidites downslope of the barrier provides evidence for steepening of the depositional slopes (Fig. 2.7C). Shoaling upward punctuated by subaerial exposure caused by minor sea-level falls characterizes the upper part of the Maryville. Finally, deposition of the Maryville Limestone was terminated in the study area by a rapid relative sea-level rise and siliciclastics derived from the craton were deposited on the platform during the "lag-time"

Figure 2. 7. Block diagrams summarizing the evolution of the platform during the deposition of the Maryville Limestone. A. Carbonate deposition on a gentle basinward sloping ramp grades downslope into shale.

B. During a period of slow down in relative sea-level rise progradation of shallower subtidal environments (oolites and cyanobacterial reefs) occurred across the ramp.

C. Establishment and migration of cyanobacterial reefs accompanied the change in the depositional mode from a ramp to a flat-topped platform fringed by steeper slopes.



after flooding (the beginning of deposition of the Nolichucky Shale).

Approximate intrashelf basin minimum water depth can be calculated by taking a depositional slope of 1° over the distance between the closest shelf edge and wholly basinal localities. Basinal depths estimated in this way are on the order of 200-300 m. A 1° slope was adopted as the lowest angle on which mass sediment movement (grain flow and debris flow) is likely to be initiated (e.g. see Foreman and others, 1991) although actual slopes were likely slightly greater. The slope localities treated here were mid- to upper-slope with maximum depths of a few tens of meters.

Conclusions

Carbonate depositional systems are fundamentally different from siliciclastic systems. Their differences must be taken into consideration when translating sequence stratigraphic concepts developed for siliciclastic systems to carbonate successions. In view of the fundamental differences, a process-oriented approach has allowed us to define the sequences, sequence boundaries, and the stacking pattern of the Maryville Limestone.

The Maryville Limestone, which is a third-order sequence, consists of two subsequences. The subsequences are characterized by a combination of aggradational, retrogradational, and progradational units as a consequence of variations in sedimentation rate, subsidence, and absolute sea-level change. The transition between the Maryville Limestone and the overlying Nolichucky Shale is a sequence boundary. This transition has been interpreted by us as a drowning unconformity. The drowning event was preceded by subaerial exposure of the outer platform. A rapid relative sea-level rise drowned the platform and siliciclastics derived from the northwest were deposited on top of the shallow water carbonates. This drowning, coupled with carbonate lag-time on the old platform, continued subsidence, and retrogradation onto the platform of siliciclastic basinal facies

converted the flat-topped platform into a ramp-like profile. The subsequent ramp deposition is represented by the lower part of the overlying Nolichucky Shale.

Our explanation for the limestone to shale transition can serve as a useful analog to other lower Paleozoic and possibly younger passive-margin sequences.

CHAPTER 3

MICROSCALE AND FABRIC SELECTIVE DISSOLUTION AND CEMENTATION DURING EARLY DIAGENESIS OF MARYVILLE LIMESTONE (MIDDLE CAMBRIAN), SOUTHERN APPALACHIANS

Introduction

Holocene shallow water carbonate deposits are composed of metastable mineral phases, aragonite, magnesian calcite, and calcite. However, this metastable assemblage varied throughout the Phanerozoic (Sandberg, 1983). In particular, lower and middle Paleozoic sequences were dominantly composed of magnesian calcite, and calcite sediments (Wilkinson and Given, 1986). Shallow platform carbonates undergo stabilization in the presence of meteoric fluids introduced during sea level lowstand and subaerial exposure. The sediments subsequently undergo recrystallization during burial. The cementation history of shallow water carbonate deposits is largely a function of their original metastable mineral assemblage. Aragonite-rich sediments will have a greater potential for cementation in meteoric environments (James and Choquette, 1984). During burial, stabilization pathways involve recrystallization where microscale dissolution and reprecipitation are believed to predominate. However, during deeper burial large scale dissolution can occur in the presence of reactive basinal brines.

There are numerous examples where fresh water diagenesis has been an important process of Quaternary and Recent carbonate sequences (Land, 1970; Steinnen and Matthews 1973; Halley and Harris, 1979; Buchbinder and Friedman, 1980; Chafetz et al., 1988; Budd, 1992). The cement morphologies associated with meteoric diagenesis are quite distinct. They include blocky clear calcite spar precipitated in vuggy porosity in the meteoric phreatic environment. However, the vadose diagenetic environment is

characterized by features such as meniscus and pendant cements. Climate plays an important role in the cementation history of carbonate sequences. For instance, under arid climatic conditions dissolution and cementation are limited.

Isotopic systematics have been successfully applied in the delineation of fresh water diagenesis in ancient as well as recent carbonates (Hudson, 1977; Allan and Matthews, 1982, Moldovanyi and Lohmann, 1984; Meyers and Lohmann, 1985 among many others). In general, meteoric calcite is characterized by depleted $\delta^{18}\text{O}$ compositions relative to contemporary seawater values. However during burial, an increase in temperature also leads to fractionation which causes a similar depletion in $\delta^{18}\text{O}$ values in precipitated diagenetic phases. Post Silurian carbonate sequences that have been subjected to fresh water diagenesis exhibit considerable depletion in $\delta^{13}\text{C}$. This depletion in $\delta^{13}\text{C}$ is caused by input of soil-gas derived light carbon. Absence of land plants during pre-Silurian time resulted in a much lower depletion in carbon isotopic compositions. Therefore, carbon isotopic signatures cannot be used as an indicator of meteoric diagenesis in most pre-Silurian carbonates. In these rocks, petrographic analysis takes on special importance.

The Middle Cambrian Maryville Limestone in the southern Appalachians provides an excellent opportunity to study the effects of sea-level changes on the cementation history of subtidal carbonates. In the study area the unit represents deposition along a rimmed shelf-edge to basin transition. The development of the Maryville sequence was controlled in part by sea-level changes, and partly by progradation of the platform toward the craton (Srinivasan and Walker, 1993, in press). The outer platform facies is punctuated by two subaerial exposure surfaces caused by sea-level lowstands. The stratigraphically lower exposure surface is restricted to the shelf-margin strata. However, the exposure surface which caps the Maryville is areally more extensive.

The main objective of this research is to describe the stabilization history of the Maryville Limestone during early diagenesis. The approach includes a combination of field work, petrography and geochemistry. Detailed petrography reveals considerable variation in the degree of burial alteration across the depositional transect from shallow platform to basin. The upper part of the Maryville depositional sequence which was affected by meteoric diagenesis shows very little evidence for deep burial diagenesis, which is probably related to the higher degree of cementation during early diagenesis. However, deep burial diagenesis was more pronounced where the effects of meteoric diagenesis were minimal or absent, particularly in slope/basin and the lower part of the Maryville sequence. Various types of dolomite, the main burial diagenetic product in these rocks, are discussed in chapter 4 of this dissertation. The present chapter is mainly concerned with early diagenesis which occurred under surficial and shallow burial conditions.

Geologic Setting

Late Precambrian crustal extension of the eastern North American continent was accompanied by the establishment of a broad regional carbonate shelf (Bird and Dewey, 1970; Read, 1989, among others) that experienced deposition from Early Cambrian through Early Ordovician time. The Middle and Upper Cambrian Conasauga rocks in northeastern Tennessee and Virginia are part of this Cambro-Ordovician sequence. In the study area, the Conasauga rocks are exposed in a series of southeasterly dipping imbricate thrust sheets. The Conasauga Group in East Tennessee conformably overlies the Rome Formation (lower Cambrian) and is in turn overlain conformably by the Knox Group (Rodgers and Kent, 1948; Harris, 1964; Palmer, 1971). During deposition of the Rome Formation the environmental pattern was influenced by linear "pull-apart" basins formed

during the breakup of the continental margin that occurred in late Precambrian and Early Cambrian time (Read, 1989). The outcrops for this study are exposed within the Copper Creek fault block (Fig. 1.2). The upper part of the Maryville Limestone in northeastern Tennessee and parts of southwestern Virginia ranges between the *Bolaspidella* zone (Middle Cambrian) and the overlying *Cedaria* zone (Dresbachian) (Derby, 1965).

Detailed stratigraphy of the Maryville Limestone is shown in Figure 2.3. In the study area it represents deposition along a rimmed platform edge-to-basin transition (Srinivasan and others, 1991; Srinivasan and Walker, 1993). The Maryville environmental array evolved over time from a gentle basinward sloping ramp to a rimmed platform. Cyanobacterial buildups marked the platform margin environments. The transition from platform-margin to basin consisted of a slightly steeper slope environment. The development of Maryville sequence was controlled by sea-level changes in part, and partly by progradation of the platform toward the craton. Deposition of the Maryville Limestone was terminated by sea-level fall and subaerial exposure. A subsequent rapid relative sea-level rise drowned the platform and during the lag time before carbonate deposition could be initiated, the platform was onlapped by basinal deposits of the Nolichucky Shale. The Maryville-Nolichucky contact has been interpreted as a sequence boundary (Srinivasan and Walker, 1992), which may have also involved nonthermal tectonic subsidence (Rankey and others, submitted).

Methods

Detailed petrographic analyses were carried out on 150 thin sections from 5 localities chosen from a total of 400 samples examined. Selected thin sections from each locality were stained with alizarin red S and a mixed stain of alizarin red S and potassium ferricyanide, according to the procedure outlined by Dickson (1965), to differentiate

calcite and dolomite and to identify ferroan phases. Selected polished thin sections were analyzed for cathodoluminescence using a nuclide ELM-2AVG luminoscope. Blocky clear calcite spar from shelf margin facies were analyzed for Ca, Mg, Fe, Mn, and Sr using a Cameca SX50 electron microprobe. Operating conditions were 20 nA beam current, 5 - 10 μ m beam spot, and count time of 40 sec for Fe, 50 sec for Mn, 20 sec for Mg, and 10 sec for Ca. The accelerating voltage was 15 keV. Detection limits in ppm for these conditions at 99% confidence are Fe = 450 ppm and Mn = 410 ppm, Sr was below detection limits. Totals greater than 102 % and less than 98% are not reported.

Samples for stable isotope analyses were drilled from polished slabs using a microscope mounted microdrill. A total of 90 samples were analyzed for carbon and oxygen isotopes at the University of Tennessee stable isotope laboratory. Sample sizes for isotopic analyses ranged between 0.2 to 8.0 mg. Isotopic analyses of large samples were carried out by CO₂ extraction from a carbonate line into sealed vessels. The CO₂ was later analyzed in the Mass spectrometer. However, isotopic analyses of small samples (less than 1 mg) were carried out using a common acid extraction line directly linked to a VG903 stable isotope mass spectrometer. Custom made glass tubes (referred to as boats) measuring approximately 1-2 cm in length and 0.5 cm in width sealed at one end served as sample holders. These sample holders were assembled sequentially onto a rectangular block. The samples were housed in a rectangular glass chamber under vacuum and maintained at 55^o C with the help of a heat tape. The sample holders or boats were dropped into the common acid bath containing 103% phosphoric acid maintained at 55^o C. The reaction time for each sample varied depending on the sample size. In-house calcite standards were run as unknowns with Maryville samples. The precision of the resulting isotopic values is better than 0.2 ‰ PDB for both carbon and oxygen. The isotopic composition was corrected for temperature fractionation. Sr-isotope analyses

were performed by Dr. Steven Goldberg at the University of North Carolina, Chapel Hill. The $^{87}\text{Sr}/^{86}\text{Sr}$ data have been normalized to the SRM 987 Sr carbonate standard.

Early Diagenesis of Maryville Limestone

Description of Depositional and Diagenetic Components

The paragenetic sequence that was established with the help of detailed standard and cathodoluminescence microscopy is summarized in Figure 3.1. The evidence for the relative timing of the various diagenetic phases is given below in the discussion of each phase. In general, the Maryville Limestone was subjected to a complex diagenetic history. As mentioned earlier, sea-level changes played an important role in the early diagenetic history. The following section provides a detailed description of different depositional and diagenetic components associated with early diagenesis. Later diagenetic phases are treated in the following chapter.

Fibrous (marine) cements

Fibrous cement occurs as a thin fringe of isopachous cement around depositional components. Because this is the first phase to have precipitated on the walls of pores, it was first in the relative timing sequence (Fig. 3.2A). In grainstone lithologies this phase occludes primary porosity (Figs. 3.2A and B). Fibrous cement in the Maryville Limestone, as is the case with all marine diagenetic phases, appears turbid and full of very tiny inclusions. Fibrous cements typically grade into turbid calcite spar and where the turbid calcite spar is absent, the intergranular pores are filled with blocky, clear calcite spar. The

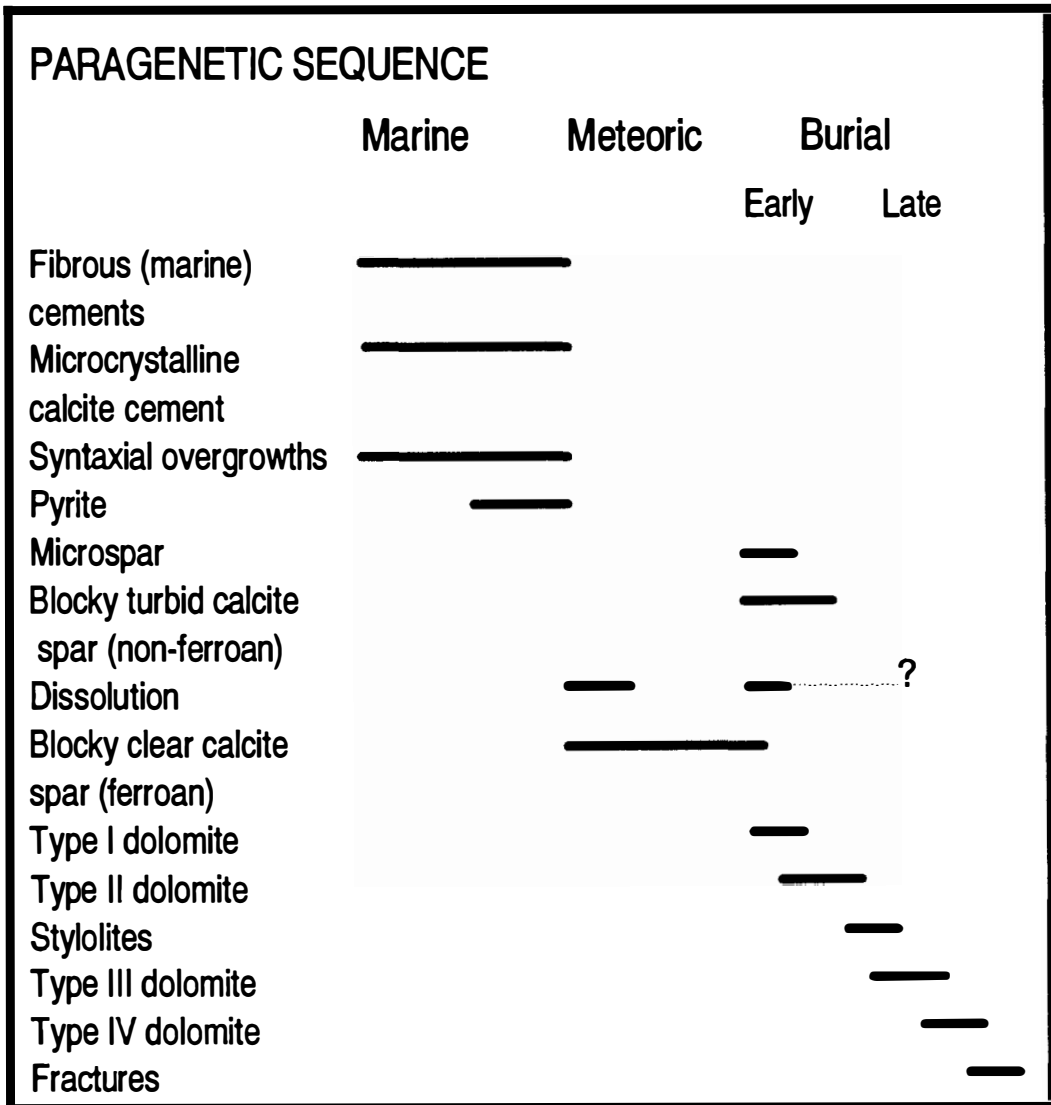
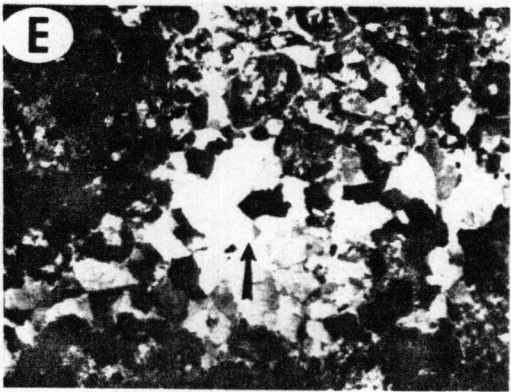
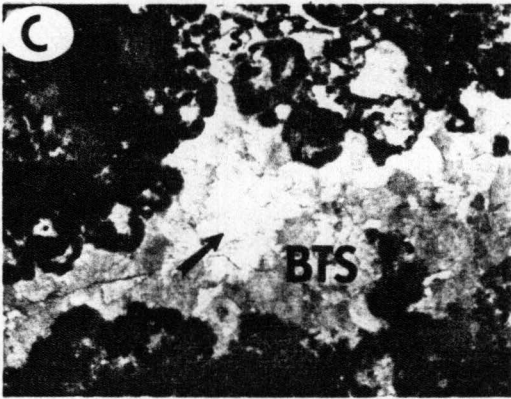
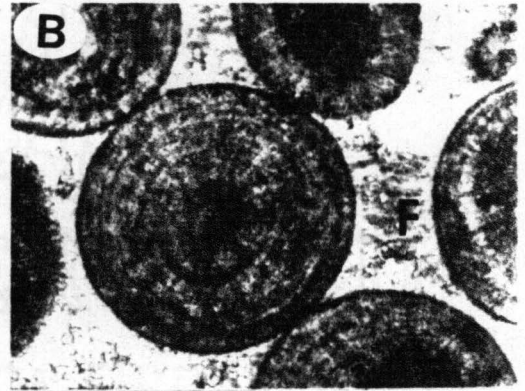
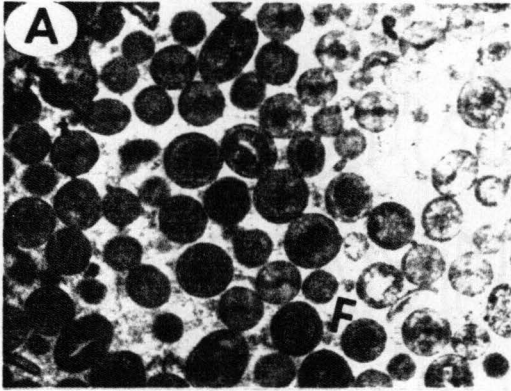


Fig 3.1. Paragenetic sequence of the Maryville Limestone. The bars indicate relative timing of the different processes and diagenetic phases.

Figure 3.2. Photomicrographs (cross-polarized light and plane light) of different diagenetic phases of the Maryville Limestone. A) Intergranular fibrous cement (F) in ooid grainstone from Thorn Hill section (field width = 6.5 mm). B) Close up of the same feature. Note the intergranular pore space is occluded by fibrous cement (F). Also note the ooid fabric is well preserved. (field width = 1.5 mm). C) Thin section plane polarized light showing intergranular blocky, turbid calcite spar (BTS) in *Renalcis* boundstone from Woods Gap section. Note, arrow points to pore central blocky, clear calcite spar (field width = 6.5 mm). D) Blocky, turbid calcite spar (BTS) in intergranular pore space. Note thin fringe of first generation fibrous cements (indicated by arrow) on depositional components (field width = 1.5 mm). E) Intergranular pore central blocky, clear calcite spar (indicated by arrow) in *Renalcis* boundstone from Woods Gap section (field width = 6.5 mm). F) Blocky, clear calcite spar (BCS) in moldic pore in oncolite grainstone from Woods Gap section. Note inclusions of dolomite rhombs (indicated by arrow) in calcite spar (field width = 1.5mm).



primary depositional fabric of fibrous cement is well preserved. Less commonly this cement type is partially replaced by dolomite.

Microcrystalline calcite and Microspar cement

Micrite occurs as cement in boundstones. However, this cement type is rare to absent in other rock types of the Maryville Limestone. Microspar commonly occurs as a mosaic of irregular crystals in micrite rich lithologies. Microspar shows variable crystal sizes, is non-ferroan, and is occasionally replaced by dolomite.

Syntaxial overgrowths

Syntaxial overgrowths on echinoderm grains are restricted to grainstone and packstone lithologies. The overgrowths generally appear turbid. Rarely the overgrowths are replaced by dolomite.

Blocky, turbid calcite spar

Blocky turbid calcite spar occludes intergranular pore spaces and burrows (Figs. 3.2C and D). This cement type is particularly abundant in grainstone and packstone lithologies. Blocky, turbid calcite spar post-dates fibrous cement. In intergranular pores, it occasionally grades into blocky clear calcite spar (Figs. 3.2C and E). In general, blocky, turbid calcite spar is non-ferroan with irregular micron sized inclusions of dolomite. Under cathodoluminescence blocky turbid calcite spar appear dull.

Blocky, clear calcite spar(intergranular pores)

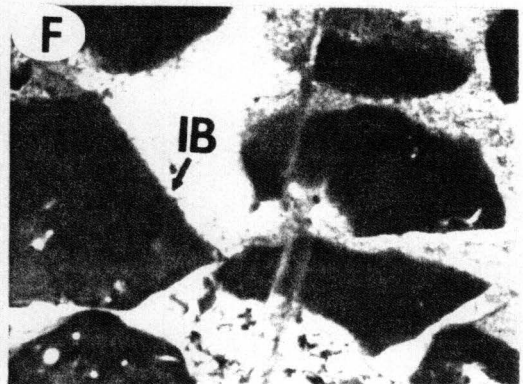
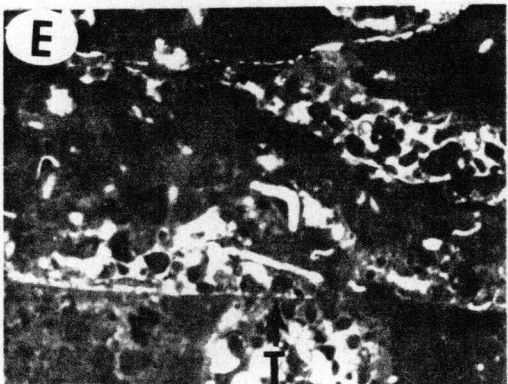
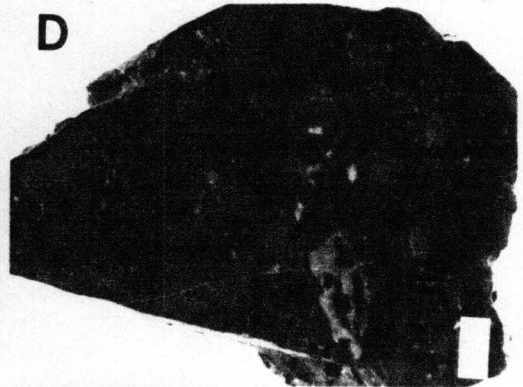
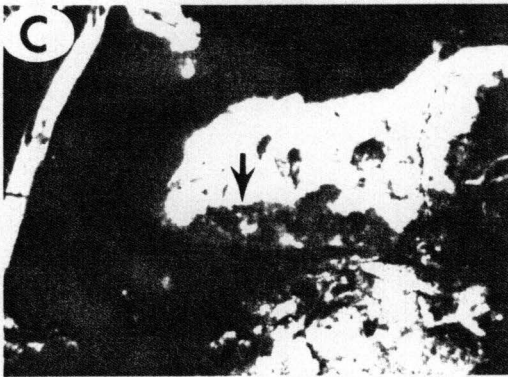
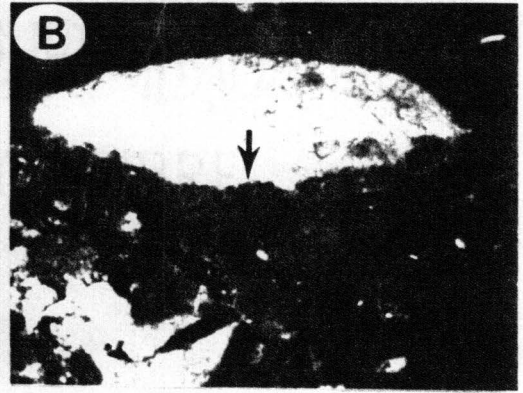
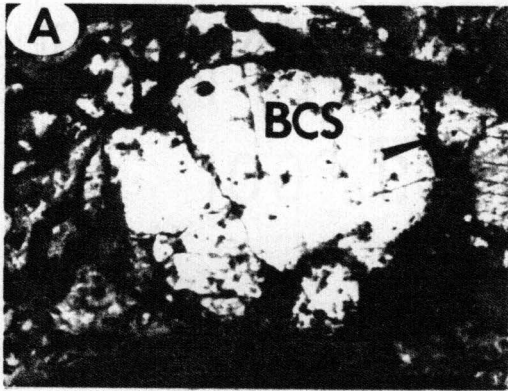
This particular cement type occurs in intergranular pores as final pore filling (Figs 3.2C and E). Blocky, clear calcite spar in intergranular pores is volumetrically less abundant than other cement phases.

Blocky clear calcite spar (moldic pores)

This particular phase commonly occurs in fabric selective dissolution voids (Fig. 3.2F) and less commonly in intergranular pores. Blocky, clear calcite spar is volumetrically more abundant in outer shelf facies, particularly in *Renalcis* and *Girvanella* boundstones. *Renalcis* is the most common constituent that has been subjected to fabric selective dissolution. This cement type occurs mainly below the prominent exposure surface at the top of the Maryville in the outer shelf facies. Field and petrographic evidence for subaerial exposure consists of blocky clear calcite spar in moldic pores (Fig. 3.3A), planar truncation surface (Figs. 3.3B and C), pores partly filled with vadose silt (Figs. 3.3D and E), and *insitu* brecciation (Fig. 3.3F).

Blocky, clear calcite spar in the Maryville Limestone is ferroan. Under CL it displays dull orange luminescence with moderately luminescent intercrystalline boundaries. The crystals commonly contain inclusions of ferroan dolomite rhombs (Fig. 3.2F). Occasionally the dolomite rhombs transect grain boundaries. There are only a few examples where blocky, clear calcite spar in moldic pores occurs in a drusy mosaic (probably because the size of most voids does not permit a clear increase in grain size towards the center of the pore).

Figure 3.3. Photomicrographs (ABDE and F) and photograph of a polished slab (C) of Maryville Limestone showing different diagenetic features. A) Blocky, clear calcite spar (BCS) in intraparticle pore. Note minor blocky, turbid calcite spar (indicated by arrow) in the same pore (field width = 1.5 mm). B) Vadose silt (indicated by arrow) and blocky, clear calcite spar in intraparticle pore (field width = 6.5 mm). C) thin section plane light showing vadose silt and blocky, clear calcite spar in intraparticle pore (field width = 1.5 mm). Slab of *Renalcis* boundstone showing subaerial exposure features, planar truncation surface (T), *insitu* brecciation (IB), and laminated vadose silt (LS) (field width = 1 cm). D) E) Thin section cross-polarized light showing planar truncation surface (T) associated with subaerial exposure (field width = 1.5 mm). F) Thin section cross-polarized showing *insitu* brecciation (IB) (field width = 1.5mm).



Intraclasts

Intraclasts are common constituents of slope/basinal lithofacies. Several different types of intraclasts have been recognized, they include peloidal, micrite, calcareous siltstone, and multigeneration clasts. The clasts in general lack compactional features such as clast breakage, peloidal flattening, and stylolites. Under CL, the clasts display a dull uniform orange luminescence. Mean carbon and oxygen isotope values for the intraclasts are -0.8 ‰ (PDB) for carbon and -8.6 ‰ (PDB) for oxygen.

Dolomite

Dolomite is the principal diagenetic phase in the Maryville Limestone formed during deeper burial. In general, the Maryville Limestone has been subjected to incomplete dolomitization. Four different types of dolomite were formed during progressive burial. Among the four dolomite types, Type I and Type II are interpreted to have formed during shallow and intermediate burial. However, Type III and Type IV dolomite represent deep burial diagenesis. A detailed discussion of dolomite formation during early as well as late burial is given in chapter 4.

Geochemistry

Stable Isotopes

Stable isotope systematics provide important clues to the effects of different diagenetic environments. Stable isotopic composition of individual depositional and diagenetic components is controlled by temperature and isotopic composition of the fluid

(Urey et al., 1951). The stable isotope composition of all the different depositional and diagenetic phases (particularly those resulting from early diagenesis) are given in Figure 3.4 and the values are summarized in Table 3.1. It is clear from Figure 3.4 that the oxygen isotopic composition of all the phases are considerably depleted (by 2 to 5 ‰ PDB) relative to Cambrian marine carbonate composition ($\delta^{18}\text{O} = -5$ ‰, Lohmann and Walker, 1989). The $\delta^{18}\text{O}$ values of depositional components such as ooids, intraclasts and syndimentary fibrous cements typically cluster around -7.5 to -9 ‰. However, $\delta^{18}\text{O}$ values of blocky clear calcite spar, which commonly occurs in moldic pores and as final fillings in intergranular pores are considerably depleted (by at least 4-5 ‰ PDB).

Elemental Composition

Dissolution of metastable carbonates results in a transfer of cations from the carbonates to the fluid. Dissolution continues until fluid saturation is reached. Eventually when precipitation is initiated, elements are partitioned between the fluid and the precipitating solid (Lohmann, 1988). The partitioning of minor and trace elements is a function of distribution coefficient and redox conditions, particularly in the case of Fe and Mn (McIntire, 1963; Kinsman, 1969). Mg and Sr which have distribution coefficients of less than unity tend to be retained in the fluid. Fe and Mn which have distribution coefficients of greater than unity preferentially enter the diagenetic phase under reducing conditions (Veizer, 1983). Electron microprobe analyses were carried out on blocky, clear calcite spar from the Maryville Limestone. The elemental composition is summarized in Table 3.1. In general, blocky, clear calcite spar is low magnesian calcite. The MgCO_3 compositions (Fig. 3.5) range from 0.5 to 1.25 mol% (avg. 0.92 mol%). Thus, these diagenetic phases are uniformly low-magnesian calcite. However, Fe and Mn

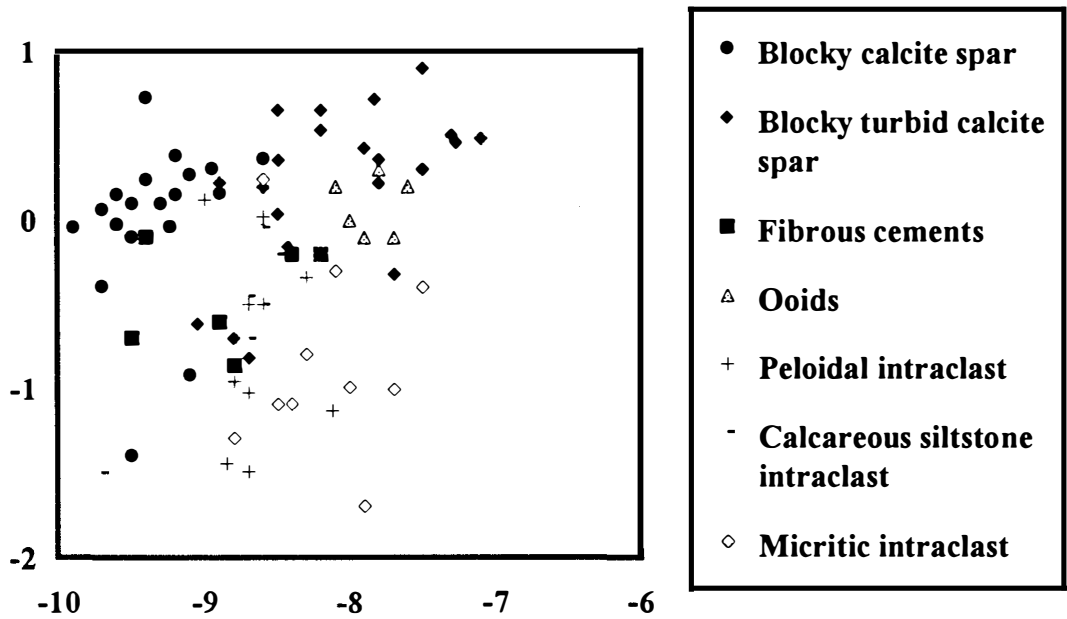


Figure 3.4. $\delta^{18}\text{O}$ versus $\delta^{13}\text{C}$ crossplot showing isotopic composition of depositional components and early diagenetic phases.

Table 3.1. Summary of all geochemical data. The number of samples (n) for $\delta^{13}\text{C}$ is the same as for $\delta^{18}\text{O}$. $^{87}\text{Sr}/^{86}\text{Sr}$ for Cambrian seawater has been estimated as 0.7094-0.7098. SD represents standard deviation for total carbonate concentrations. BD represents below detection limits.

COMPONENT	$\delta^{18}\text{O}$ ‰ PDB (n)	$\delta^{13}\text{C}$ ‰ PDB	MgCO_3 mol% (sd)	CaCO_3 mol% (sd)	Fe (ppm)	Mn (ppm)	$^{87}\text{Sr}/^{86}\text{Sr}$ (n)
Fibrous (marine) cements	-8.8 (10)	-0.4					
Ooids	-7.8 (6)	0.5					
Blocky turbid calcite spar	-8.2 (23)	0.2					0.7095 (2)
Blocky clear calcite spar (ferroan)	-9.2 (24)	0.01	0.92 (0.22)	98.74 (0.27)	1600	B.D.	0.7098 (1)
Type II dolomite					15,460	410	
Type III dolomite	-8.1 (6)	0.94	44.83 (1.8)	53.11 (1.52)	14,715	420	0.7133 (3)
Type IV dolomite	-7.2 (14)	1.16	43.02 (1.65)	53.49 (1.49)	27,427	1010	0.7124 (3)
Intraclasts	-7.8 (27)	-0.7					

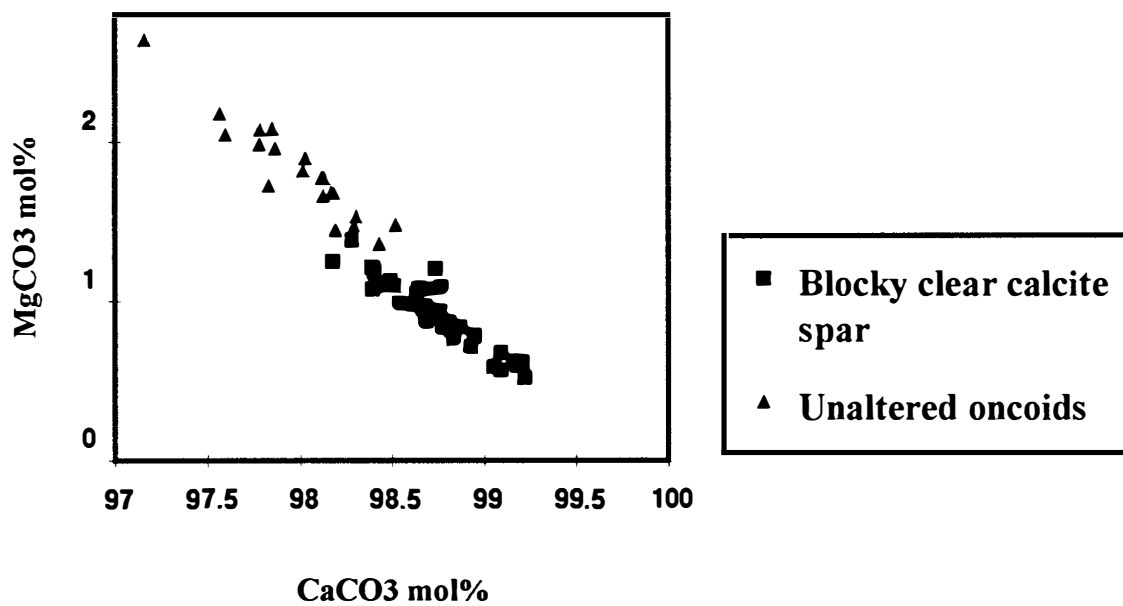


Figure 3.5. MgCO_3 and CaCO_3 content of blocky, clear calcite spar in moldic pores and unaltered oncoids.

distributions are variable. A cross plot of Fe vs Mg (Fig. 3.6) reveals that Fe values in the blocky, clear calcite spar range up to a maximum of 2,200 ppm (avg. 1,600 ppm).

However, Mn values are below the detection limit of 400 ppm. A similar range of Fe and Mn values were reported by Holail (1992) for Jurassic-Pleistocene meteoric cements from Egypt.

Sr Isotopes

The equilibrium Sr-isotopic compositions of marine carbonate and seawater of the same age should be equal (Faure, 1986). The Sr isotope ratios in seawater is derived from a mix of three different sources consisting of young volcanic rocks, sialic continental rocks, and Phanerozoic carbonate rocks (Faure, 1986). The Sr isotope ratio in seawater has fluctuated during the entire Phanerozoic. It is estimated to have been the highest for Cambrian and present day sea-water (Burke et al., 1982). According to Burke et al (1982) Cambrian values ranged from 0.7090 - 0.7095. Sr isotope ratios provide important constraints on the timing of cementation and fluid source (Banner et al., 1988; Vahrenkamp et al., 1991). Three Sr-isotope analyses were performed on the early diagenetic phases of the Maryville Limestone. The $^{87}\text{Sr}/^{86}\text{Sr}$ values for blocky turbid calcite spar range from 0.7096 to 0.7094 and 0.7096 - 0.7098 for blocky, clear calcite spar (Fig. 3.7). These values are within the range of values for Cambrian seawater

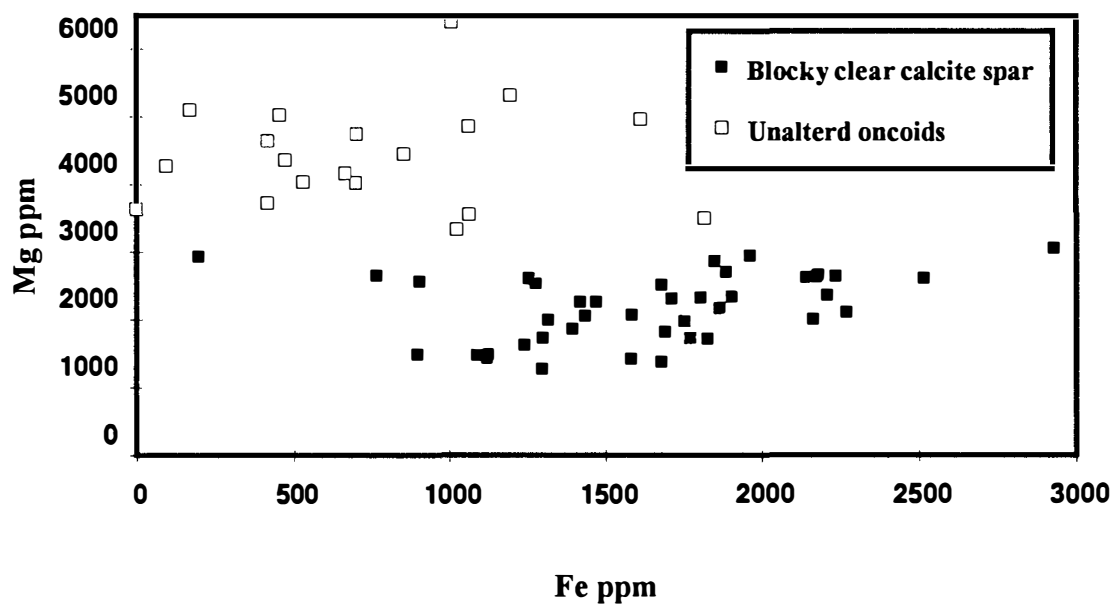


Figure 3.6. Fe and Mg content of blocky, clear calcite spar in moldic pores and unaltered oncoids.

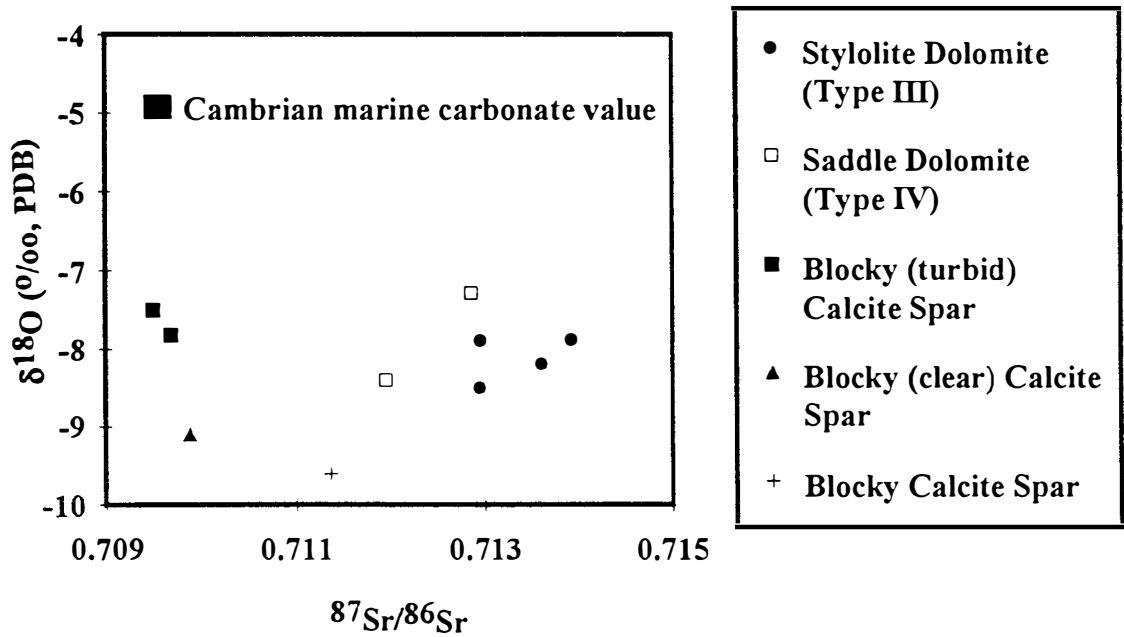


Figure 3.7. $\delta^{18}\text{O}$ versus $^{87}\text{Sr}/^{86}\text{Sr}$ crossplot of early and late burial diagenetic phases.

Discussion of Stabilization Processes

Shallow Burial (microscale dissolution and reprecipitation)

Stabilization of shallow water carbonate sediments can take place by wholesale dissolution and reprecipitation in response to the influx of undersaturated meteoric fluids or by microscale dissolution and reprecipitation during burial compaction. Given that seawater is saturated with respect to calcite and aragonite, very little dissolution is expected at the sediment-water interface. However, several reactions near the sediment-water interface occur that can contribute to undersaturation of pore waters with respect to carbonate (McKenzie and Morse, 1990). Undersaturation and dissolution takes place under both aerobic and anaerobic conditions. It is being increasingly recognized that dissolution occurs related to sulfate reduction in shallow marine environments. Sulfate reduction typically results in increased alkalinity which can cause carbonate precipitation (Bernier, 1971; Baker and Kastner, 1981; Compton, 1988; Slaughter and Hill, 1991). However, the concomitant decrease in pH, may cause carbonate dissolution (Morse et al, 1985; Walter and Burton, 1987; Stoessell, 1992; Morse et al., 1992). Depositional components (syndimentary fibrous and micritic cements) provide evidence for microscale dissolution and reprecipitation. Fibrous cements associated with Quaternary reefs are generally Mg-calcite in composition (Aissaoui, 1988 and references cited therein). Foreman et al (1989) hypothesized that shallow water ooids and fibrous cements from the upper Cambrian Nolichucky Shale were probably Mg-calcite in composition (Figs 3.5 and 3.6). In Maryville Limestone, preservation of the primary fabric of syndimentary fibrous (marine) cements and ooids suggests that wholesale dissolution did not take place. However, stable isotopic composition of fibrous cements provides constraints on diagenetic stabilization. $\delta^{18}\text{O}$ values of fibrous cements which

cluster around -8.0 ‰ PDB are considerably depleted when compared to Cambrian marine carbonate values (-5.0 ‰ PDB, Lohmann and Walker, 1989). It is well established that depletion in isotopic composition is generally caused by interaction with depleted meteoric fluids or an increase in temperature. Lack of evidence for wholesale dissolution and preservation of fibrous cement ultrastructure suggest that stabilization was largely microscale. The depleted oxygen isotopic composition is attributed to an increase in temperature of pore fluids during burial. There is considerable spread in the $\delta^{18}\text{O}$ values of fibrous cements indicating a variable degree of stabilization compared to other primary components such as ooids. Diagenetic stabilization probably took place in the presence of modified marine fluids. The non-ferroan nature and absence of CL zonation indicates that the pore fluids were probably oxidizing or alternatively that there was no supply of Fe for the pore fluids. Since all the marine phases and cements of shallow burial origin display a similar range of isotopic composition, stabilization of marine phases (ooids, fibrous cements, and intraclasts) and precipitation of shallow burial pore filling cements probably occurred in diagenetic fluids of similar composition. According to Land (1989) dissolution and reprecipitation, both wholesale and microscale, is neither a closed system nor a open system process and the degree of openness of the system is usually variable. The degree of openness of the system during early diagenesis of the Maryville Limestone is difficult to evaluate. Quantitative modeling can probably help resolve this question. However, quantitative modeling is still in its infancy and is beyond the scope of this project.

Subaerial Exposure & Meteoric Diagenesis (fabric selective dissolution and cementation)

Carbonate platform shelf-margin facies typically build up to sea-level. During sea-level lowstand the shelf-margin settings are the most common locales to be affected by

meteoric diagenesis. An array of diagenetic features are associated with subaerial exposure and meteoric diagenesis. In general, the different hydrologic regimes associated with meteoric diagenesis such as vadose and phreatic environments are commonly characterized by distinct cement morphologies (James and Choquette, 1984, Walker, 1989). While dissolution occurs in vadose environments, cementation is the dominant process in phreatic environments.

Sea-level fluctuations punctuated the development of the Maryville depositional sequence (Srinivasan and Walker, in press). In particular, outer platform facies of the Maryville depositional sequence appear to have been more affected by meteoric diagenesis. Several workers have suggested that HMC allochems can undergo fabric selective dissolution in both meteoric and deep burial diagenetic realms (Donath et al., 1980; Mazzullo, 1981; James and Klappa, 1983; Budd, 1992). Sandberg (1983) suggested that skeletal molds can form in both aragonitic and calcitic components. In the Maryville Limestone, moldic pores are widely developed in *Renalcis* which is generally believed to have been Mg calcite in original composition (Pratt, 1984) and less commonly in other constituents such as *Girvanella* and trilobite grains.

Although dissolution commonly occurs during subaerial exposure, cementation may not occur (Land, 1987). Cementation of pores is largely a function of supersaturation of pore fluids with LMC (Morse and Mackenzie, 1990). The presence of textural evidence in the form of fabric selective dissolution in the Maryville shelf margin facies supports emergence and meteoric diagenesis. Cementation occurred in both primary as well as in secondary pores. Precipitation of blocky, clear calcite spar in fabric selective dissolution voids probably occurred in downdip portions under reducing conditions of a regional ground water system. Reducing conditions for the pore fluids is reflected by enriched Fe concentrations in blocky, clear calcite spar. Depleted $\delta^{18}\text{O}$ composition of blocky, clear calcite spar with respect to Cambrian marine values ($\delta^{18}\text{O} = -5.0\text{‰}$)

PDB, Lohmann and Walker, 1989) is consistent with a meteoric interpretation. A depletion of 4 ± 2 in meteoric calcites compared to marine calcites is commonly seen in Holocene settings (Lohmann, 1988; Budd and Land, 1990). In general, depleted $\delta^{18}\text{O}$ values can result from depleted meteoric fluids or from an increase in temperature during precipitation (Wagner and Matthews, 1982).

Middle and Upper Paleozoic and younger carbonate rock sequences that have been subjected to subaerial exposure exhibit considerable depletion in carbon signatures. This depletion in carbon signatures is caused by input of soil-gas derived light carbon related to the respiration of land plants. However, it is not surprising that meteoric blocky, clear calcite spar from the Maryville Limestone shows little shift in its carbon isotopic composition, suggesting that lack of negative shift in carbon isotopic values is probably due to the absence of land plants developed on the surface during exposure. Sr isotopic composition of blocky clear calcite spar which are similar (0.7098) to the host carbonate composition (0.7095) also supports meteoric origin.

Given that it is difficult to demonstrate unequivocally subaerial exposure and meteoric diagenesis, we have applied field, textural, and geochemical criteria to support meteoric diagenesis in the Maryville Limestone. Such an integrated approach is clearly needed, particularly in the case of lower Paleozoic carbonate sequences.

Conclusions

- 1) An integrated approach consisting of field, petrography and geochemistry resulted in the recognition of microscale dissolution and reprecipitation and fabric selective dissolution and cementation during early diagenesis of the Maryville Limestone.

2) Preserved ultrastructures and depleted oxygen isotopic composition of depositional components such as ooids (mean $\delta^{18}\text{O} = -8.7$ ‰ PDB) and intraclasts (mean $\delta^{18}\text{O} = -8.2$ ‰ PDB) and synsedimentary fibrous cements (mean $\delta^{18}\text{O} = -8.4$ ‰ PDB) suggest stabilization by microscale dissolution and reprecipitation during shallow burial.

3) Fabric selective dissolution occurred in response to subaerial exposure and influx of meteoric fluids. Blocky clear calcite spar commonly occludes moldic pores. Depleted oxygen isotopic composition (mean $\delta^{18}\text{O} = -9.2$ ‰ PDB) values for blocky clear calcite spar are consistent with subaerial exposure and meteoric diagenesis. $^{87}\text{Sr}/^{86}\text{Sr}$ values which are similar to Cambrian seawater values lend support to this interpretation.

4) Finally, enriched Fe concentrations in blocky clear calcite spar suggests that some of the phreatic part of the meteoric system was relatively stagnant which promoted reducing conditions.

CHAPTER 4

PETROGRAPHIC AND GEOCHEMICAL CONSTRAINTS FOR FLUID SOURCE AND POSSIBLE PATHWAYS DURING BURIAL DIAGENESIS OF MARYVILLE LIMESTONE (MIDDLE CAMBRIAN) SOUTHERN APPALACHIANS

Introduction

Various mechanisms for formation of dolostone in platform carbonates have been summarized by Hardie (1987). Among these hypotheses, dolomitization related to hypersaline brines, mixed meteoric and sea-water, and deep basinal brines have found popular acceptance. Massive dolomitization of platform carbonates requires a large reservoir that can supply adequate quantities of Mg. In general, sea water is the biggest storehouse of Mg (Land, 1980; 1985; Morrow 1982 and others). The dolomitization in question in the present study is incomplete and non-evaporite related. This research is focused on burial dolomitization of subtidal limestone deposits. Burial dolomitization of subtidal carbonates typically occurs in the presence of modified marine and/or deep basinal brines derived from compaction of fine grained basinal sediments (Illing, 1959). Mass balance considerations require large volumes of compaction derived fluids to form regional bodies of dolomite (Morrow, 1982). The Maryville Limestone in our study area is only partially dolomitized, so large volumes of extraformational fluids were probably not involved.

This chapter has been submitted to *Sedimentology*.

Srinivasan, K., Walker, K. R., and Goldberg, S. A., 1993, Petrographic and geochemical constraints for fluid source and possible pathways during burial diagenesis of Maryville Limestone (Middle Cambrian) Southern Appalachians.

Four different generations of dolomite have been identified along a platform-to-basin depositional transect, using standard and cathodoluminescent microscopy. The different dolomite types display distinct trends in their distribution and chemistry, and formed during different stages of progressive burial diagenesis. In this study, petrographic and geochemical data are used to identify fluid source(s) during deep burial diagenesis of the Maryville Limestone. This study offers an important insight into hydrologic events, regional burial dolomitization and cementation history of the Maryville and, by implication of the entire Conasauga Group.

Geologic Setting

The Cambrian Conasauga Group in the southern Appalachians constitutes part of a thick, pericratonic, Cambro-Ordovician passive-margin sequence along the eastern North American continent. The Maryville Limestone (Middle Cambrian) of the Conasauga Group is entirely subtidal in the study area. It is well-exposed within the Copper Creek fault block in eastern Tennessee (Fig. 1.2). The detailed stratigraphy of the Maryville Limestone is shown in Figure 2.3. It represents deposition along a rimmed platform edge to basin transition (Srinivasan et al., 1991; Srinivasan and Walker, 1993 in press). The Maryville environmental array evolved over time, from a gentle basinward sloping ramp to a rimmed platform. Cyanobacterial buildups marked the platform margin environments (Srinivasan and Walker, in press). The transition from platform-margin to basin consisted of a slightly steeper slope environment. The development of the Maryville sequence was controlled by sea-level changes in part, and partly by progradation of the platform toward the craton. Deposition of the Maryville Limestone in the study area was terminated by sea-level fall and subaerial exposure. A subsequent rapid relative sea-level rise drowned the platform and during the lag time before carbonate deposition could be initiated the

platform was overlapped by basinal deposits of the Nolichucky Formation. The Maryville-Nolichucky contact has been identified as a sequence boundary (Srinivasan and Walker, in press), which may have also involved nonthermal tectonic subsidence (Rankey et al., submitted).

Methods

Detailed petrographic analyses were carried out on 120 thin sections from 5 localities, chosen from a total of 400 samples examined. Selected thin sections from each locality were stained with alizarin red S and a mixed stain of alizarin red S and potassium ferricyanide according to the procedure outlined by Dickson (1965) to differentiate calcite and dolomite and to identify ferroan phases. Selected polished thin sections were analyzed for cathodoluminescence using a nuclide ELM-2AVG luminoscope (operating conditions 12-14 keV and 45 - 60 μ amp). Various phases in twelve carbon-coated thin sections from critical samples were analyzed for Ca, Mg, Fe, Mn, and Sr using a Cameca SX50 electron microprobe. Operating conditions were 20 nA beam current, 5 - 10 μ m beam spot, count time of 40 sec for Fe, 50 sec for Mn, 20 sec for Mg, and 10 sec for Ca, and the accelerating voltage was 15 keV. Detection limits in ppm for these conditions at 99% confidence are Fe (450 ppm) and Mn (410 ppm). Totals greater than 102 % and less than 98% are not reported. Samples for stable isotope analyses were drilled from polished slabs using a microscope mounted microdrill assembly. A total of twenty samples were analyzed for carbon and oxygen isotopes at the University of Tennessee stable isotope laboratory. Saddle dolomite (14 samples) was analyzed using a timed extraction procedure outlined by Al-Aasm et al. (1990) for mixed calcite-dolomite samples. The samples were reacted in 100% phosphoric acid at 55^o C for 16-18 hrs. However, stylolite-associated dolomite was reacted with 100% phosphoric acid at 25^o C for 48

hours. In-house dolomite standards were run as unknowns with Maryville samples. The precision is better than 0.2 ‰ PDB for both carbon and oxygen. Sr-isotope analyses were performed by Dr. Steven Goldberg at the University of North Carolina, Chapel Hill. Isotopic data were collected on a VG sector 54 in a quintuple-collector dynamic mode which yielded a value of 0.710250 ± 0.000016 for the SRM 987 Sr carbonate standard.

Burial Diagenesis and Dolomitization

Petrographic and Cathodoluminescence Characteristics

Petrographic analyses reveal that dolomite is the principal burial diagenetic phase in the Maryville Limestone samples examined. The paragenetic sequence that was established with the help of detailed standard and cathodoluminescence microscopy is given in Figure 4.1. Based on petrographic characteristics, geochemical considerations, and cross cutting relationships we have identified four different generations of dolomite. The crystal shape classification in our petrographic work is based on Sibley & Gregg (1987).

Type I Dolomite

This type occurs as anhedral and rarely as subhedral crystals (Fig. 4.2A). The size of individual crystals is variable, ranging from 2 to a few tens of μm . Type I dolomite preferentially replaced micrite and is abundant in wackestone lithologies. The replacement of micrite is typically partial to complete. Under cathodoluminescence, these dolomite crystals appear uniformly dull orange. In rare cases, the crystals coalesce to form a mosaic

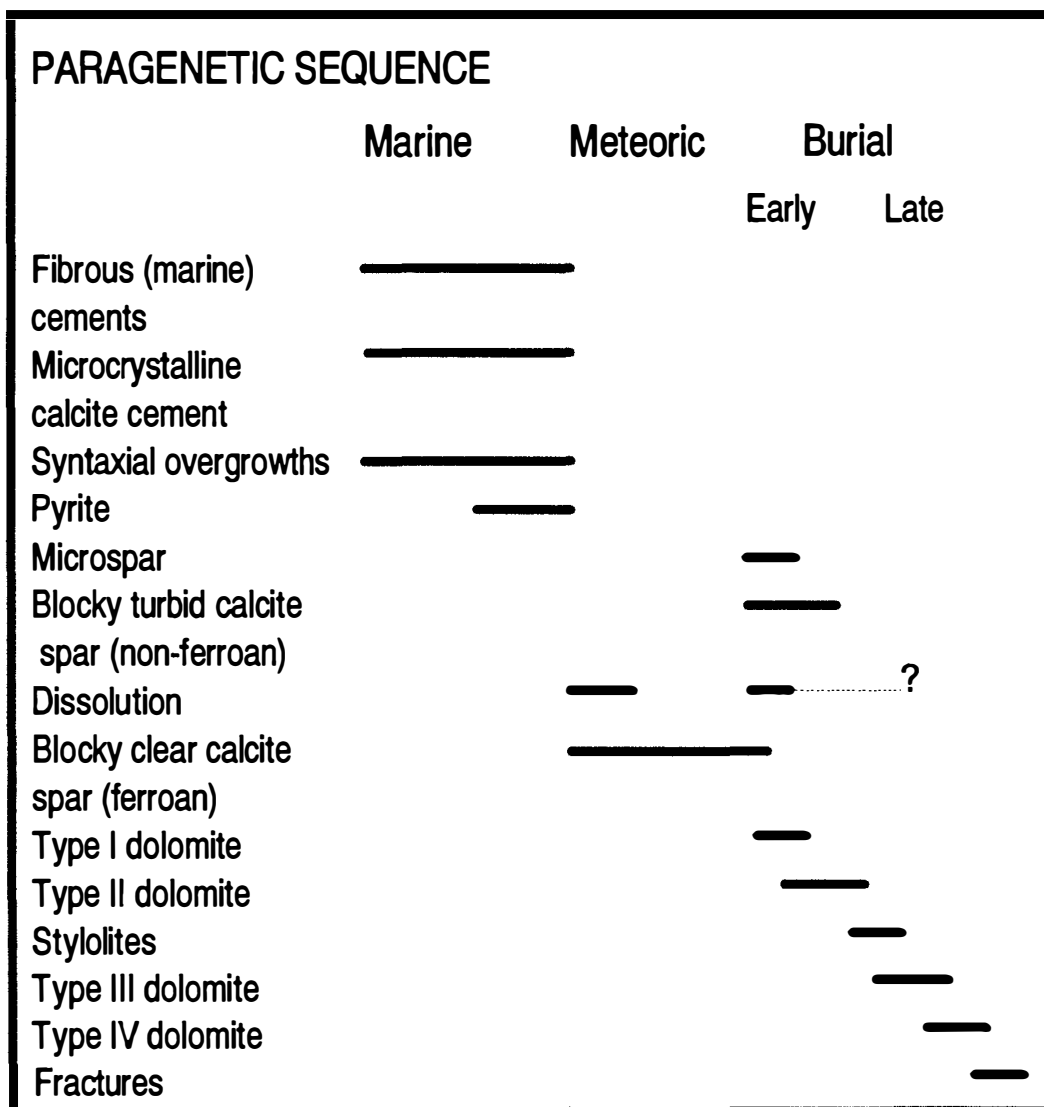
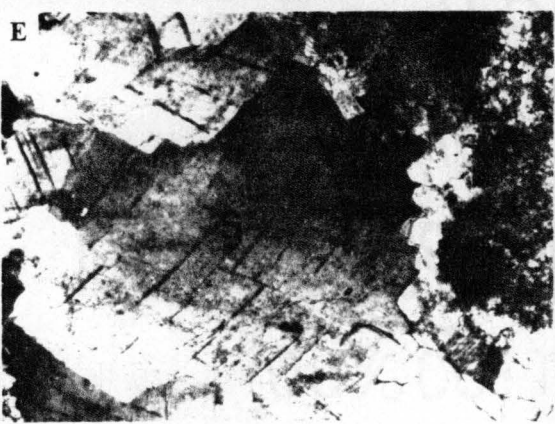
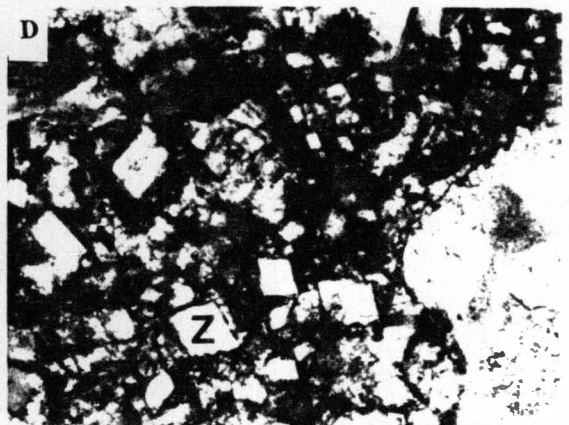
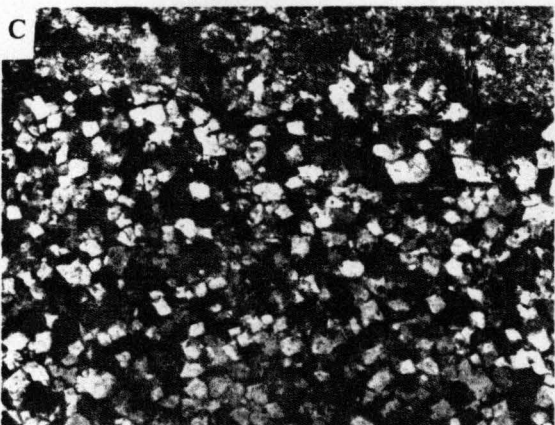
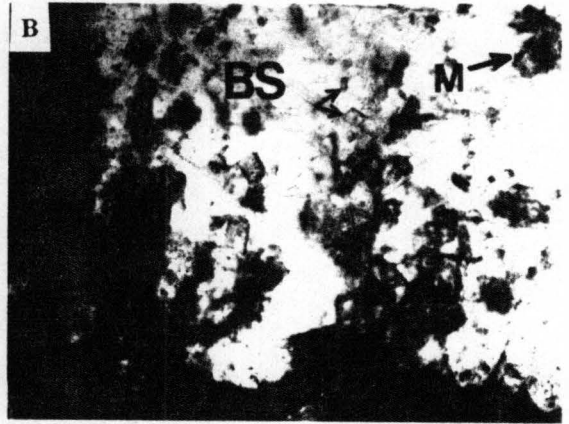
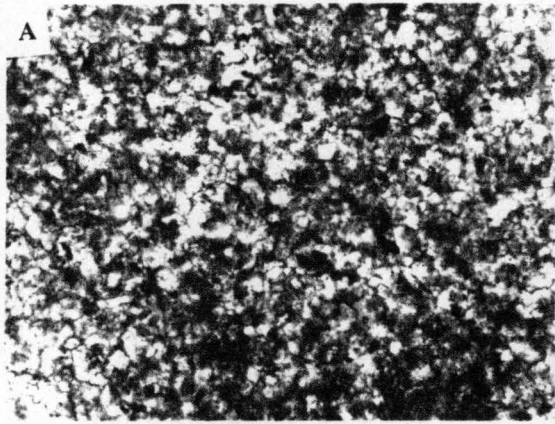


Figure 4.1. Paragenetic sequence of the Maryville Limestone. The bars indicate relative timing of the different phases.

Figure 4.2. Photomicrographs of different dolomite types of Maryville Limestone in the study area. A) Example of irregular dolomite disseminations (indicated by arrow) in micrite also note abundant rhombs. Plane light, field width = 0.7mm. B) Inclusions (at arrows) of planar dolomite rhombs (Type II) in blocky clear calcite spar. Occasionally rhombs form a mosaic (M). Cross-polarized light, field width = 1.5mm. C) Example of dolomite type associated with stylolites (arrow). Cross-polarized light, field width = 1.5mm. D) Zoned dolomite associated with stylolites under cathodoluminescence. Note the rims appear bright. field width = 1mm. E) Saddle dolomite (S); note the coarse crystal size and curved crystal boundaries. Under cross-polarized light, field width = 1.5mm. F) Void-filling saddle dolomite (S), cross-cut by fracture (indicated by arrow). Under cross polarized light, field width = 6.5mm.



of anhedral crystals. Staining reveals that Type I dolomite is generally only weakly ferroan, but larger mosaics of anhedral crystals appear to be slightly more ferroan.

Type II Dolomite

Type II dolomite is commonly a replacement phase and occurs as planar euhedral rhombs (Fig. 4.2B). The grain size is variable, ranging from 5 to 300 μm . This planar-e dolomite commonly occurs as inclusions in blocky, and clear (ferroan) calcite spar, which is interpreted as meteoric in origin on the basis of crystal fabric, and stable isotope and trace element compositions. Typically Type II dolomite is concentrated along intercrystalline boundaries between blocky, clear calcite spar grains, but in rare instances the rhombs transect grain boundaries. The crystals also occur along cleavage planes in blocky calcite spar. The degree of dolomite replacement typically decreases away from pore walls and toward pore centers. Under cathodoluminescence, Type II dolomite appears as non-luminescent rhombs. The crystals may coalesce to form dense mosaics of planar crystals. The formation of this dolomite type was controlled by intercrystalline porosity, as evidenced by the concentration of rhombs along grain boundaries.

Type III Dolomite

Type III Dolomite consists of euhedral to subhedral and occasionally anhedral crystals, ranging from approximately 10 to 150 μm in size. Type III dolomite occurs in grainstone, packstone, wackestone and mudstone, but is more common in mudstone and wackestone. Type III dolomite occurs as thin seams along stylolites and as thick bands measuring a few mm commonly bounded by stylolites (Fig. 4.2C). The individual crystals typically appear as planar rhombs with a turbid core and less commonly as zoned crystals

(Fig. 4.2D). Intercrystalline boundaries are marked by iron oxide staining. Under cathodoluminescence, Type III dolomite is non-luminescent, or consists of zoned rhombs with a dark core and bright rim, or orange luminescent rhombs. Zoned dolomite crystals and crystals with orange luminescence are restricted to shelf-margin lithofacies. The individual rhombs usually crosscut by stylolites, but very rarely crosscut stylolites.

Type IV Dolomite

Type IV dolomite is the saddle or baroque dolomite of Radke and Mathis (1980). Type IV dolomite typically occurs as void fillings (Fig. 4.2E) and rarely in the matrix. In general, saddle dolomite is abundant in grainstone and packstones. The subhedral to anhedral crystals are variable in size from 100 μm to 1500 μm . Saddle dolomite is ferroan and displays undulose extinction. Under cathodoluminescence the crystals are typically non-luminescent. Saddle dolomite crystals commonly are crosscut by post cementation fractures (Fig. 4.2F).

Saddle dolomite displays regional and local variations in its distribution. It increases in abundance basinward from the shelf margin. However, at the shelf margin, this dolomite type is restricted to the lower part of the reefal complex of the upper Maryville.

Stratigraphic Distribution

Dolomitization of the Maryville Limestone is incomplete with the degree of dolomitization greatest in muddy facies. In contrast, in grainstone and packstone facies, dolomite occurrence is restricted to intragranular pores. There are local as well as regional variations in the occurrence of the individual varieties of dolomite. Type II

dolomite, which occurs as inclusions in clear blocky spar, is typically restricted to the shallow-platform lithofacies. Type III zoned crystals and crystals with orange luminescence are restricted to the shelf-margin strata. Volumetrically, Type III dolomite is more abundant. Coarse baroque dolomite is abundant in shelf-margin and slope/basin lithofacies and is less abundant in the shallow platform rock types.

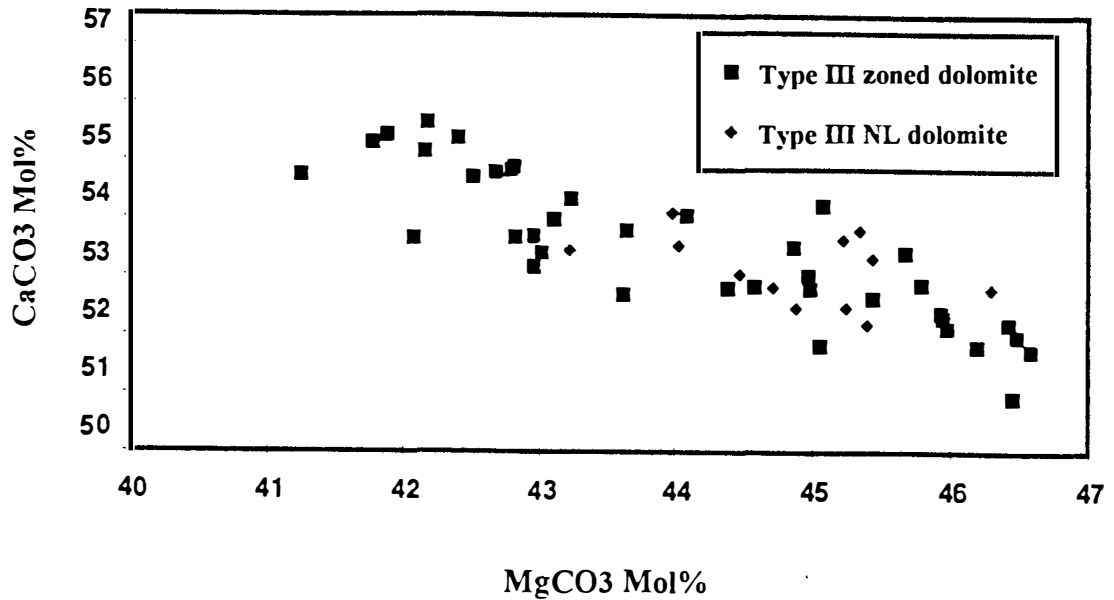
Geochemistry

Major Element Geochemistry

Ideal dolomite is stoichiometric and well ordered (Graf and Goldsmith, 1956; Goldsmith and Graf, 1958; Lumsden and Chimahusky, 1980). Numerous workers have noted that dolomites associated with Holocene carbonates is typically nonstoichiometric (McKenzie, 1981; Carballo et al., 1987, and many others). Stoichiometry of recent dolomite increases with age (Gregg et al., 1992). However, ancient dolomite generally tends to show a higher degree of stoichiometry. This increase in stoichiometry is attributable to neomorphic alteration (Mazzullo, 1992).

In the Maryville Limestone, major element chemistry of the different dolomite types has been determined from electron probe analyses of individual crystals. Microprobe analyses were largely done on Type III and Type IV dolomite. However, a limited number of analyses were carried out on Type II dolomite. Because of the limitation imposed by the crystal size, no microprobe analysis was carried out on Type I dolomite.

Stylolite bounded dolomite (Type III) shows both stoichiometric and non-stoichiometric compositions (Fig. 4.3A). XRD patterns of a limited number of samples indicate that the dolomite is well ordered. The MgCO_3 molar compositions of Type III



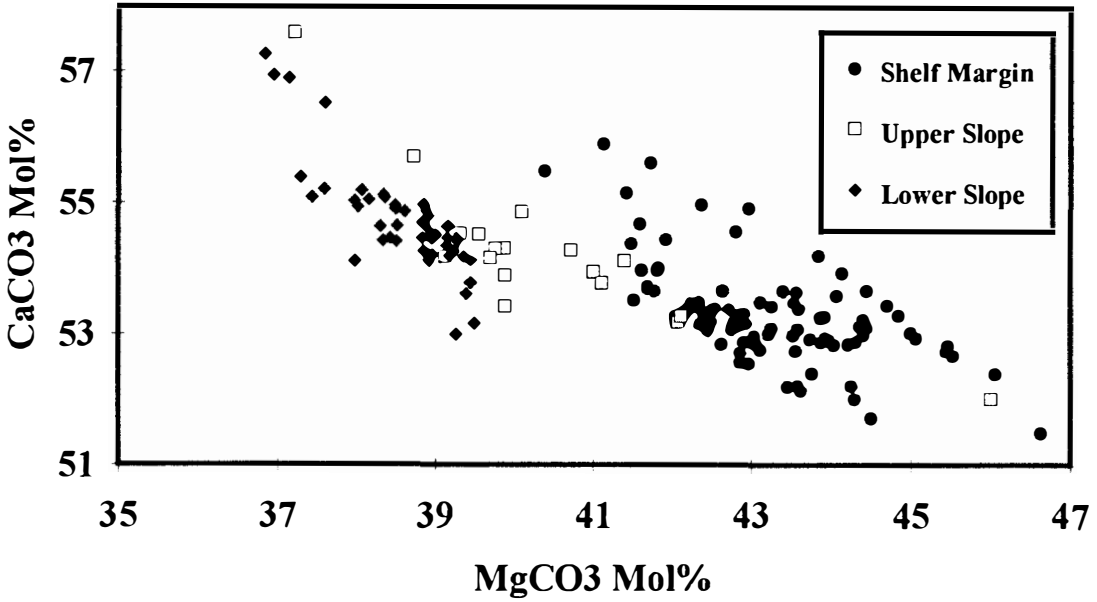
A

Figure. 4.3. Electron microprobe data of Maryville dolomite types. (A) MgCO₃ and CaCO₃ content of dolomite associated with stylolites (Type III); (B) MgCO₃ and CaCO₃ content of saddle dolomite; (C) Fe and Mn content of stylolite dolomite (zoned and non-luminescent, Type III) and dolomite inclusions (Type II) in blocky, clear calcite spar. Most Type II dolomite have Mn values below detection limits, unlike most Type III dolomite. (D) Fe and Mn content of saddle dolomite (Type IV). Note that saddle dolomite displays chemical trends from slope/basin (southwest) to shelf margin (northeast). Note that Mn compositions of those samples with Mn less than about 450 ppm may have any value between 0 ppm and 449 ppm.

zoned dolomite are variable from core to rim of individual crystals. In general, the cores are more stoichiometric and analyses close to the rim are calcian. However, the rims could not be analyzed because the width of the rim is smaller than the beam diameter. Type III dolomite does not display spatial lateral trends in its geochemistry. In contrast, Type IV late-stage, void-filling baroque dolomite displays distinct spatial lateral trends (Fig. 4.3B). This phase shows both calcian and near stoichiometric compositions varying from nonstoichiometric composition in downslope facies to near stoichiometric compositions (Fig. 4.3B) in platform edge facies.

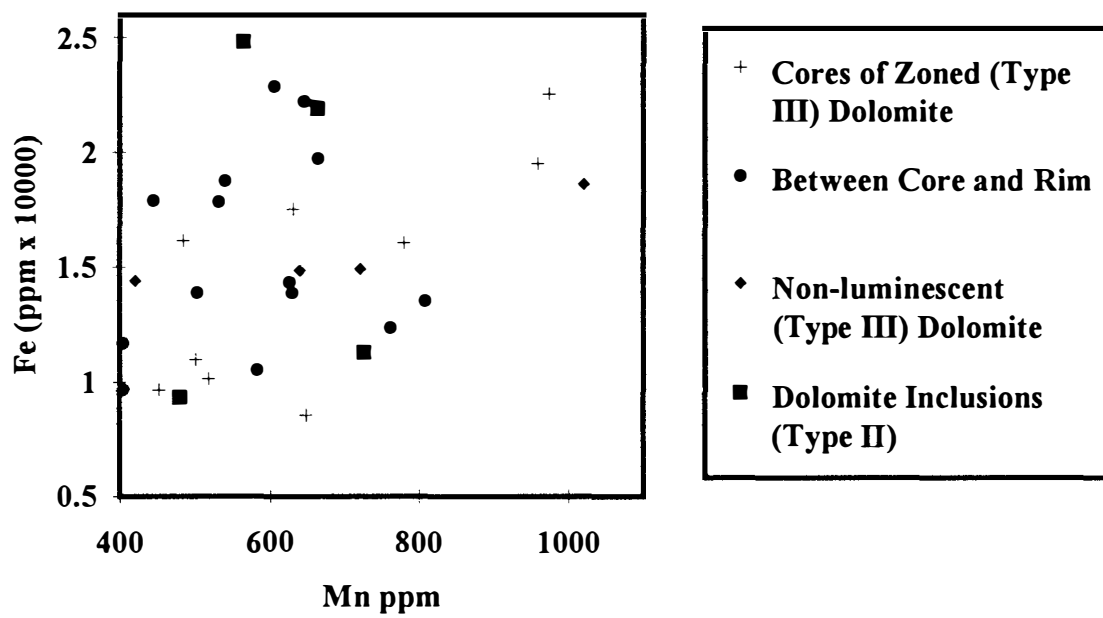
Minor and Trace Elements

A limited number of electron microprobe analyses were performed on Type II and Type III dolomites. However, a large number of analyses were carried out on Type IV or saddle dolomite. The heterogeneous Distribution Law predicts that trace elements with distribution coefficients greater than 1 tend to become depleted in the precipitating solid in the direction of flow (Machel, 1988). Machel (1988) suggested that trends in the distribution of trace elements can be used to determine the direction of fluid flow. Gregg & Shelton (1989) employed similar lateral trends in the distributions of Fe, Mn, and Sr in the Bonneterre Dolomite (Cambrian) to interpret fluid flow direction. In the Maryville Limestone, Fe and Mn contents show a general enrichment from Type II to Type IV dolomite. Fe and Mn concentrations in Type II dolomite are 0.93-2.5 wt % Fe and a maximum of 700 ppm Mn (4.3C). Type III dolomite is commonly more enriched in Fe and Mn when compared to Type II dolomite with values ranging from 1.2-2.6 wt% Fe and a maximum of 1000 ppm Mn (Fig. 4.3C). Although Fe and Mn contents of Type III dolomite are variable, there are no distinct vertical or lateral spatial trends. However, zoned crystals of Type III dolomite display chemical zonation, with cores enriched in Fe



B

Figure 4.3 (continued)



C

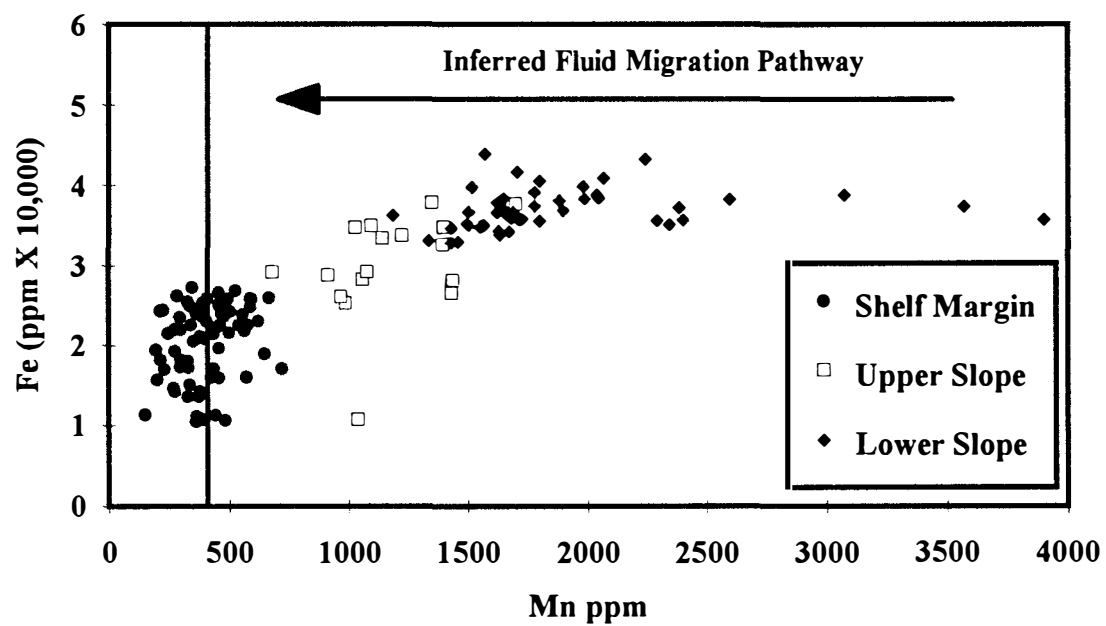
4.3 (continued)

and decreasing Fe from core to rim. The bright luminescent rims represent an increased incorporation of Mn. These differences in chemistry are also reflected in the luminescence characteristics of Type III dolomite as described earlier.

Type IV or saddle dolomite displays distinct lateral spatial trends in the distribution of Fe and Mn (Fig. 4.3D). Values decrease from 3.5-4.5 wt % Fe and 0.1-0.3 wt% Mn in the west (slope/basin) to 1.5-2.5 wt % Fe and less than 600 ppm Mn in the east (platform-margin).

Stable Isotopes

Stable oxygen and carbon isotope composition of a precipitating phase is a function of temperature, fluid composition, and the isotopic composition of the ambient rock (Banner et al., 1988). The stable isotope compositions of Type III and Type IV dolomite are given in Figure 4.4. Note that in Figure 4.4, the stylolite-related dolomite (Type III) and saddle dolomite (Type IV) show a similar variation. The $\delta^{18}\text{O}$ values for stylolite-bounded dolomite range from -7.5‰ to -8.5‰ PDB and that of saddle dolomite from -6.75‰ to -8.75‰ PDB. $\delta^{13}\text{C}$ values for both the dolomite types range from 0.3‰ to 1.7‰ PDB. The isotopic compositions of other associated phases are as follows: fibrous (marine) cements, $\delta^{18}\text{O} = -6.5\text{‰}$ to 8.0‰ and $\delta^{13}\text{C} = -0.5$ to $+0.5\text{‰}$ PDB; blocky, clear calcite spar, $\delta^{18}\text{O} = -9.0\text{‰}$ to -10‰ PDB and $\delta^{13}\text{C} = -0.5\text{‰}$ to $+0.5\text{‰}$ PDB. In general, oxygen isotope compositions of Type III and Type IV dolomite are significantly depleted when compared to the estimated original Cambrian marine carbonate value ($\delta^{18}\text{O} = -5.5\text{‰}$ PDB, Lohmann & Walker, 1989). The depleted oxygen isotopic compositions of Type III and Type IV dolomites suggest that the fluids were not in isotopic equilibrium with the host rock. It is reasonable



D

Figure 4.3 (continued)

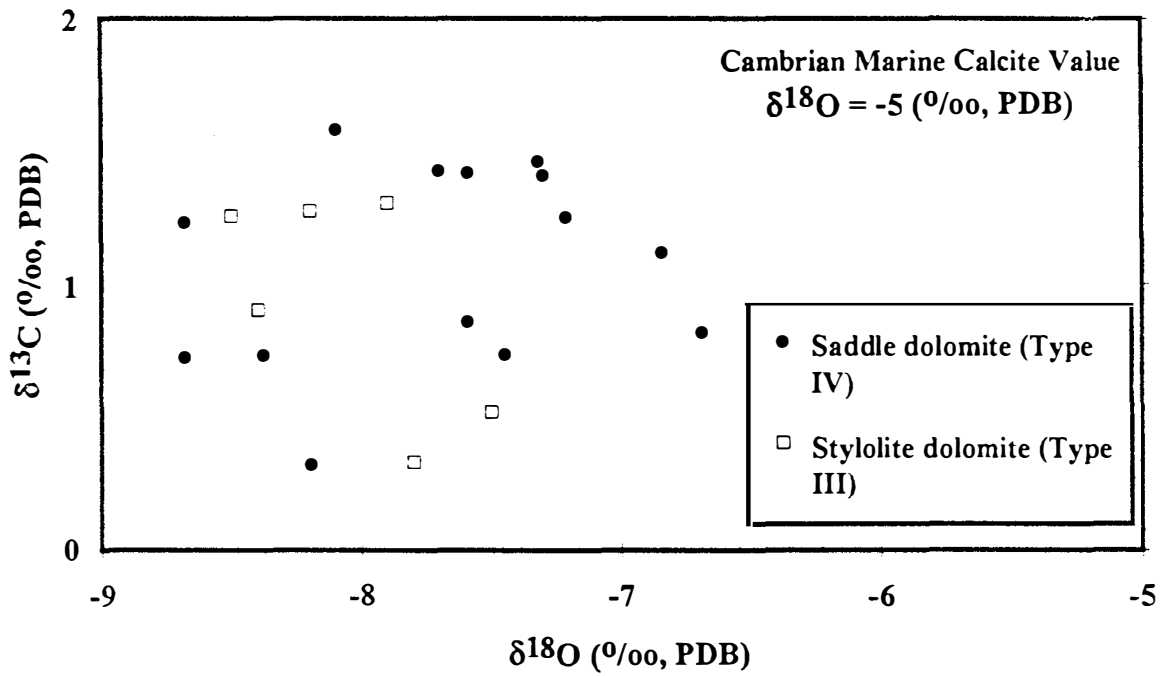


Figure 4.4. $\delta^{18}\text{O}$ versus $\delta^{13}\text{C}$ crossplot of replacement stylolite dolomite (Type III) and void filling saddle dolomite (Type IV).

to suggest that temperature calculations based on oxygen isotope compositions of saddle dolomite will reflect the minimum temperature of precipitation. Such a calculation yields a temperature of about 85° to 105° C for the precipitation of Type IV dolomite.

Strontium Isotopes

The timing of dolomitization and fluid source can be constrained by using Sr-isotope ratios (Scholle & Halley, 1985; Banner et al., 1988; Vahrenkamp et al., 1991). Seawater Sr-isotope ratio was constant for any particular time period, but has varied through time during the Phanerozoic. Secular variation of Sr-isotope ratios of sea-water for the entire Phanerozoic has been summarized by several workers (e.g., Burke et al., 1982). The Sr-isotope ratios of seawater for the Phanerozoic is estimated to be the highest for Cambrian and present-day seawater (.70907; Burke et al., 1982).

Burial phases with radiogenic Sr-isotope ratios higher than coeval seawater have been attributed to basinal brines (Moore, 1985; Scholle and Halley, 1985). Several studies have reported Sr-isotope ratios for dolomite cementation and dolomitization associated with burial diagenesis (e.g., Kaufmann et al., 1990; Kupecz and Land, 1991; Banner et al., 1988). In the Maryville Limestone, Sr-isotope ratios determined for Type III and Type IV dolomite range from 0.7104-0.7139 (Fig. 4.5). The Sr-isotope ratios of Type III dolomite appear to be slightly more enriched (0.71336) than Type IV dolomite (0.71195). These values are considerably higher than Cambrian marine values (Burke et al., 1982).

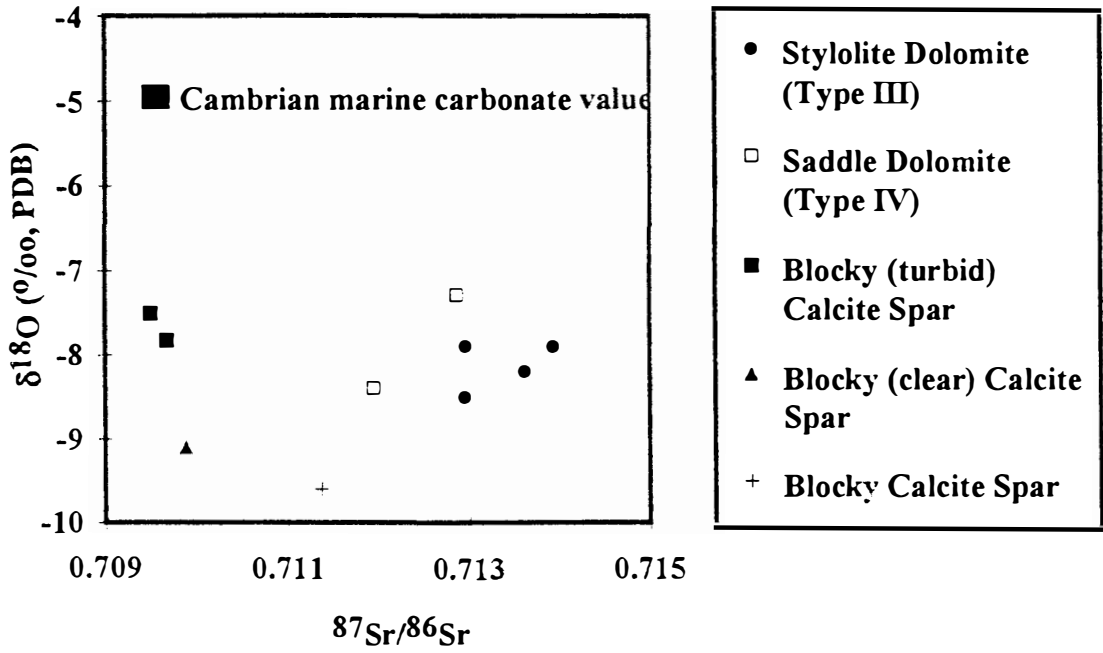


Figure 4.5. $\delta^{18}\text{O}$ versus $^{87}\text{Sr}/^{86}\text{Sr}$ crossplot of saddle dolomite (Type IV), stylolite dolomite (Type III) and other associated cement phases.

Burial History

Maximum burial temperatures can be approximated from burial history curves. The maximum burial of the Maryville Limestone is estimated from the thickness of overburden units, which range in age from Late Cambrian to Middle Pennsylvanian. Overburden thickness and biostratigraphic age data to construct the burial curves were extracted from Cattermole (1966), Milici et al. (1979), Breland (1980), Borowski (1982), Walker (1985), Englund et al. (1985), and Hatcher (1989).

The estimated maximum burial depth of the Maryville Limestone in the study area was approximately 4-4.5 kms (Fig. 4.6). Taking an average geothermal gradient of 30^o C and a surface temperature of 20^o C, estimated maximum burial temperatures were approximately 140^o-150^o C. Calculated temperatures from stable oxygen isotope compositions of Type III and Type IV dolomite range from 85^o-105^o C. The temperature calculations are based on Land's (1985) equation, $10^3 \ln \alpha_{\text{dolomite-fluid}} = 2.78 * 10^6 T^{-2} (K) + 0.91$. From a comparison of the probable temperature of formation of burial dolomite with the maximum burial temperatures, it is evident that the dolomite formed prior to maximum burial. These rocks probably reached the dolomite formation temperature in the middle Paleozoic. A consideration of a regional set of burial curves (Walker et al., 1992) suggests that the shale sections of the basin coeval with the Maryville were buried slightly more rapidly than the Maryville and that these shale deposits reached temperatures of about 100^o C during the Middle to Late Ordovician.

Discussion of Fluid Source and Diagenetic Pathways

Textural and chemical variations of the Maryville dolomite types as described above suggest that they represent different episodes of diagenesis. Although the major

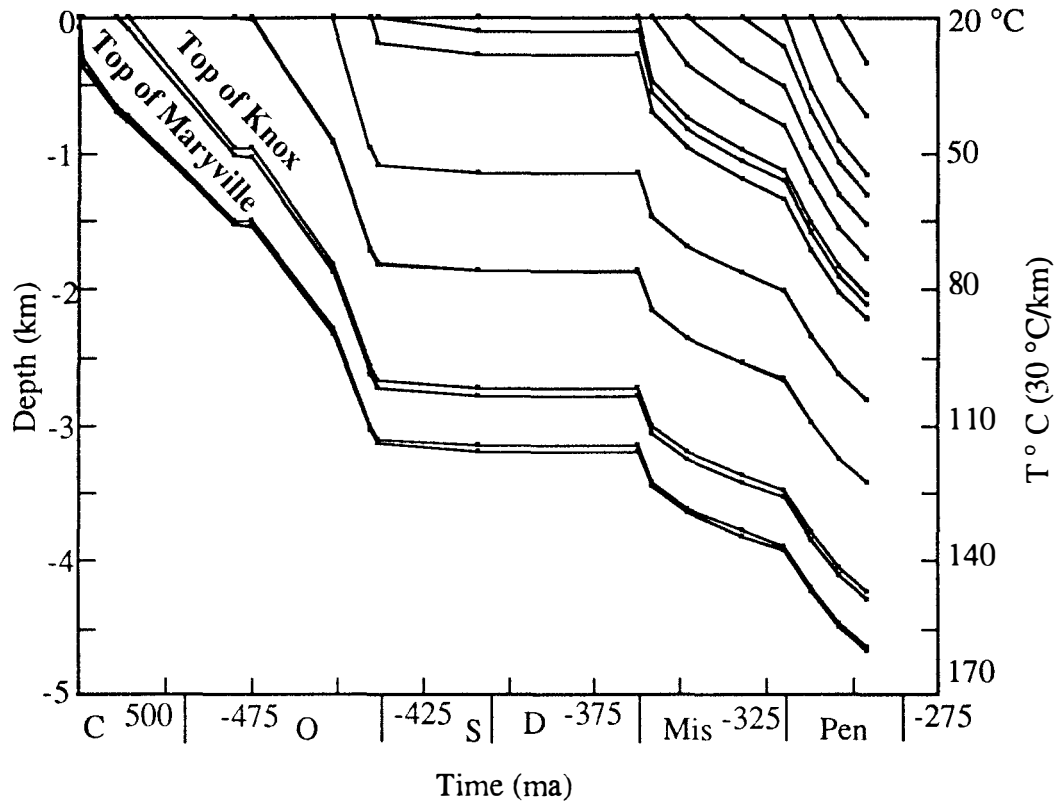


Figure 4.6. Burial history plot for Maryville Limestone. The burial history plot is based on overburden thickness. Note that surface temperature is assumed to be 20°C and geothermal gradient is assumed to be 30°C per km.

emphasis of this research is on the fluid source and pathways during late stage burial diagenesis, we discuss here the origin of all the dolomite types in order to provide a complete burial diagenetic history of the Maryville Limestone. The different dolomite types formed during progressive burial, based on their petrographic characteristics and differences in chemistry described in the section above.

Early Dolomitization

Type I and Type II dolomite likely formed during shallow and intermediate burial diagenesis. A shallow subsurface origin for Type I dolomite is interpreted based on crystal size and low iron content as revealed by staining. Type II dolomite, which occurs as inclusions of planar dolomite rhombs in blocky, clear (meteoric) calcite spar, is interpreted as having formed during shallow to intermediate burial. Gregg & Sibley (1984) and Gregg & Shelton (1990) proposed that planar crystal boundaries are indicative of early diagenesis and nonplanar boundaries of deep burial diagenesis. A shallow to intermediate burial origin for this dolomite type is proposed based on the following petrographic and chemical relationships: (a) planar crystal boundaries, (b) association with shallow platform lithologies, (c) position in the overall paragenetic sequence revealed by petrography, and (d) enriched in Fe (1-2.4 wt%) and Mn (up to a maximum of 700ppm) concentrations (Fig. 4.3C).

Since Type I dolomite is commonly associated with subtidal fine grained lithofacies, the fluids involved in the formation of this dolomite type were non-evaporite related. Mg liberated from stabilization of Mg-calcites probably served as a local source of Mg^{+2} for dolomite formation. The occurrence of microspar (see Figure 4.1, paragenetic sequence) in fine grained lithofacies provides evidence for neomorphic alteration of micrite. Numerous workers have proposed that dolomite formation is

promoted during early diagenesis by bacterial reduction of sulfate, which results in increased alkalinity and dolomite supersaturation (Baker & Kastner, 1981; Compton, 1988; Slaughter & Hill, 1991). In the Maryville Limestone, evidence for sulfate reduction during early diagenesis is provided by the occurrence of pyrite. Although we do not have any control to estimate the depth of dolomite formation, it is conceivable that Type I dolomite formation occurred in the first few meters of burial because sulfate reduction occurs fairly early. We propose that Mg^{+2} and Ca^{+2} were probably derived from the dissolution of precursor carbonates and by diffusion from overlying seawater. Diffusion of Mg from the overlying sea water is facilitated by the high degree of porosity and permeability in sediments during early diagenesis.

In the case of Type II dolomite, it is difficult to evaluate whether Mg, Fe and Mn were supplied by the precursor carbonate. This dolomite type is enriched in Fe (unlike marine and other early diagenetic phases) which could be the result of initial formation from Fe rich fluids. It is conceivable that iron oxide coatings formed during subaerial exposure (see Srinivasan & Walker, in press) on detrital grains may have served as a local source of Fe under later reducing conditions of diagenesis. Alternatively, neomorphic alteration (Mazzullo, 1992) of early fine-grained dolomite (poorly ordered and less stoichiometric) during burial in the presence of compaction derived basinal fluids may have contributed to elevated Fe^{+2} concentrations. Sibley and Gregg (1987) suggested that planar crystal boundaries can be retained during neomorphism at higher temperatures. In general, Holocene dolomites are fine crystalline ($< 10\mu m$), low in Fe and non stoichiometric (Land, 1985; Hardie, 1987; Sibley, 1990; Mazzullo, 1992). However, the coarse planar textures and the higher stoichiometry observed in the case of Maryville Type II dolomite suggest that it has undergone neomorphic alteration.

Late Burial Dolomitization

Type III dolomite (stylolite associated) and Type IV dolomite (saddle/baroque dolomite) are recognized as products of intermediate and deep burial diagenesis. Because Type III dolomite is associated with stylolites and increases in abundance towards stylolites, the formation of this dolomite type probably was associated with the process of stylolitization. An intermediate to deep burial origin for Type III dolomite is consistent with the following petrographic and chemical relationships: (a) association with stylolites, (b) elevated Fe (1.2 - 2.6 wt%) and Mn (maximum of 1000 ppm) concentrations when compared to Type II dolomite (c) depleted $\delta^{18}\text{O}$ compositions with respect to Cambrian seawater composition, and (d) enriched Sr-isotope ratios.

Void filling saddle or baroque dolomite (Type IV) formed during late burial diagenesis. This is the latest phase in the paragenetic sequence prior to the formation of fractures. A late burial diagenetic origin for saddle dolomite is consistent with the following petrographic and geochemical relationships: (a) occurrence as void fillings, (b) elevated Fe and Mn concentrations compared to other dolomite types of burial origin, (c) depleted $\delta^{18}\text{O}$ compositions compared to Cambrian sea water composition, (d) enriched Sr-isotope ratios compared to Cambrian marine values, and (e) the inferred elevated temperature of formation of this phase.

Compositional zoning in Type III zoned dolomite can be explained by fluctuations in pore-water chemistry such as decrease in the supply of Fe and a relative increase in Mn concentrations in the fluid. Increased incorporation of Mn, which serves as luminescence activator (Machel, 1985) towards the rims of zoned dolomite crystals, resulted in bright luminescent rims. Given that zoned dolomite crystals have a limited stratigraphic distribution, it is conceivable that fluctuations in pore water chemistry were local.

Constraints on Fluid Source from Carbon, Oxygen, and Sr-isotope ratios

In trying to evaluate fluid source, it is imperative that fluid sources such as seawater, meteoric and deep basinal brines be considered. In general, fluids derived from the zone of sulfate reduction tend to be characterized by isotopically light carbon values (Burns et al., 1988). Isotopically heavy carbon values of Type III and Type IV dolomite of Maryville Limestone suggest fluid derivation far removed from the zone of sulfate reduction.

Oxygen and Sr-isotope ratios of Type III and Type IV dolomite provide constraints on the fluid source, composition and possible pathways. In general, the $\delta^{18}\text{O}$ values of Type III and Type IV dolomite are depleted relative to the Cambrian marine value. Depleted $\delta^{18}\text{O}$ values can result from depleted meteoric fluids or elevated temperatures. However, a meteoric origin is not consistent with the relatively high radiogenic Sr-isotope ratios of Type III and Type IV dolomite of the Maryville Limestone. The range in $\delta^{18}\text{O}$ values of void filling baroque dolomite suggests that precipitation occurred over a range of temperatures. Alternatively, heavier values can be attributed to isotopically heavy basinal fluids. The calculated temperatures, which are based on Land's (1985) equation, range from 85° C to 105° C. In our temperature calculations, we assumed a $\delta^{18}\text{O}$ of 5 ‰ SMOW for the burial fluids. This assumption is based on SMOW values of modern subsurface brines. Our burial history curve (Fig. 8) indicates that the estimated temperatures are consistent with the overall burial history of the Maryville Limestone and that elevated temperatures can be accounted for by burial alone (over 4 km of burial).

A siliciclastic source for the burial fluids is proposed on the basis of elevated Sr-isotope ratios of Type III and Type IV dolomite. Radiogenic Sr-isotope ratios reflect sources external to the Maryville Limestone. Regional stratigraphic relationships suggest

that the Cambrian intrashelf basin that flanked the western margin of the carbonate platform may have served as a potential fluid source during burial. During progressive burial silicate reactions serve as a potential source of radiogenic strontium to basinal fluids (Steuber et al., 1984). Numerous workers proposed that burial diagenetic transformation of smectite to illite is accompanied by the release of metal ions to the pore fluid. The potential of basinal shale to serve as a source of Ca, Fe, Mg, Na and Si during deep burial diagenesis is well documented in the literature (Dunoyer de Segonzac, 1970; Boles and Franks, 1979; McHargue and Price, 1982; Lee and Friedman, 1987; Gregg, 1988; Kaufmann et al., 1990). Fe and Mg in the smectite layers typically tend to get released at higher temperatures of transformation (Boles and Frank, 1979) and the smectite-to-illite conversion takes place over a temperature range of 50 to 125 ° C (burial depths of 2 to 4 km with normal geothermal gradients). Freed and Peacor (1992) documented a sudden increase in the proportion of illite relative to smectite in Gulf Coast shale over a depth range of 2-2¹/₂ kms. Similarly, basinal shale may have supplied the necessary metal ions for dolomitization of the Maryville Limestone. Because we interpret Type II and Type III dolomite as neomorphic products of early formed dolomite, it is not difficult to account for a source of magnesium. However, in the case of void-filling saddle dolomite, Mg for dolomite formation was supplied by basinal fluids. Also, this phase is volumetrically less abundant. Hence it is not difficult to envision basinal shale as the main source of Mg for Type IV dolomite formation.

Given that the geochemical attributes of Type III and Type IV dolomite of the Maryville Limestone support a siliciclastic source, fluid migration pathways can be inferred from spatial lateral trends in the distribution of Fe and Mn in saddle dolomite. Spatial lateral trends, consisting of a decrease in Fe and Mn values from slope/basin to the shelf-margin, suggest a fluid source to the west and/or southwest of the platform. Warm

basinal fluids derived from the Cambrian intrashelf basin migrated updip into the adjacent carbonate platform (see Fig. 2.8).

The geochemistry of late burial dolomite types clearly indicates that an active hydrologic system was operative during burial of the Maryville Limestone. Several mechanisms have been proposed for regional subsurface fluid flow, and these include gravity-driven fluid flow (Garven and Freeze, 1984), compaction driven fluid flow (Noble, 1963; Bethke, 1985), and episodic dewatering of basinal sediments (Cathles and Smith, 1983). Qing and Mountjoy (1992) postulated tectonism and sedimentary loading to explain regional fluid migration in western Canada sedimentary basin. A similar scenario can be envisioned for deep basinal fluid migration in the southern Appalachians. Tectonic compression in the southern Appalachians related to arc collision was initiated during the early part of the Middle Ordovician (Quinlan and Beaumont, 1984; Hatcher, 1987). Burial history curves suggest that by the end of Middle Ordovician time, the Maryville Limestone was buried to depths of approximately 3 to 3 1/2 kms. Thus fluid migration responsible for dolomite recrystallization and dolomite cementation in the Maryville Limestone may have occurred in response to tectonic compression and sediment loading. By the end of the Middle Ordovician time, two potential basinal fluid sources existed, the Cambrian intrashelf basin that flanked the western margin of the carbonate platform and the Middle Ordovician Sevier Basin that developed in response to thrust and sediment loading (Shanmugam and Lash, 1982, Quinlan and Beaumont, 1984). However, probable pressure gradients (Walker et al., 1992) from the Sevier Basin do not correlate with the inferred fluid migration pathways involved in burial diagenesis of Cambrian rocks, which are based on minor and trace element compositions of late-stage saddle dolomite. Therefore, deep basinal fluids originated in the Cambrian shale basin juxtaposed against the carbonate platform and migrated from west to east into the adjacent platform carbonates. Given that void-filling saddle dolomite is abundant in grainstone and

packstone lithologies, it is conceivable that warm fluids migrated through these relatively more porous and permeable units that served as conduits for focused fluid flow.

Fluid-rock ratios, variations in $\delta^{18}\text{O}$, $^{87}\text{Sr}/^{86}\text{Sr}$ isotope compositions

Basinal fluids evolve progressively along the migration path as a result of water-rock interaction. Progressive water-rock interactions will be reflected in the O and Sr isotope ratios, which generally shift toward host-carbonate values depending on the extent of water-rock reactions. Banner et al. (1988) explained the observed variations in C, O and Sr ratios of Burlington dolomite by changes in fluid-rock ratios.

We propose an evolutionary pathway involving water-rock interaction to explain the depleted $\delta^{18}\text{O}$ and enriched radiogenic Sr-isotope ratios of Type III dolomite. Water-rock interaction at low water-rock ratios will shift the isotopic composition toward the host carbonate composition. In contrast, continued water-rock interaction at high water-rock ratios will result in isotopically light $\delta^{18}\text{O}$ values relative to the host carbonate composition. Depleted but nonetheless uniform oxygen isotopic values of Type III dolomite are suggestive of high water-rock ratios involved in the recrystallization of Type III dolomite. Fluid-rock interaction at low water-rock ratios would have shifted the Sr-isotopic composition toward Cambrian carbonate values. However radiogenic Sr-isotope ratios of Type III dolomite support recrystallization at high water-rock ratios. Alternatively, the isotopic compositions may reflect little interaction with the host rock.

In the case of Type IV, or saddle dolomite the observed scatter in $\delta^{18}\text{O}$ values could have been caused by any one or a combination of the following: (a) variation in water-rock ratios, (b) changes in temperature, and (c) changes in $\delta^{18}\text{O}$ composition of the fluid. As in Type III dolomite, depleted oxygen and enriched Sr-isotopic ratios reflect

fluid rock interaction at high water-rock ratios. The observed range of $\delta^{18}\text{O}$ values may simply reflect changes in temperature, or alternatively, changes in water composition.

Conclusions

(1) Petrographic and geochemical studies reveal that several stages of dolomitization occurred during progressive burial.

(2) Early burial dolomitization involved normal marine fluids. Mg was derived from overlying seawater and stabilization of Mg calcite phases.

(3) Late burial dolomitization and dolomite cementation involved deep basinal brines.

(4) Depleted $\delta^{18}\text{O}$ and enriched $^{87}\text{Sr}/^{86}\text{Sr}$ values compared to Cambrian seawater values suggest that fluids were warm and radiogenic. Temperatures ranged from 85° to 105° C. This is consistent with burial history.

(5) Fe and Mn values in saddle dolomite decrease from 3.5 -4.5 wt% Fe, and 0.1-0.3 wt% Mn in the west (slope/basin) to 1.5-2.5 wt% Fe, and less than 600 ppm Mn in the east (shelf-margin) indicating fluid migration from west to east. Fluids responsible for late dolomitization were derived from the Cambrian intrashelf basin.

CHAPTER 5

CONCLUSIONS

1. Carbonate depositional systems are fundamentally different from siliciclastic systems. Their differences must be taken into consideration when translating sequence stratigraphic concepts developed for siliciclastic systems to carbonate successions. In view of the fundamental differences, a process-oriented approach is applied to define the sequences, sequence boundaries, and the stacking pattern of the Maryville Limestone.

2. The Maryville Limestone, which is a third-order sequence, consists of two subsequences. The subsequences are characterized by a combination of aggradational, retrogradational, and progradational units as a consequence of variations in sedimentation rate, subsidence, and absolute sea-level change.

3. The transition between the Maryville Limestone and the overlying Nolichucky Shale is interpreted to be a sequence boundary. This transition is a drowning unconformity. The drowning event was preceded by subaerial exposure of the outer platform. A rapid relative sea-level rise drowned the platform and siliciclastics derived from the northwest were deposited on top of the shallow water carbonates. This drowning, coupled with carbonate lag-time on the old platform, continued subsidence, and retrogradation onto the platform of siliciclastic basinal facies converted the flat-topped platform into a ramp-like profile. The subsequent ramp deposition is represented by the lower part of the overlying Nolichucky Shale.

4. The Maryville Limestone was subjected to a complex diagenetic history. An integrated approach consisting of field, petrography and geochemistry resulted in the recognition of microscale dissolution and reprecipitation and fabric selective dissolution and cementation during early diagenesis of the Maryville Limestone.

5. Preserved primary fabrics and depleted oxygen isotopic composition of depositional components such as ooids (mean $\delta^{18}\text{O} = -8.7\text{‰}$ PDB) and intraclasts

(mean $\delta^{18}\text{O} = -8.2$ ‰ PDB) and synsedimentary fibrous cements (mean $\delta^{18}\text{O} = -8.4$ ‰) suggest stabilization by microscale dissolution and reprecipitation occurred during shallow burial.

6. Fabric selective dissolution occurred in response to subaerial exposure and influx of meteoric fluids. Blocky clear calcite spar commonly occlude moldic pores. Depleted oxygen isotopic composition (mean $\delta^{18}\text{O} = -9.2$ ‰ PDB) values for blocky clear calcite spar relative to Cambrian marine calcite values (-5 ‰ PDB) are consistent with subaerial exposure and meteoric diagenesis. $^{87}\text{Sr}/^{86}\text{Sr}$ values which are similar to Cambrian seawater values lend support to this interpretation.

7. Finally, enriched Fe concentrations in blocky clear calcite spar suggests that some of the phreatic part of the meteoric system was relatively stagnant which promoted reducing conditions.

8. Petrographic and geochemical studies reveal that several stages of dolomitization occurred during progressive burial.

9. Dolomitization of the Maryville Limestone during early burial involved normal marine fluids. Mg was derived from overlying seawater and stabilization of Mg calcite phases.

10. Late burial dolomitization and dolomite cementation involved deep basinal brines.

11. Depleted $\delta^{18}\text{O}$ and enriched $^{87}\text{Sr}/^{86}\text{Sr}$ values of late burial dolomite phases relative to Cambrian marine calcite values and dolomite precipitated in equilibrium with seawater suggest that fluids were warm and radiogenic. Temperatures ranged from 85° to 105° C. This is consistent with burial history.

12. Fe and Mn values in saddle dolomite decrease from 3.5 -4.5 wt% Fe, and 0.1-0.3 wt% Mn in the west (slope/basin) to 1.5-2.5 wt% Fe, and less than 600 ppm Mn in the east (shelf-margin) indicating fluid migration from west to east. Fluids responsible for late

dolomitization were derived from the adjacent intrashelf basin. Late burial fluid movement was related to shale diagenesis.

LIST OF REFERENCES

LIST OF REFERENCES

- Aissaoui, D.M., 1988, Magnesian calcite cements and their diagenesis: dissolution and dolomitization, Mururoa Atoll: *Sedimentology*, v. 35, p. 821-841.
- Aitken, J.D., 1966, Middle Cambrian to Middle Ordovician cyclic sedimentation, southern Rocky Mountains of Alberta: *Bulletin of Canadian Petroleum Geology*, v. 14, p. 405-441.
- Al-Aasm, I.S., Taylor, B.E., and South B., 1990, Stable isotope analysis of multiple carbonate samples using selective acid extraction: *Chemical Geology*, v. 80, 119-125.
- Allan, J.R., and Matthews, R.K., 1982, Isotope signatures associated with early meteoric diagenesis: *Sedimentology*, v. 29, p. 797-817.
- Baker, P.A., and Kastner, M., 1981, Constraints on the formation of sedimentary dolomite: *Science*, v. 213, p. 214-216.
- Ball, M.M., 1967, Carbonate sand bodies of Florida and the Bahamas: *Journal of Sedimentary Petrology*, v. 37, p. 556-591.
- Banner, J.L., Hanson, G.N., and Meyers, W.J., 1988, water-rock interaction history of regionally extensive dolomites of the Burlington-Keokuk Formation (Mississippian): Isotopic evidence. *in* Shukla, V., and Baker, P.A., eds., *Sedimentology and Geochemistry of Dolostones*: Society of Economic Paleontologists and Mineralogists Special Publication 43, p. 97-114.
- Barnaby, J.R., and Read, J.F., 1990, Carbonate ramp to rimmed shelf evolution: Lower to Middle Cambrian continental margin, Virginia Appalachians: *Geological Society of America Bulletin*, v. 102, p. 391-404.
- Berner, R.A., 1971, *Principles of Chemical Sedimentology*: McGraw-Hill, New York, 240p.

- Bethke, C.M., 1985, A numerical model of compaction driven ground-water flow and heat transfer, and its application to the paleohydrology of intracratonic sedimentary basins: *Journal Geophysical Research*, v. 90, p. 6817-6828.
- Bird, J.M., and Dewey, J.F., 1970, Lithosphere plate continental margin tectonics and the evolution of the the Appalachian orogen: *Geological Society of America Bulletin*, v. 81, p. 1031-1060.
- Boles, J.R. & Franks, S.G., 1979, Clay diagenesis in Wilcox sandstones of southwest Texas: Implications of smectite diagenesis on sandstone cementation. *Journal of Sedimentary Petrology*, v. 49, p. 55-70.
- Borowski, W.S., 1982, Petrology, depositional environments, and stratigraphic analysis of a part of the Middle Ordovician Chickamauga Group Limestones near Clinton, Tennessee: Unpublished Ph.D. dissertation, University of Tennessee Knoxville, 239 pp.
- Breland, F.C. Jr., 1980, Stratigraphic, paleoenvironmental, and echinoderm distributional patterns in an unfaulted Middle Ordovician (Chickamauga Group) shelf-edge to on-shelf transect in east Tennessee: Unpublished Ph.D. dissertation, University of Tennessee Knoxville, 217 pp.
- Buchbinder, L.G., and Friedman, G.M., 1980, Vadose, phreatic and marine diagenesis of Pleistocene-Holocene carbonates in a borehole-Mediterranean coast of Isreal: *Journal of Sedimentary Petrology*, v. 50, p. 395-409.
- Budd, D.A., and Land, L.S., 1990, Geochemical imprint of meteoric diagenesis in Holocene ooid sands; Schooner Cays, Bahamas: correlation of calcite cement geochemistry with extant groundwaters: *Journal of Sedimentary Petrology*, v. 60, p. 361-378.
- Budd, D.A., 1992, Dissolution of high- Mg calcite fossils and the formation of biomolds during mineralogical stabilization: *Carbonates and Evaporites*, v. 7, p. 74-81.

- Burke, W.H., Denison, R.E., Hetherington, E.A., Koepnick, R.B., Nelson, H.F., and Otto, J.B., 1982, Variation of seawater $^{87}\text{Sr}/^{86}\text{Sr}$ throughout Phanerozoic time: *Geology*, v. 10, p. 516-519.
- Burns, S.J., Baker, P.A., and Showers, W.J., 1988, The factors controlling the formation and chemistry of dolomite in the organic-rich sediments: Miocene Drakes Bay Formation, California, *in* Shukla, V., and Baker, P.A., eds., *Sedimentology and Geochemistry of Dolostones: Society of Economic Paleontologists and Mineralogists Special Publication 43*, p. 41-52.
- Carballo, J.D., Land, L.S., and Miser, D.E., 1987, Holocene dolomitization of supratidal sediments by active tidal pumping, Sugarloaf Key, Florida: *Journal of Sedimentary Petrology*, v. 57, p. 153-165.
- Cathles, L.M., and Smith, A.T., 1983, Thermal constraints on the formation of Mississippi valley-type lead-zinc deposits and their applications for episodic basin dewatering and deposit genesis: *Economic Geology*, v. 78, p. 983-1002.
- Cattermole, J.M., 1966, Geologic map of the Fountain City Quadrangle, Knox county, Tennessee. United States Geological Survey.
- Chafetz, H.S., McIntosh, A.G., and Rush, P.F., 1988, Freshwater phreatic diagenesis in the marine realm of recent Arabian Gulf carbonates: *Journal of Sedimentary Petrology*, v. 58, p. 433-440.
- Compton, J.S., 1988, Sediment composition and precipitation of dolomite and pyrite in the Neogene Monterey and Sisquoc Formations, Santa Maria Basin Area, California, *in* Shukla, V., and Baker, P.A., eds, *Sedimentology and Geochemistry of Dolostones: Society of Economic Paleontologists and Mineralogists*, v. 43, p. 53-65.
- Demico, R.V., 1985, Platform and off-platform carbonates of the Upper Cambrian of western Maryland, U.S.A.: *Sedimentology*, v. 32, p. 1-22.

- Derby, J.R., 1965, Paleontology and stratigraphy of Nolichucky Formation in southwest Virginia and northeast Tennessee: Unpublished Ph.D. dissertation, Virginia Polytechnic Institute and State University, Blacksburg, 468 p.
- Dickson, J.A.D., 1965, Modified staining technique for carbonates in thin section: *Nature*, v. 205, p. 587.
- Donath, F.A., Carozzi, A.V., Fruth, L.S., Jr., and Rich, D.W., 1980, Oomoldic porosity experimentally developed in Mississippian oolitic limestone: *Journal of Sedimentary Petrology*, v. 50, p. 1249-1260.
- Dunoyer De Segonsac, G., 1970, The transformation of clay minerals during diagenesis and low-grade metamorphism: a review: *Sedimentology*, v. 15, p. 281-345.
- Eberli, G., and Ginsburg, R.N., 1989, Cenozoic progradation of northwestern Great Bahama Bank, a record of lateral platform growth and sea-level fluctuations, in Crevello, P.D., Wilson, J.L., Sarg, J.F., and Read, J.F., eds., *Controls on Carbonate Platform and Basin Development: Society of Economic Paleontologists and Mineralogists Special Publication 44*, p. 339-352.
- Englund, K.J., Gillespie, W.H., Cecil, B.C., Windolph, J.F., Jr., and Crawford, T.J., 1985, Characteristics of the Mississippian-Pennsylvanian boundary and associated coal-bearing rocks in the southern Appalachians: Open file report United States Geological Survey, 85-577.
- Erwin, P.N., 1981, Stratigraphy, depositional environments, and dolomitization of the Maryville and the Upper Honaker formations (Cambrian), Tennessee and Virginia: Unpublished M.S. thesis, Duke University, Durham, 232 p.
- Faure, G., 1986, *Principles of Isotope Geology*, John Wiley and Sons, 589 p.
- Flügel, E., 1982, *Microfacies analysis of limestone*: Springer-Verlag, New York, 633 p.

- Foreman, J.L., 1991, Petrologic and geochemical evidence for water-rock interaction in the mixed carbonate-siliciclastic Nolichucky Shale (Upper Cambrian) in east Tennessee: unpublished Ph.D. dissertation, University of Tennessee, Knoxville, 228 p.
- Foreman, J.L., Walker, K.R., Weber, L.J., Driese, S.G., and Dreier, R.B., 1991, Slope and basinal carbonate deposition in the Nolichucky Shale (Upper Cambrian), East Tennessee: effect of carbonate suppression by siliciclastic deposition on basin-margin morphology, *in* Lomando, A.J., and Harris, P.M., eds., Mixed carbonate-siliciclastic sequences: Society of Economic Paleontologists and Mineralogists core workshop 15, p. 511-540.
- Freed, R.L., and Peacor, D.R., 1992, Diagenesis and the formation of authigenic illite-rich I/S crystals in Gulf Coast Shales: TEM study of clay separates: *Journal of Sedimentary Petrology*, v. 62, p. 220-234.
- Garven, G. and Freeze, R.A., 1984, Theoretical analysis of the role of groundwater flow in the genesis of stratabound ore deposits: 2 quantitative results: *American Journal of Science*, v. 284, p. 1125-1174.
- Gebelein, C.D., 1976, Open marine subtidal and intertidal stromatolites (Florida, The Bahamas and Bermuda), *in* Walter, M.R., ed., *Stromatolites*: Elsevier, New York, p. 381-388.
- Ghibaudo, G., 1992, Subaqueous sediment gravity flow deposits: practical criteria for their description and classification: *Sedimentology*, v. 39, p. 423-454.
- Ginsburg, R.N., 1960, Ancient analogs of Recent stromatolites: 21st International Geological Congress Report, Part 22, p. 26-35.
- Goldsmith, J.R., and Graf, D.L., 1958, Relations between lattice constants and composition of the Ca-Mg carbonates: *American Mineralogist*, 43, 84-101.
- Graf, D.L., and Goldsmith, J.R., 1956, Some hydrothermal syntheses of dolomite and protodolomite: *Journal of Geology*, v. 64, p.173-186.

- Gregg, J.M., and Sibley, D.F., 1984, Epigenetic dolomitization and the origin of xenotopic dolomite texture: *Journal of Sedimentary Petrology*, v. 54, p. 908-931.
- Gregg, J.M., 1988, Origins of dolomite in the offshore facies of the Bonneterre Formation (Cambrian), southeast Missouri, *in* Shukla, V., and Baker, P.A., eds, *Sedimentology and Geochemistry of Dolostones: Society of Economic Paleontologists and Mineralogists Special Publication 43*, p. 67-84.
- Gregg, J.M., and Shelton, K.L., 1989, Minor- and trace-element distributions in the Bonneterre dolomite (Cambrian), Southeast Missouri: evidence for possible multiple-basin fluid sources and pathways during lead-zinc mineralization: *Bulletin of Geological Society of America*, v. 101, p. 221-230.
- Gregg, J.M., and Shelton, K.L., 1990, Dolomitization and dolomite neomorphism in the back reef facies of the Bonneterre and Davies formations (Cambrian), southeastern Missouri: *Journal Sedimentary Petrology*, v. 60, p. 549-562.
- Gregg, J.M., Howard, S.A., and Mazzullo, S.J., 1992, Early diagenetic recrystallization of Holocene (< 3000 years old) peritidal dolomites, Ambergris Cay, Belize: *Sedimentology*, v. 39, p. 143-160.
- Halley, R.B., and Harris, P.M., 1979, Fresh-water cementation of a 1000-year-old oolite: *Journal of Sedimentary Petrology*, v. 49, p. 969-988.
- Hardie, L.A., 1987, Dolomitization: a critical view of some current views: *Journal of Sedimentary Petrology*, v. 57, p. 166-183.
- Harris, L.D., 1964, Facies relations of exposed Rome Formation and Conasauga Group of northeastern Tennessee with equivalent rocks in the subsurface of Kentucky and Virginia: *United States Geological Survey Professional Paper 501-B*, p. B25-B29.
- Harris, P.M., 1979, Facies anatomy of a Bahamian ooid shoal: *sedimenta VII*, The Comparative Sedimentology Laboratory, The university of Miami, 163 p.

- Harris, P.M., 1984, Carbonate sands-a core workshop: Society of Economic Paleontologists and Mineralogists, a core workshop 5, 464 p.
- Harris, P.M., Moore, C.H., and Wilson, J.L., 1986, Carbonate depositional environments, modern and ancient, part 2, carbonate platforms: Colorado School of Mines Quaterly, v. 80, 60 p.
- Hasson, K.O., and Haase, C.S., 1988, Lithofacies and paleogeography of the Conasauga Group (Middle and Late Cambrian) in the Valley and Ridge Province of east Tennessee: Geological Society of America Bulletin, v. 100, p. 234-246.
- Hatcher, R.D. Jr., 1987, Tectonics of the southern and central Appalachian internides: Annual Reviews of Earth and Planetary Science, v. 15, p. 337-362.
- Hatcher, R.D. Jr., 1989, Tectonic synthesis of the U.S. Appalachians, in Hatcher, R.D. Jr., Thomas, W.A., Viele, G.W., eds., The Appalachian-Ouachita in the United States: Geological Society of America, The Geology of North America, F-2, p. 511-535.
- Holail, H., 1992, Coordinated petrography-isotopic-chemical investigation of meteoric calcite cement (Jurassic-Pleistocene), Egypt: Carbonates and Evaporites, v. 7, p. 48-55.
- Illing, L.V., Wells, A.J., and Taylor, J.C.M., 1965, Penecontemporaneous dolomite in the Persian Gulf, in Pray, L.C., and Murray, R.C., eds., Dolomitization and Limestone Diagenesis: a Symposium Society of Economic Paleontologists and Mineralogists 13, p. 88-111.
- James, N. P., 1981, Megablocks of calcified algae in the Cow Head Breccia, western Newfoundland; vestiges of a lower Paleozoic continental margin: Geological Society of America Bulletin, v. 92, p. 799-811.
- James, N.P., and Stevens, R.K., 1986, Stratigraphy and correlation of the Cambro-Ordovician Cow Head Group, western Newfoundland: Geological Society of Canada Bulletin, v. 366, 143 p.

- James, N.P., and Gravestock, D.I., 1990, Lower Cambrian shelf and shelf margin buildups, Flinders Ranges, South Australia: *Sedimentology*, v. 37, p. 455-480.
- James, N.P., and Choquette, P.E., 1984, Diagenesis 9 - Limestones - The meteoric diagenetic environment: *Geoscience Canada*, v. 11, p. 161-194.
- Kaufmann, J., Meyers, W.J., and Hanson, G.N., 1990, Burial cementation in the Swan Hills Formation (Devonian), Rosevear Field, Alberta, Canada: *Journal of Sedimentary Petrology*, v. 60, p. 918-939.
- Kendall, G.St.C., and Schlager, W., 1981, Carbonates and relative changes in sea-level: *Marine Geology*, v. 44, p. 181-212.
- Kinsman, D.J.J., 1969, Interpretation of Sr⁺² concentrations in carbonate minerals and rocks: *Journal of Sedimentary Petrology*, v. 39, p. 486-508.
- Kozar, M.G., Weber, L.J., and Walker, K.R., 1986, Transport mechanisms and genesis of limestone-clast conglomerates with examples from the Cambrian of east Tennessee: *American Association of Petroleum Geologists Bulletin abstracts*, v. 70, p. 609.
- Kozar, M.G., 1986, The stratigraphy, petrology, and depositional environments of the Maryville Limestone (Middle Cambrian) in the vicinity of Powell and Oak Ridge, Tennessee: unpublished M.S. thesis, University of Tennessee, Knoxville, 242 p.
- Kozar, M.G., Weber, J.L., and Walker, K.R., 1990, Field and Modeling studies of Cambrian carbonate cycles, Virginia Appalachians-Discussion: *Journal of Sedimentary Petrology*, v. 60, p. 790-794.
- Kriesa, R.D., 1981, Storm-generated sedimentary structures in subtidal marine facies with examples from the Middle and Upper Ordovician of southwest Virginia: *Journal of Sedimentary Petrology*, v. 51, p. 823-848.
- Kupecz, J.A. and Land, L.S., 1991, Late-stage dolomitization of the Lower Ordovician Ellenburger Group, west Texas: *Journal of Sedimentary Petrology*, v. 61, p. 551-574.

- Land, L.S., 1970, Phreatic versus vadose diagenesis of limestones: evidence from a fossil water table. *Sedimentology*, v. 14, p. 175-185.
- Land, L.S., 1980, The isotopic and trace element geochemistry of dolomite: the state of the art, *in* Zenger, D.H., Dunham, J.B., and Ethington, R.L., eds., *Concepts and Models of Dolomitization*, Society of Economic Paleontologists and Mineralogists, v. 28, p. 87-110.
- Land, L.S., 1985, The origin of Massive dolomites: *Journal of Geological Education*, v. 33, p. 112-125.
- Lee, Y.I. and Friedman, G.M., 1987, Deep-burial dolomitization in the Ordovician Ellenburger Group carbonates, west Texas and southeastern New Mexico: *Journal of Sedimentary Petrology*, v. 57, p. 544-557.
- Logan, B.W., Rezak, R., and Ginsburg, R.N., 1964, Classification and environmental significance of algal stromatolites: *Journal of Geology*, v. 72, p. 68-83.
- Logan, B.W., Harding, J.L., Ahr, W.M., Williams, J.D., and Snead, R.G., 1969, Carbonate sediments and reefs, Yucatan shelf, Mexico: *American Association of Petroleum Geologists Memoir 11*, p. 1-198.
- Lohmann, K.C., and Walker, J.C.G., 1989, The $\delta^{18}\text{O}$ record of Phanerozoic abiotic marine calcite cements: *Geophysical Research Letters*, v. 16, p. 319-322.
- Lohmann, K.C., 1988, Geochemical patterns of meteoric diagenetic systems and their application to paleokarst, *in* Choquette, P.W., and James, N.P., eds., *Paleokarst*, Springer-Verlag, New York, p. 55-80.
- Lumsden, D.N. and Chimahusky, J.S., 1980, Relationship between dolomite nonstoichiometry and carbonate parameters, *in* Zenger, D.H., Dunham, J.B., Ethington, R.L., eds., *Concepts and Models of Dolomitization*, Society of Economic Paleontologists and Mineralogists, v. 28, p. 123-137.

- Machel, H.G., 1985, Cathodoluminescence in calcite and dolomite and its chemical interpretation: *Geoscience Canada*, v. 12, p. 139-147.
- Machel, H.G., 1988, Fluid flow direction during dolomite formation as deduced from trace-element trends, *in* Shukla, V., and Baker, P.A., eds., *Sedimentology and Geochemistry of Dolostones*, Society of Economic Paleontologists and Mineralogists 43, p. 115-127.
- Markello, J.R., and Read, J.F., 1981, Carbonate ramp-to-deeper shale shelf transitions of an upper Cambrian intrashelf basin, Nolichucky Formation, southwest Virginia Appalachians: *Sedimentology*, v. 28, p. 573-597.
- Markello, J.R., and Read, J.F., 1982, Upper Cambrian intrashelf basin, Nolichucky Formation, southwest Virginia Appalachians: *American Association of Petroleum Geologists Bulletin*, v. 66, p. 860-878.
- Mazzullo, S.J., 1981, Facies and burial diagenesis of a carbonate reservoir: Chapman deep (Atoka) field, Delaware basin, Texas: *American Association of Petroleum Geologists Bulletin*, v. 65, p. 850-865.
- Mazzullo, S.J., 1992, Geochemical and neomorphic alteration of dolomite, a review: *Carbonates and Evaporites*, v. 7, p. 21-37.
- McHargue, T.R. & Price, R.C., 1982, Dolomite from clayin argillaceous or shale-associated marine carbonates: *Journal of Sedimentary Petrology*, v. 52, p. 873-886.
- McIntire, W.L., 1963, Trace element partition coefficients - a review of theory and application to geology: *Geochimica Cosmochimica Acta*, v. 27, p. 1209 - 1264.
- McKenzie, J.A., 1981, Holocene dolomitization of calcium carbonate sediments from the coastal sabkhas of Abu Dhabi, U.A.E.: A stable isotope study: *Journal of Geology*, v. 89, p. 185-198.

- Morse, J.W., and MacKenzie, F.T., 1990, *Geochemistry of Sedimentary Carbonates*: New York, Elsevier, 707 p.
- Meyers, W.J., and Lohmann, K.C., 1985, Isotope geochemistry of regionally extensive calcite cement zones and marine components in Mississippian limestones, New Mexico, *in* Schneidermann, N., and Harris, P.M., eds., *Carbonate Cements*, Society of Economic Paleontologists and Mineralogists Special Publication 36, p. 223-239.
- Milici, R.C., Briggs, G., Knox, L.M., Sitterly, D.P., and Statler, A.T., 1979, The Mississippian and Pennsylvanian (Carboniferous) systems in the United States-Tennessee: United States Geological Survey Professional Paper 1110-G.
- Mitchum, R.M., Jr., Vail, P.R., and Thompson, S., III, 1977, Seismic stratigraphy and global changes of sea level, Part 2: The depositional sequence as a basic unit for stratigraphic analysis, *in* Payton, C., ed., *Seismic stratigraphy-Applications to hydrocarbon exploration*: American Association of Petroleum Geologists Memoir 26, p. 53-62.
- Moldovanyi, E.P., and Lohmann, K.C., 1984, Isotopic and petrographic record of phreatic diagenesis: Lower Cretaceous Sligo and Cupido formations: *Journal of Sedimentary Petrology.*, v. 54, p. 972-985.
- Moore, C.H. (1985) Upper Jurassic subsurface cements: A case history, *in* Schneidermann, N., and Harris, P.M., eds., *Carbonate Cements*, Society of Economic Paleontologists and Mineralogists Special Publication 36, p. 291-308.
- Morrow, D.W., 1982, Diagenesis II. Dolomite-part II: dolomitization models and ancient dolostones: *Geoscience Canada*, v. 9, p. 95-107.
- Morse, J.W., Zullig, J.J., Bernstein, L.D., Millero, F.J., Milne, P., Mucci, A., and Choppin, G.R., 1985, Chemistry of calcium carbonate-rich shallow water sediments in the Bahamas: *American Journal of Science*, v. 285, p. 147-185.

- Morse, J.W., Cornwell, J.C., Arakaki, T., Saulwood Lin, and Miguel Huerta-Diaz, 1992, Iron sulfide and carbonate mineral diagenesis in Baffin Bay, Texas: *Journal of Sedimentary Petrology*, v. 62, p. 671-680.
- Newell, N.D., Purdy, E.G., and Imbrie, J., 1960, Bahamian oolite sand: *Journal of Geology*, v. 68, p. 481-497.
- Noble, E.A., 1963, Formation of ore deposits by waters of compaction: *Economic Geology*, v. 58, p. 1145-1156.
- Osleger, D.A., and Read, J.F., 1991, Relation of eustasy to stacking patterns of meter-scale carbonate cycles, Late Cambrian, U.S.A.: *Journal of Sedimentary Petrology*, v. 61, p. 1225-1252.
- Palmer, A.R., 1971, The Cambrian of the Great Basin and adjacent areas of the western United States, *in* Holland, C.H., ed., *Lower Paleozoic Rocks of the World: Cambrian of the New World*, v. 1, Wiley Interscience, New York.
- Pfeil, R.W., and Read, J.F., 1980, Cambrian carbonate platform margin facies, Shady Dolomite, southwestern Virginia, U.S.A.: *Journal of Sedimentary Petrology*, v. 50, p. 91-116.
- Pratt, B.R., 1984, *Epiphyton* and *Renalcis*-diagenetic microfossils from calcification of coccoid blue-green algae: *Journal of Sedimentary Petrology*, v. 54, p. 948-971.
- Pratt, B.R., 1984, *Epiphyton* and *Renalcis*-diagenetic microfossils from calcification of coccoid blue-green algae: *Journal of Sedimentary Petrology*, v. 54, p. 948-971.
- Qing, H., and Mountjoy, E.W., 1992, Large-scale fluid flow in the Middle Devonian Presqu'ile barrier, western Canada sedimentary basin: *Geology*, v. 20, p. 903-906.
- Quinlan, G.M., and Beaumont, C., 1984, Appalachian thrusting, lithospheric flexure, and the Paleozoic stratigraphy of the eastern interior of North America: *Canadian Journal of Earth Sciences*, v. 21, p. 973-996.

- Radke, B.M., and Mathis, R.L., 1980, On the formation and occurrence of Saddle Dolomite: *Journal Sedimentary Petrology*, 50, 1149-1168.
- Rankey, E.C. Srinivasan, K. Walker, K.R. and Tobin, K.J., 1992, Middle Cambrian tectonism and the development of stratigraphic "Grand Cycles": A case study from the southern Appalachians (submitted, *Geology*).
- Read, J.F., and Pfeil, J.W., 1983, Fabrics of allochthonous reefal blocks, Shady Dolomite (Lower to Middle Cambrian), Virginia Appalachians: *Journal of Sedimentary Petrology*, v. 53, p.761-778.
- Read, J.F. 1989, Controls on evolution of Cambrian-Ordovician passive margin, U.S. Appalachians, *in* Crevello, P., Wilson, J.L., Sarg, J.F., Read, J.F., eds., Controls on carbonate platform and basin development: Society of Economic Paleontologists and Mineralogists Special Publication No. 44, p. 147-166.
- Reading, H.G., 1986, *Sedimentary Environments and Facies*; London, Blackwell Scientific Publications, 612 p.
- Reinhardt, J., 1977, Cambrian off-shelf sedimentation, central Appalachians, *in* Cook, H.E., and Enos, P., eds., Deep-water carbonate environments: Society of Economic Paleontologists and Mineralogists Special Publication No. 25, p. 83-112.
- Rodgers, J., and Kent, D.F., 1948, Stratigraphic section at Lee Valley, Hawkins County, Tennessee. Tennessee Division of Geology Bulletin, v. 55, 47 p.
- Rodgers, J., 1953, Geologic map of east Tennessee with explanatory text: Tennessee Division of Geology Bulletin, v. 58, 168 p.
- Rodgers, J., 1968, The eastern edge of the North American continent during the Cambrian and Early Ordovician, *in* Zen, E.A., and others, eds., *Studies of Appalachian Geology: Northern and Maritime*. New York, John Wiley, p. 141-150.
- Sandberg, P.A., 1983, An oscillating trend in Phanerozoic non-skeletal carbonate mineralogy: *Nature*, 305, 19-22.

- Schlager, W., 1981, The paradox of drowned reefs and carbonate platforms: Geological Society of America Bulletin, v. 92, p. 197-211.
- Schlager, W., 1989, Drowning unconformities in carbonate platforms, *in* Controls on carbonate platform and basin development: Society of Economic Paleontologists, and Mineralogists Special Publication 44, p. 15-25.
- Schlager, W. 1991, Depositional bias and environmental change-important factors in sequence stratigraphy: Sedimentary Geology, v. 70, p. 109-130.
- Scholle, P.A., and Halley, R.B., 1985, Burial diagenesis: Out of sight, out of mind, *in* Carbonate Cements, Schneidermann, N., and Harris, P.M., Society of Economic Paleontologists and Mineralogists Special Publication 36, p. 309-334.
- Sepkoski, J., Jr., 1982, Flat-pebble conglomerates, storm deposits and the Cambrian bottom fauna, *in* Einsele, G., and Seilacher, A., eds., Cyclic and Event Stratification: Springer-Verlag, Berlin, p. 371-385.
- Shanmugam, G., and Lash, G.C., 1982, Analogous tectonic evolution of the Ordovician foredeeps, southern and central Appalachians. Geology, v. 10, 562-566.
- Sibley, D.F., and Gregg, J.M., 1987, Classification of dolomite rock textures: Journal of Sedimentary Petrology, 57, 967-975.
- Sibley, D.F., 1990, Unstable to stable transformations during dolomitization: Journal of Geology, v. 98, p. 739-748.
- Simmons, W.A., 1984, Stratigraphy and depositional environments of the Middle Cambrian Maryville Limestone (Conasauga Group) near Thorn Hill, Tennessee [M.S. thesis]: Knoxville, Tennessee, University of Tennessee, Knoxville, 276 p.
- Slaughter, M., and Hill, R.J., 1991, The influence of organic matter in organogenic dolomitization. Journal of Sedimentary Petrology, 61, 296-303.
- Srinivasan, K., Walker, K.R., and Foreman, J.L., 1990, Early submarine cementation as a mechanism for the origin of intraclasts: evidence from petrography and stable

- isotope composition: Geological Society of America abstracts with programs, v. 22, no. 7, A 90.
- Srinivasan, K., Walker, K. R., Foreman, J.L., 1991, Cambrian flooding event: implications for Middle and Upper Cambrian sequence stratigraphy, southern Appalachians. Society for Economic Paleontologists and Mineralogists first annual theme meeting, Portland, Oregon, August 15-18.
- Srinivasan, K., and Walker, K.R., 1993, Sequence stratigraphy of an intrashelf carbonate ramp to basin transition in the Maryville Limestone (Middle Cambrian), southern Appalachians: Geological Society of America Bulletin (in press).
- Srinivasan, K., Walker, K.R., and Goldberg, S.A., 1993, Petrographic and geochemical constraints for fluid source and possible pathways during burial diagenesis of Maryville Limestone (Middle Cambrian) southern Appalachians. (Sedimentology, submitted).
- Steinen, R.P., and Matthews, R.K., 1973, Phreatic versus vadose diagenesis: Stratigraphy and mineralogy of a cored borehole on Barbados, W.I: Journal of Sedimentary Petrology, v. 43, 1012-1020.
- Steuber, A.M., Pushkar, P., and Hetherington, E.A., 1984, A strontium isotopic study of Smackover brines and associated solids, southern Arkansas: Geochimica Cosmochimica Acta, v. 48, p. 1637-1649.
- Stockman, K.W., Ginsburg, R.N., and Shinn, E.A., 1967, The production of lime mud by algae in South Florida: Journal of Sedimentary Petrology, v. 37, p. 633-648.
- Stoessell, R.K., 1992, Effects of sulfate reduction on CaCO₃ dissolution and precipitation in mixing-zone fluids: Journal of Sedimentary Petrology, 62, 873-880.
- Stow, D.A.V., and Shanmugam, G., 1980, Sequence of structures in fine-grained turbidites, comparison of recent deep-sea and ancient flysch sediments: Sedimentary Geology, v. 25, p. 23-42.

- Urey, H.C., Lowenstam, H.A., Epstein, S. and Mckinney, J.C.R., 1951, Measurement of paleotemperatures in the Upper Cretaceous of England, Denmark, and the southeastern United States. *Geological Society of America Bulletin*, v. 62, p. 399-416.
- Vahrenkamp, V.C., Swart, P.K., and Ruiz, J., 1991, Episodic dolomitization of late Cenozoic carbonates in the Bahamas: Evidence from strontium isotopes: *Journal of Sedimentary Petrology*, v. 61, p. 1002-1014.
- Van Wagoner, J.C., Posamentier, H.W., Mitchum, R.M., Vail, P.R., Sarg, J.F., Loutit, T.S., and Hardenbol, J., 1988, An overview of the fundamentals of sequence stratigraphy and key definitions, *in* Wilgus, C.K., Hastings, B.S., Kendall, C.G.St.C., Posamentier, H.W., Ross, C.A., and Van Wagoner, J.C., eds., *Sea-level changes: an integrated approach*: Society of Economic Paleontologists and Mineralogists Special Publication 42, p. 39-45.
- Veizer, J., 1983, Trace elements and isotopes in sedimentary carbonates, In: R.J. Reeder (Ed., *Carbonates: Mineralogy and Chemistry*. *Reviews in Mineralogy*, 11. Mineralogical Society of America, p. 267-300.
- Wagner, P.D., and Matthews, R.K., 1982, Porosity preservation in the Upper Smackover (Jurassic) carbonate grainstone, Walker Creek Field, Arkansas: Response of paleophreatic lenses to burial processes: *Journal of Sedimentary Petrology*, v. 52, p. 3-18.
- Walker, K.R., Foreman, J.L., Roberson, K.E., Srinivasan, K., and Steinhauff, D.M., 1989, Cambrian original marine calcite carbon and oxygen isotopic composition determined from unaltered ooids and fibrous cements: *Geological Society of America abstracts with programs*, v. 21, A222.
- Walker, K.R., Foreman, J.L., Roberson, K.E., Srinivasan, K., and Steinhauff, D.M., 1989, Cambrian original marine calcite carbon and oxygen isotopic composition

- determined from unaltered ooids and fibrous cements: Geological Society of America abstracts with programs, v. 21, A222.
- Walker, K.R., Foreman, J.L., and Srinivasan, K., 1990, The Cambrian Conasauga Group of eastern Tennessee: A preliminary general stratigraphic model with a more detailed test for the Nolichucky Formation: Appalachian Basin Industrial Associates, v. 17, p. 184-189.
- Walker, K.R. Ed., 1985, The Geologic History of the Thorn Hill Paleozoic Section (Cambrian-Mississippian), eastern Tennessee: University of Tennessee Studies in Geology 10, TN, 128 p.
- Walker, K.R., Steinhauff, D.M., and Roberson, K.E., 1992, Uppermost Knox Group, the Knox unconformity, the Middle Ordovician transition from shallow shelf to deeper basin near Dandridge, Tennessee, and a possible source for mineralizing fluids, in Misra, K.C., Fulweiler, R.E., and Walker, K.R., eds., Zinc Deposits in East Tennessee, Society of Economic Geology Guidebook 14, 79 p.
- Walter, L., and Burton, E.A., 1987, Active dissolution in modern shallow marine carbonate sediments: Global implications. Geological Society of America Annual Meeting and Exposition, Phoenix Arizona, 880.
- Weber, L.J., 1988, Paleoenvironmental analysis and test of stratigraphic cyclicity in the Nolichucky Shale and Maynardville Limestone (Upper Cambrian) in central east Tennessee: unpublished Ph.D. dissertation, University of Tennessee, Knoxville, 389p.
- Wilkinson, B.H., and Given, R.K., 1986, Secular variation in abiotic marine carbonates: constraints on Phanerozoic atmospheric carbon dioxide contents and oceanic Mg/Ca ratios: Journal of Geology, v. 94, p. 321-334.
- Wilson, J.L., 1969, Microfacies and sedimentary structures in "deeper water" lime mudstones, in Friedman G.M., ed., Depositional environments in carbonate rocks:

Society of Economic Paleontologists and Mineralogists Special Publication

14, p. 4-19.

APPENDICES

APPENDIX A
STANDARD MEASUREMENT CONVENTIONS

STANDARD MEASUREMENT CONVENTIONS

Bed thickness terminology used in the description of measured sections follows Ingram (1954). Grain size descriptions are based on Wentworth scale (1922).

Bed Thickness

Thick-bedded	30.0 - 100.0 cm
Medium-bedded	10.0 - 30.0 cm
Thin-bedded	3.0 - 10.0 cm
Very thin-bedded	1.0 - 3.0 cm
Laminated	0.3 - 1.0 cm

Grain Size

Coarse-Grained	Grains visible to the unaided eye (> 1 mm).
Medium-Grained	Grains visible with hand lens and readily identifiable (0.25 - 1.0 mm).
Fine-Grained	Grains visible with hand lens but not readily identifiable (0.1 - 0.25 mm).
Very fine-grained	Grains not visible with hand lens (< 0.1 mm).

APPENDIX B

DESCRIPTION OF STRATIGRAPHIC SECTIONS

NOTE

1. Field descriptions are given in ascending order from base of the section to the top.
2. Thin sections were cut for samples that are underlined. Polished slabs were prepared for samples from the Thorn Hill section. However, thin sections prepared by Simmons (1984) were used for petrographic studies
3. For sample identification with respect to locality and stratigraphic interval, a combination of alpha-numeric code is used. For example:

Th = Thorn Hill (for e.g. Th 2.5 mab)

WG = Woods Gap

GS = Graveston

NF = Norris Freeway

CH = Clinton Highway

mab after each sample number represents meters above base of the measured section.

THORN HILL SECTION AND SAMPLES

The Maryville Limestone is well exposed in this area along U.S. highway 25 E in northern Grainger County, Tennessee (Howard Quarter and Avondale Quadrangles). Exposed is 120 m of Maryville Limestone at this outcrop. Contact with the underlying Rogersville Shale is sharp. Measurement and description begins at the base of the Maryville Limestone.

<u>UNIT</u>	<u>THK (m)</u>	<u>CUM. TKN (m)</u>	<u>DESCRIPTION</u>
1	2.3	2.3	<u>Maryville Limestone</u> : Intraclastic oncolitic packstone/grainstone. Dark gray colored, the clasts measure up to 4 cm. Base of this unit is marked by lag. Contact with the underlying Rogersville is sharp. this unit also consists of oncolidal packstone/grainstone layers. Individual oncolids are large and appear dark gray colored. Occasional occurrence of hardgrounds. Thin dark gray to black colored bioturbated layers also occur. The burrows are filled with sparry calcite. Samples: 0.2 mab, 0.8 mab, 1.5 mab.
2	2.2	4.5	<u>Maryville Limestone</u> : Burrow mottled limestone, dark colored. Fabric not clearly visible, because outcrop is fresh. Mottled layers typically weather to buff color. Samples: 3.2 mab, 4.0 mab.
3	4.0	8.5	<u>Maryville Limestone</u> : Burrow mottled limestone. Light gray colored with pale yellow stringers of dolomite. Black spots on the surface could be pyrite. Thin grainy layers consisting of ostracods are discernible. Samples: 5.3 mab, 6.8 mab, 8.5 mab.
4	13.1	21.6	<u>Maryville Limestone</u> : Burrow mottled limestone: Contact with underlying unit sharp. Dark gray to light gray, burrows commonly filled with calcite spar. The intensity of burrowing commonly varies in this unit. Burrows commonly dolomitized. Thin grainy layers consisting of ostracods and trilobites common. Coarsening and fining upward layers common. Occasional occurrence of thin intraclastic layers. Samples: 9.5 mab, 12.0

mab, 13.5 mab, 15.4 mab, 17.4 mab, 18.0 mab, 18.5 mab, 20.0 mab, 21.2 mab, 21.6 mab.

- | | | | |
|---|-----|------|---|
| 5 | 7.9 | 29.5 | <p><u>Maryville Limestone</u>: Lime mudstone, bioturbated, burrows appear both horizontal and vertical. Appears light gray to dark gray in color. Outcrop is fresh. Thin layers of dolomite weather to buff color. The dolomite layers occur parallel to bedding. Contact with the upper unit is sharp. Minor occurrence of fossils. Thin grainy layers with ooids and fossils occur in the upper part of this unit. The top of this unit is marked by a thin oncolite layer.</p> |
| 6 | 1.7 | 31.2 | <p><u>Maryville Limestone</u>: Oncolite/oolite packstone: Contact with the lower unit sharp. This unit appears dark gray to light gray. Bioturbated, mostly horizontal burrows. The ooid part of the unit appears light gray. Upper part of this unit is ooid packstone/grainstone. Thin intraclastic layers common towards the upper part of this unit.</p> |
| 7 | 4.8 | 36.0 | <p><u>Maryville Limestone</u>: Ooid grainstone/packstone: Well exposed. Contact with the underlying unit, sharp. The unit appears massive. Light gray in color. Thin intraclastic layers occur. Individual clasts appear elongated. Faintly cross laminated towards the upper part of the unit. Bioturbated near the top. Samples: 31.2 mab, 31.7 mab, 32.1 mab, 32.5 mab, 33.9 mab, 34.8 mab, 35.6mab, 35.7 mab</p> |
| 8 | 4.0 | 40.0 | <p><u>Maryville Limestone</u>: Oolitic intraclastic Packstone/grainstone: Light gray to dark gray, thick bedded. Thin shale layers interspersed within the intraclastic layers. The intraclastic layers pinchout. Samples: 39.0 mab, 40.0 mab.</p> |
| 9 | 5.5 | 45.5 | <p><u>Maryville Limestone</u>: Burrow mottled limestone: Thin layers oolitic limestone alternate. Thin layers of dolomite commonly weathers to buff color. Thin to medium bedded. Oolitic/intraclastic layers within this unit appear light gray in color. Burrows filled with calcite spar commonly occur. Top of this unit is marked by oolitic/intraclastic packstone. Samples: 40.2 mab, 40.9 mab, 43.0 mab, 44.8 mab, 45.5 mab.</p> |

10	0.7	46.2	<u>Maryville Limestone</u> : Oolitic intraclastic grainstone/packstone: Intraclastic at the bottom and oolitic at the top. Contact with the underlying sharp to scoured. Light gray colored. No discernible sedimentary structures. Abundant stylolites.
11	1.8	48.0	<u>Maryville Limestone</u> : Burrow mottled and oolitic limestone. Thin to medium bedded. Fine to medium grained. Light gray colored. Well exposed. Some <i>Renalcis</i> towards the top. Coarsening upward. Intraclastic layers towards the top of this unit. The individual clasts vary in size. Intraclastic part appears gray. Samples: 47.2 mab, 48.0 mab.
12	2.5	50.5	<u>Maryville Limestone</u> : Oolitic oncolitic intraclastic grainstone/packstone: Grayish colored, thin to medium bedded, coarsening upward. Intraclastic towards the top. Thin dolomite layers alternate within the intraclastic layers. Dolomite layers weather to buff color. Contact with the underlying unit is sharp. Minor <i>Renalcis</i> . Oolitic intraclastic unit appears gray to dark gray.
13	3.5	53.5	<u>Maryville Limestone</u> : Light gray colored. Alternating layers of dolomite/silt and thin ooid layers. The dolomite layers are thinly bedded. Fine to medium grained. Stylolitic, contact with the underlying unit sharp. The unit is coarsening upward. The upper part of this unit is oolitic. Samples: 51.5mab, 52.8 mab, 53.5 mab.
14	1.8	55.3	<u>Maryville Limestone</u> : Well exposed ooid grainstone, dark gray colored. Contact with the underlying unit is diffuse. No macro fossils. The unit typically fines upward. Samples: 53.8 mab, 54.5 mab, 54.9 mab, 55.0 mab.
15	3.7	59.0	<u>Maryville Limestone</u> : Intraclastic/oolitic grainstone. Intraclastic at the base and oolitic grainstone/packstone towards the top. Thin to medium bedded, also medium to coarse grained. Alternating mudstone layers occur. Base of this unit appears scoured. Gray to light gray.

16	4.0	63.0	<p>Burrows commonly occur in the muddy layers. Samples: 55.5 mab, 56.3 mab, 56.6 mab, 57.3 mab. <u>Maryville Limestone</u>: Oolitic intraclastic grainstone packstone: Base of this unit scoured. Intraclasts occur as lag on the scoured base. Intraclasts occur sub parallel to inclined to bedding. Light gray colored. Medium to thick bedded. The percentage of ooids increases towards the central part of this unit. The oolitic beds are faintly cross laminated. Few hardgrounds. Coarsening upward unit. Thin layers of burrow mottled limestone commonly occur. Thin oncolite layers occur toward the top. The oncolite layers are gray to dark gray. Samples: 59.5 mab, 60.4 mab, 60.5 mab, 61.3 mab, 61.7 mab.</p>
17	6.4	69.6	<p><u>Maryville Limestone</u>: Burrow mottle limestone-quartz silty peloidal packstone: Alternating layers of mudstone and siltstone. Siltstone layers consist of abundant quartz, typically fining upwards. Also, thin intraclastic, oolitic/oncolitic, and bioclastic layers which typically occur towards the top of this unit. Alternating coarsening and fining upward layers. The siltstone layers are 3-4 cm thick. Samples: 63.3 mab, 63.4 mab, 64.1 mab, 64.5 mab, 65.1 mab, 65.5 mab, 67.3 mab, 68.2 mab, 69.0 mab.</p>
18	4.8	74.4	<p><u>Maryville Limestone</u>: Alternating calcareous siltstone layers: The siltstone layers are typically fining upwards. Weather to buff color, thin bedded. The unit generally becomes argillaceous towards the top. Siltstone layers display parallel and low angle cross laminations. The limestone layers are grainy with intraclasts. The intraclasts range from sub parallel to inclined to bedding. Samples: 70.1 mab, 70.5 mab, 72 mab, 73 mab, 74 mab, 74.4mab.</p>
19	2.0	76.5	<p><u>Maryville Limestone</u>: Limestone with thin siltstone layers. Contact with the underlying bed, sharp. Limestone at the bottom, siltstone at the top. Siltstone layers parallel to low angle cross laminated. Intraclasts commonly occur. Siltstone layers range from 8-10 cm thick. Medium bedded intraclastic packstone with thin shale layer toward</p>

the upper part of the unit. Samples: 75 mab, 75.5 mab, 75.9 mab.

20	11.5	88.0	<p><u>Maryville Limestone</u>: Nodular limestone with thin siltstone and intraclastic layers: Moderate to poorly exposed. Thin argillaceous layers alternate. Argillaceous layers weather to buff color. The limestone layers are 8-10 cm thick and are thinly laminated. The upper part of the outcrop is poorly exposed. Siltstone layers appear thin bedded with minor intraclasts. Samples: 77.5 mab, 79.5 mab, 80.5 mab, 82 mab, 82.8 mab, 85 mab, 86.1 mab.</p>
21	9.0	97.0	<p><u>Maryville Limestone</u>: Burrow mottled limestone: Contact with the lower unit, sharp. Thin nodular limestone, oolitic grainstone layers occur. The limestone layers appear gray in color. The mottled layers weather to buff color. The mottled layers are thin and continuous. Samples: 88 mab, 89 mab, 90.5 mab, 92.9 mab, 93.8 mab, 95.5 mab.</p>
22	6.0	103.0	<p><u>Maryville Limestone</u>: Oolitic/intraclastic grainstone with thin mudstone layers: Contact with the lower unit diffuse. Coarsening upward. Oolitic grainstone is grayish colored, medium to thick bedded with cross bedding. Intraclastic layers are medium to thick bedded. Mudstone layers are thin bedded. Minor <i>Renalcis</i>. Upper oolitic layer appears massive. Samples: 97.2 mab, 97.5 mab, 98.5 mab, 99.7 mab, 101.5 mab, 102.9 mab.</p>
23	2.4	105.4	<p><u>Maryville Limestone</u>: Intraclastic oolitic grainstone/packstone with thin mudstone layers: Light gray to dark gray. Thin to thick bedded. Few scoured surfaces occur overlain by bioclastic layers. Minor <i>Renalcis</i>, although it is difficult to recognize them where the outcrop is fresh. The mudstone layers are bioturbated. Burrows dolomitized. Thin coarsening and fining upward layers.</p>
24	1.8	107.2	<p><u>Maryville Limestone</u>: Limestone with thin dolomitized layers: Dark gray colored. Contact with the lower unit sharp. Thin bedded, no macro fossils. Samples: 106.4 mab, 107.2 mab.</p>

25	9.1	116.3	<u>Maryville Limestone</u> : Contact with the lower unit sharp. Well exposed. Thin dolomitized layers commonly weather to buff color. Bioturbated, burrows occur as both vertical and horizontal to bedding. Fossils include, <i>Renalcis</i> , trilobites, and few ostracods. Samples: 108.1 mab, 108.8 mab, 110.2 mab, 113.0 mab, 114.1 mab, 115.7 mab.
26	3.0	119.3	<u>Maryville Limestone</u> : Oolitic intraclastic grainstone: Well exposed, contact with the lower unit sharp. Cross bedded. Light gray colored. Intraclastic at the bottom, grading upward into oolitic grainstone. Thin to thick bedded. Thin dolomitized layers occur. Abundant intergranular cements. The oolitic grainstones are dolomitized. Stylolites are common. No macroscopic fossils. Samples: 116.4 mab, 116.7 mab, 117.6 mab, 118.2 mab, 119.3 mab.
27	1.8	120.8	Covered Interval. The top of the Maryville Limestone is a sequence boundary.
28	4.8	125.6	<u>Nolichucky</u> : Poor to moderately exposed. Bioclastic grainstone, thin intraclastic and mudstone layers. Gray to dark gray. Fossils include, ostracods, trilobites, ooids and oncooids. Bioturbated, burrows filled with sparry cement. Lower contact of this unit not visible. Typically fining upward. Mudstone layer becomes more common upward in the unit. Upper 1 m of this unit is covered. Samples: 121.4 mab, 121.6 mab, 123 mab, 124 mab.
29	4.8	130.4	<u>Nolichucky</u> : Bioclastic, oolitic, intraclastic grainstone. Lower part of this unit is well exposed, upper part poorly exposed. Light gray colored. Oolitic layers dolomitized. Individual clasts appear parallel and randomly oriented to bedding. Thin argillaceous layers common.
30	8.6	141.0	<u>Nolichucky</u> : Moderate to poorly exposed. Bioturbated lime mudstone, oolitic grainstone, and intraclastic packstone. Thin to thick bedded. Intraclastic layers are thick bedded.

The outcrop is located in Luttrell Quadrangle on 61 west. The outcrop is a quarry located adjacent to Bull Run Creek. Base of the outcrop is covered, however the top of this outcrop is well exposed. Description and measurement begins at the first exposed massive limestone layer.

<u>UNIT</u>	<u>THK(m)</u>	<u>CUM THK(M)</u>	<u>DESCRIPTION</u>
1	0.8	0.8	<u>Maryville Limestone</u> : Oolitic grainstone with thin bioclastic layers. Well exposed, gray to dark gray. Macro fossils consist of well preserved trilobites and ostracods. Oolitic grainstone weathers to buff color. Samples: <u>0.0</u> mab, <u>0.7</u> mab.
2	1.5	2.3	<u>Maryville Limestone</u> : Alternating layers of laminated limestone and mudstone. Poorly exposed, fining upward. This unit is followed by a thin covered interval. Samples: <u>2.3</u> mab.
3	1.5	3.8	<u>Maryville Limestone</u> : Oolitic grainstone with intraclasts. Poorly exposed, weathers to buff color. Contact with the lower unit not exposed. Oolitic grainstone layer contains abundant bioclasts. This unit is followed by a small covered interval. Samples: <u>3.2</u> mab, <u>3.5</u> mab.
4	1.2	5.0	Covered Interval.
5	2.1	7.1	<u>Maryville Limestone</u> : Well exposed grainstone, mudstone layer at the top which appears bioturbated. Light gray to gray colored. Contact with the underlying not visible. No discernible macro fossils or sedimentary structures. Fining upward unit. Samples: <u>5.4</u> mab, <u>6.5</u> mab, <u>7.1</u> mab.
6	6.9	14.0	<u>Maryville Limestone</u> : <i>Renalcis</i> boundstone with thin packstone and grainstone layers. Well exposed, contact with the underlying unit sharp. A well developed hardground marks the base of this unit. Macrofossils include, <i>Renalcis</i> , trilobites, and ostracods. The grainstone layers are composed of oncoids. Abundant intergranular fibrous cements. Bioturbated. Samples: <u>7.1</u> mab, <u>7.5</u>

mab, 8.0 mab, 9.2 mab, 11.0 mab, 12.1 mab, 13.0 mab, 14.0 mab.

- | | | | |
|----|-----|------|---|
| 7 | 6.4 | 20.4 | <p><u>Maryville Limestone</u>: <i>Renalcis-Girvanella</i> boundstone with thin packstone and grainstone layers. Well exposed, weathers to buff color. The grainstone layers are composed of oncoids. The proportion of oncolite layers increase towards the top. Abundant intergranular cements. Coarsening upward. When viewed from a distance, the unit appears biohermal in shape. Fabric is not clearly visible, because the outcrop is fresh. Samples: <u>14.9</u> mab, <u>15.2</u> mab, <u>15.3</u> mab, <u>16.3</u> mab, <u>17.0</u> mab, <u>17.8</u> mab, <u>18.6</u> mab, <u>19.4</u> mab.</p> |
| 8 | 0.2 | 20.6 | <p><u>Maryville Limestone</u>: Exposure surface 1. The surface is characterized by a micro scalloped surface. Evidence for exposure also consists of reddening and <i>insitu</i> brecciation. Abundant bioclasts. Samples <u>20.4</u> mab.</p> |
| 9 | 3.0 | 23.6 | <p><u>Maryville Limestone</u>: <i>Girvanella-Renalcis</i>-sponge boundstone with thin bioclastic layers. Dark gray to gray colored. Bioclastic layers consist sponge spicules. Well exposed. Contact with the underlying unit sharp. The fabric is not clear because of the freshness of the outcrop. Commonly bioturbated. Intergranular cements in bioclastic layers. Samples: <u>21.2</u> mab, <u>21.6</u> mab, <u>22.4</u> mab, <u>23.1</u> mab, <u>23.6</u> mab.</p> |
| 10 | 4.4 | 28.0 | <p><u>Maryville Limestone</u>: Boundstone with thin packstone and grainstone layers, components include, <i>Renalcis</i>, <i>Girvanella</i>, sponge, and trilobite fragments. Well exposed. Contact with the underlying unit sharp. Geometry of the unit is biohermal when viewed from a distance. Unit appears gray to dark gray. Abundant oncoids in the upper part of the unit. Bioturbated. Grainstone layers increase towards the top. Samples: <u>24.8</u> mab, <u>25.0</u> mab, <u>26.0</u> mab, <u>26.6</u> mab, <u>27.6</u> mab.</p> |
| 11 | 4.0 | 32.0 | <p><u>Maryville Limestone</u>: Oncoidal grainstone/packstone with thin mudstone and</p> |

- bioclastic layers. Light gray to dark gray, bioturbated, burrows filled with dolomite. Contact with the underlying unit sharp. Well exposed. Generally becomes grainstone upwards. The unit generally turns bioclastic upwards. Samples: 28.3 mab, 28.9 mab, 29.0 mab, 30.2 mab, 31.1 mab, 31.8 mab.
- 12 1.5 33.5 Maryville Limestone: Oncoidal limestone with thin bioclastic layers. Well exposed, contact with the underlying unit sharp. Oncoidal at the base grading upwards into bioclastic layers. Samples: 32.4 mab, 32.9 mab, 33.2 mab.
- 13 1.7 35.2 Maryville Limestone: Oncoidal packstone/wackestone with thin mudstone layers. Contact with underlying unit sharp. Well exposed, gray to dark gray, weathers to tan color. The wackestone and mudstone layers are bioturbated. No visible macro fossils. Sponge spicules can be identified in freshly broken samples. Few oncoids at the base of the unit with increasing proportion of oncoids towards the top. Oncoids appear dissolved and replaced with blocky clear calcite spar. Samples: 33.5 mab, 33.8 mab, 34.8 mab.
- 14 2.8 38.0 Maryville Limestone: Oncoidal grainstone/packstone with few bioclastic layers. Well exposed, contact with the underlying unit sharp. Light gray. The top of the Maryville Limestone is at 38.0 mab. Top is marked by a microscalloped surface with a thin layer of skeletal lag and abundant spar. The microscalloped surface is marked by a thin dark colored crust. Samples: 35.2 mab, 36.1 mab, 36.5 mab, 37.3 mab, 38.0 mab.
- The top of the Maryville Limestone is interpreted to be a sequence boundary. It is interpreted to be an exposure as well as a drowning surface.
- 15 6.0 44.0 Nolichucky Shale: Well exposed, contact sharp with the underlying unit. The lime nodules at the base of this unit appears bioturbated. No macrofossils. The carbonate layers are thinly laminated occasionally

appearing as microhummocky cross laminated.
Sparse intraclasts. Upper part of this unit is poorly exposed. Samples: 38.2 mab, 39.1 mab, 40.5 mab, 42.0 mab.

GRAVESTON OUTCROP AND SAMPLES

136

Outcrop is located in the Graveston Quadrangle. This outcrop is a roadcut located adjacent to the Bull Run Creek on 144 W. Base of the outcrop is covered, however the top of this outcrop is well exposed. Description and measurement begins at the first exposed massive limestone layer.

<u>UNIT</u>	<u>THK(m)</u>	<u>CUM.THK(m)</u>	<u>DESCRIPTION</u>
1	3.0	3.0	<u>Maryville Limestone</u> : Oolitic-intraclastic grainstone. Thin layers of bioclastic grainstone. Well exposed, light gray colored unit. Weathers to buff color. Contact with the underlying unit not exposed. Macro fossils include trilobites and ostracods. Individual clasts measure up to 2 - 3 cm. Samples: <u>0.0 mab</u> , <u>1.5 mab</u> , <u>2.0 mab</u> , <u>2.7 mab</u> , <u>2.8 mab</u> .
	1.5	4.5	Covered interval.
2	4.5	9.0	<u>Maryville Limestone</u> : Nodular limestone and intraclastic grainstone/packstone. Contact with the underlying unit not exposed. This unit is moderately exposed. Intraclastic at the base and nodular towards the top. The intraclastic beds are 5 - 10 cm thick. Light gray to gray colored. The nodular beds appear bioturbated. Samples: <u>4.5 mab</u> , <u>5.1 mab</u> , <u>5.4 mab</u> , <u>6.9 mab</u> , <u>8.0 mab</u> .
3	0.7	9.7	<u>Maryville Limestone</u> : Oolitic grainstone. Well exposed, cross-bedded. Contact with the underlying unit sharp. Weathers to buff. No macro fossils. This unit is overlain by a thin covered interval. Samples: <u>9.1 mab</u> .
	0.5	10.2	Covered interval.
4	3.0	13.2	<u>Maryville Limestone</u> : Oolitic-intraclastic grainstone. Contact with the underlying unit not exposed. Macro fossils include trilobites and ostracods. Thin bioclastic layers occur. Light gray colored, no distinct sedimentary structures. Thin argillaceous layers occur. Stylolites common. Samples: <u>10.5 mab</u> , <u>10.8 mab</u> , <u>11.6 mab</u> , <u>12.2 mab</u> , <u>13.2 mab</u> .

- | | | | |
|---|------|-------|--|
| 5 | 2.4 | 15.6 | <p><u>Maryville Limestone</u>: Oolitic/oncolitic/bioclastic packstone and wackestone. Well exposed, contact with the underlying unit not visible. gray to light gray in color. Weathers buff to tan color. Few <i>Renalcis</i> fragments. Individual oncoids appear large with concentric laminae. Thin argillaceous laminae commonly occur. Abundant spar cement. Samples: <u>13.7 mab</u>, <u>14.4 mab</u>.</p> |
| 6 | 15 | 30.6 | <p><u>Maryville Limestone</u>: <i>Renalcis</i> boundstone with thin grainstone and packstone layers. Contact with the underlying unit sharp. Macro fossils consist of few trilobite fragments. Moderately well exposed. Light gray to greyish in color. Grainstone layers contain abundant intergranular cements. Well bedded. Boundstone layers are composed of thin argillaceous layers which are dolomitized. The proportion of oncoids increases toward the top of this unit. Individual oncoids display well developed concentric laminations. No distinct sedimentary structures. Samples: <u>15.6 mab</u>, <u>16.0 mab</u>, <u>17.0 mab</u>, <u>18.2 mab</u>, <u>18.6 mab</u>, <u>19.4 mab</u>, <u>20.0 mab</u>, <u>21.0 mab</u>, <u>21.6 mab</u>, <u>22.7 mab</u>, <u>24.0 mab</u>, <u>25.6 mab</u>, <u>27.0 mab</u>, <u>28.3 mab</u>, <u>29.6 mab</u>, <u>30.4 mab</u>.</p> |
| 7 | 0.8 | 31.4 | <p><u>Maryville Limestone</u>: Oncolitic packstone. Well exposed. Contact with the underlying unit is irregular and scoured. Gray to dark gray. Oncoids are fairly large. Sparse intraclasts towards the top of this unit. Samples: <u>30.6 mab</u>, <u>30.7 mab</u>.</p> |
| 8 | 0.87 | 32.27 | <p><u>Maryville Limestone</u>: Oncoidal packstone/grainstone. Individual oncoids appear rounded to bean shaped. There is a well defined hardground within this unit. Oncoids display evidence for dissolution and replacement by spar. Contact with the overlying unit sharp.</p> |
| 9 | 3.5 | 35.77 | <p><u>Maryville Limestone</u>: Light gray to dark gray. Abundant biotic fragments and oncoids. Well exposed. Thin interspersed argillaceous layers. Biotic fragments appear to be trilobites. This unit</p> |

grades up into Nolichucky Shale. The contact with the overlying unit is sharp.

Nolichucky Shale

The outcrop is located in Fountain City Quadrangle approximately 6 miles from Halls Crossroads on 441 N. This outcrop here is well exposed. Description and measurement begins at the base of the Maryville Limestone.

<u>UNIT</u>	<u>THK(m)</u>	<u>CUM. THK(m)</u>	<u>DESCRIPTION</u>
1	4.5	4.5	<u>Maryville Limestone</u> : Limestone with thin shale interbeds. Base is marked by a well developed hardground. This unit is underlain by shale. Intraclastic units commonly alternate with thinly laminated limestone units. The intraclastic beds are medium to thick bedded. Coarsening upward. The shale layers are 2 - 3 cm thick. In general limestone layers become increasingly numerous and thicker towards the upper part of this unit. Samples: <u>0.35</u> mab, <u>1.2</u> mab, <u>1.55</u> mab, <u>1.60</u> mab, <u>3.5</u> mab, <u>4.5</u> mab.
2	0.8	5.3	<u>Maryville Limestone</u> : Shale with limestone interbeds. Thin paper laminated dark colored shale beds alternate with laminated limestone beds.
3	1.9	7.2	<u>Maryville Limestone</u> : Intraclastic grainstone/packstone with thin interbeds of shale and limestone. Fining upward. The intraclastic beds are medium to thick bedded. Well exposed. Base of this unit is scoured. Samples: <u>6.05</u> mab, <u>6.25</u> mab.
4	1.0	8.2	<u>Maryville Limestone</u> : Shale
5	0.7	8.9	<u>Maryville Limestone</u> : Thick bedded intraclastic grainstone. Glauconite common in intraclastic layers. Fining upward unit, well exposed. Contact sharp with the underlying unit. Samples: <u>8.3</u> mab, <u>8.8</u> mab.
6	9.0	17.9	<u>Maryville Limestone</u> : Limestone and shale interbeds with thin to medium bedded intraclastic grainstone/packstone layers. Abundant nodular limestone layers towards the top of this unit. The lower part of the unit is poorly exposed. Contact with the underlying unit diffuse. Fining upward unit. Few scoured surfaces commonly occur within this

unit. The limestone interbeds are commonly parallel to low angle cross lamination. Clasts within the intraclastic unit are subparallel to randomly oriented. They measure up to few cm. Samples: 9.1 mab, 9.7 mab, 10.0 mab, 12.4 mab, 13.5 mab, 14.2 mab, 16.0 mab, 16.9 mab.

7	10.0	27.9	Covered interval
8	3.0	30.9	<u>Maryville Limestone</u> : Shale and limestone interbeds. Shale is abundant at the bottom grading into limestone towards the top. Coarsening upward. The top of this unit is marked by a thick bedded intraclastic layer. The base of intraclastic bed is marked by scour marks. Samples: <u>28.9</u> mab, <u>29.05</u> mab, <u>30.7</u> mab.
9	2.0	32.9	<u>Maryville Limestone</u> : Shale and limestone and calcareous siltstone interbeds. Moderately exposed. The limestone beds range from 2-3 cm thick, thinly laminated. Samples: <u>31.6</u> mab.
10	0.35	33.4	<u>Maryville Limestone</u> : Thick bedded intraclastic grainstone. Base of this unit is scoured. Well exposed. Abundant glauconite. Clasts subparallel to randomly oriented. Clasts display evidence for micritization. This unit is not laterally continuous even in outcrop scale. Samples: <u>33.0</u> mab.
11	3.5	36.9	<u>Maryville Limestone</u> : Limestone and shale interbeds. Moderate to poorly exposed. Coarsening upward. The top of this unit is marked by a medium bedded intraclastic layer. Intraclastic layer is typically capped by thin laminated limestone layer. The limestone interbeds measure up to a few cm and are thinly laminated. Samples: <u>35.9</u> mab, <u>36.4</u> mab, <u>36.5</u> mab.
12	4.0	40.9	<u>Maryville Limestone</u> : Alternating intraclastic packstone, nodular limestone and shale interbeds. Contact with the lower unit sharp. Lower part of this unit is poorly exposed. This unit contains coarsening and fining upward layers. The intraclastic beds are typically thin, medium, and thick bedded. In

thickbedded layers, a thin shale layer occurs between two intraclastic layers. Clasts in the intraclastic beds appear subparallel to irregularly oriented. Limestone interbeds are thinly laminated. Polished slabs of limestone interbeds display partial Bouma sequence. Samples: 37.0 mab, 37.25 mab, 37.5 mab, 38.3 mab, 38.5 mab, 38.7 mab, 39.05 mab, 39.25 mab, 40.2 mab, 40.5 mab, 40.6 mab.

- | | | | |
|----|------|-------|--|
| 13 | 0.75 | 41.65 | <p><u>Maryville Limestone</u>: Oolitic intraclastic grainstone/packstone. Well exposed, massive. Gray in color, weathers to buff. The individual ooids appear large and appear to be dolomitized. Contact with the underlying unit is sharp. Samples: <u>41.2</u> mab.</p> |
| 14 | 2.0 | 43.65 | <p><u>Maryville Limestone</u>: Limestone and shale interbeds with thin intraclastic packstone layers. Contact with the underlying unit sharp. Coarsening and fining upward unit. The intraclastic packstone beds exhibit planar contact with the underlying beds. The intraclastic beds are thin to medium bedded and commonly coarse grained. Limestone interbeds are commonly nodular. Shale interbeds appear dark. Samples: <u>41.7</u> mab, <u>42.0</u> mab, <u>42.2</u> mab, <u>42.5</u> mab, <u>43.0</u> mab, <u>43.1</u> mab, <u>43.3</u> mab, <u>43.5</u> mab.</p> |
| 15 | 0.25 | 43.9 | <p><u>Maryville Limestone</u>: Intraclastic grainstone/packstone. Medium bedded (25 cm), contact with the underlying unit sharp. Interspersed within this unit is a thin shale layer.</p> |
| 16 | 1.35 | 45.25 | <p><u>Maryville Limestone</u>: Interbedded shale, intraclastic packstone and nodular limestone. Shale interbeds are much thinner compared to limestone beds. Coarsening upward unit. The intraclastic beds are amalgamated. There are several intraclastic layers each separated by a thin shale layer. Samples: <u>44.0</u> mab, <u>44.5</u> mab, <u>44.7</u> mab.</p> |
| 17 | 1.15 | 46.4 | <p><u>Maryville Limestone</u>: Interbeds of limestone/shale and intraclastic packstone. Limestone interbeds appear light to dark gray with thin planar laminations. Shale appears as thin dark beds.</p> |

Samples: 45.4 mab, 45.7 mab, 45.9 mab, 46.1 mab, 46.3 mab.

18	3.0	49.4	<u>Maryville Limestone</u> : Well exposed interbedded planar laminated limestone, intraclastic grainstone, and oolitic packstone with thin shale layers. Base of this unit consists of planar laminated layer grading upward into thin to thick bedded intraclastic layers. In general the intraclastic layers are thin bedded. Samples: 46.5 mab, 46.9 mab, 47.2 mab, 47.5 mab, 48.0 mab, 48.25 mab.
19	3.6	53.0	<u>Maryville Limestone</u> : Interbedded laminated limestone, intraclastic packstone, and shale layers. This unit is followed by a large covered interval. Measurement and description continues on the opposite of the road cut where the upper part of the Maryville Limestone is well exposed. Samples: 49.7 mab, 50.8 mab, 51.4 mab, 52.0 mab.
	15.0	68.0	Covered interval
20	0.3	68.3	<u>Maryville Limestone</u> : Laminated argillaceous limestone. Poorly exposed. Contact with the underlying unit not exposed. Weathers to yellowish brown. Laminations occur as parallel to low angle cross laminations.
	1.5	69.8	Covered interval
21	0.6	70.4	<u>Maryville Limestone</u> : Laminated mudstone. Moderately exposed. Dark gray in color. Weathers to dark brown. Samples: <u>70.0</u> mab.
22	1.0	71.4	<u>Maryville Limestone</u> : Laminated argillaceous limestone. Poorly exposed. Contact with the underlying unit diffuse.
23	1.0	72.4	<u>Maryville Limestone</u> : Laminated limestone and oolitic intraclastic grainstone. Basal part of this unit is poorly exposed. Upper part consists of thick bedded oolitic intraclastic grainstone. Coarsening upward. Weathers to buff. Samples: <u>72.0</u> mab.

- | | | | |
|----|-----|------|--|
| 24 | 1.4 | 73.8 | <u>Maryville Limestone</u> : Intraclastic packstone, laminated mudstone and thin shale layers. Well exposed. Gray to dark gray in color. The interbedded mudstone layers display thin laminations. Samples: <u>72.5</u> mab, <u>73.2</u> mab, <u>73.8</u> mab. |
| 25 | 1.2 | 75.0 | <u>Maryville Limestone</u> : Laminated limestone. Moderate to poorly exposed. Contact with the underlying unit sharp. Dark gray in color. Laminations appear as planar to low angle cross laminations. Samples: <u>74.6</u> mab, <u>74.8</u> mab. |
| 26 | 1.3 | 76.3 | <u>Maryville Limestone</u> : Lime mudstone, laminated limestone and intraclastic packstone. Contact with the underlying unit sharp. Mudstone beds appear dark in color. Intraclastic beds are thin to medium bedded. Coarsening upward. Intraclastic beds are commonly separated by thin argillaceous layers. Samples: <u>75.0</u> mab, <u>75.7</u> mab, <u>75.8</u> mab. |
| 27 | 0.9 | 77.2 | <u>Maryville Limestone</u> : Interbedded intraclastic grainstone and laminated limestone. Contact with the underlying unit, sharp. Fining upward unit. Intraclastic beds range from thin to medium bedded. Base of thin bedded intraclastic layers marked by tool marks. Clasts are parallel laminated. Laminated lime mudstone interbeds range in thickness from 3-5 cm. Samples: <u>76.4</u> mab, <u>76.6</u> mab, <u>77.2</u> mab. |
| 28 | 1.1 | 78.3 | <u>Maryville Limestone</u> : Interbedded intraclastic packstone and laminated silty limestone. Well exposed. Contact sharp with the underlying unit. Intraclastic beds are typically capped by a thin argillaceous layer. Individual clasts range from less than 1 cm to about 4 cm. They are parallel to imbricated. Intraclastic layers range from mud to clast supported. Laminations in silty limestone layers consist of parallel and low angle cross laminations. Undersides of these beds are marked by tool marks. Samples: <u>77.3</u> mab, <u>77.5</u> mab, <u>77.6</u> mab, <u>77.9</u> mab, <u>78.2</u> mab. |

29	2.2	80.5	<u>Maryville Limestone</u> : Intraclastic grainstone/packstone with thin shale layers. Well exposed, thick bedded. Intraclastic layers capped by a thin shale layer. Intraclastic beds are laterally discontinuous. Samples: <u>79.1</u> mab, <u>79.9</u> mab.
30	1.0	81.5	<u>Maryville Limestone</u> : Laminated limestone. Well exposed. Overlying this unit is a poorly exposed unit. Samples: <u>80.6</u> mab.
31	4.5	86.0	<u>Maryville Limestone</u> : Intraclastic limestone with thin shale layers. Poorly exposed unit. Light to dark gray in color. Samples: <u>81.8</u> mab, <u>85.8</u> mab.
32	4.0	90.0	<u>Maryville Limestone</u> : <i>Renalcis</i> boundstone. Exceptionally well exposed. Base of this unit is marked by a thin intraclastic layer. Fabric is not very clear probably because of dolomitization. Unit appears massive. Cross laminations?. Samples: <u>86.0</u> mab, <u>86.6</u> mab, <u>86.9</u> mab, <u>87.4</u> mab, <u>88.0</u> mab, <u>89.4</u> mab, <u>90.0</u> mab.
33	2.0	92.0	<u>Nolichucky Shale</u>

CLINTON HIGHWAY OUTCROP AND SAMPLES

Outcrop is located on the northeast side of Clinton Highway between Stradler Road (Brushy Valley Road) and the bridge over Bull Run Creek. Contact with the underlying Rogersville shale is covered. For this outcrop thin sections prepared by Kozar (1986) were used for petrographic studies.

APPENDIX C

ELECTRON MICROPROBE DATA

Table: Electron Microprobe Analysis of Unaltered oncoids									
Sample Id/Sample No.	MgCO ₃ wt%	MgCO ₃ mol%	CaCO ₃ wt%	CaCO ₃ mol%	MnCO ₃ wt%	MnCO ₃ mol%	FeCO ₃ wt%	FeCO ₃ mol%	Total wt%
Unaltered oncoid WG 28.8	1.223	1.450228	98.288	98.18613	0.023	0.020006	0.377	0.325348	99.938
Unaltered oncoid WG 28.8	1.404	1.665145	98.207	98.12222	0.087	0.075688	0.11	0.094946	99.87
Unaltered oncoid WG 28.8	1.771	2.09137	98.354	97.84627	0.003	0.002599	0.035	0.03008	100.21
Unaltered oncoid WG 28.8	1.26	1.4806	99.521	98.5194	0	0	0	0	100.78
Unaltered oncoid WG 28.8	1.613	1.901448	98.705	98.02324	0	0	0.087	0.074639	100.41
Unaltered oncoid WG 28.8	1.515	1.779404	99.159	98.11469	0	0	0.098	0.083769	100.81
Unaltered oncoid WG 28.8	1.294	1.537707	98.194	98.30238	0.08	0.069735	0.087	0.075241	99.677
Unaltered oncoid WG 28.8	0.731	1.730595	49.05	97.8266	0	0	0.257	0.442801	50.038
Unaltered oncoid WG 28.8	1.488	1.777952	97.48	98.12341	0.067	0.058724	0.02	0.017392	99.088
Unaltered oncoid WG 28.8	1.546	1.825645	98.524	98.01414	0	0	0.177	0.152117	100.26
Unaltered oncoid WG 28.8	1.239	1.481563	97.572	98.29103	0.04	0.035086	0.221	0.192326	99.072
Unaltered oncoid WG 28.8	2.221	2.642585	96.931	97.15898	0.02	0.017455	0.209	0.180977	99.381
Unaltered oncoid WG 28.8	1.689	1.985983	98.709	97.77832	0.054	0.046576	0.221	0.189119	100.67
Unaltered oncoid WG 28.8	1.843	2.186553	97.611	97.56034	0.037	0.0322	0.248	0.214133	99.749
Unaltered oncoid WG 28.8	1.723	2.047075	97.506	97.59322	0.05	0.043575	0.335	0.289661	99.653
Unaltered oncoid WG 28.8	1.158	1.361421	99.38	98.42891	0.017	0.014661	0.213	0.182247	100.79
Unaltered oncoid WG 28.8	1.746	2.083217	97.278	97.77884	0.047	0.041135	0.095	0.082492	99.187
Unaltered oncoid WG 28.8	1.398	1.682599	96.828	98.17804	0.013	0.011477	0.146	0.127886	98.385
Unaltered oncoid WG 28.8	1.644	1.959537	97.457	97.85988	0.05	0.043716	0.146	0.126649	99.312
Unaltered oncoid WG 28.8	1.447	1.691683	99.667	98.16162	0.003	0.002573	0.138	0.117416	101.3

Table: Electron Microprobe Analysis of Blocky clear calcite spar in moldic pores									
Sample Id/Sample No.	MgCO3 wt%	MgCO3 mol%	CaCO3 wt%	CaCO3 mol%	MnCO3 wt%	MnCO3 mol%	FeCO3 wt%	FeCO3 mol%	Total wt%
Blocky clear calcite spar WG 28.8	0.802	0.952845	98.581	98.6691	0.059	0.051419	0.355	0.306954	99.826
Blocky clear calcite spar WG 28.8	0.939	1.115811	98.364	98.46935	0.087	0.075834	0.392	0.339007	99.782
Blocky clear calcite spar WG 28.8	1.001	1.189172	98.321	98.4004	0.09	0.078429	0.384	0.332001	99.796
Blocky clear calcite spar WG 28.8	0.7	0.837865	97.952	98.77101	0	0	0.449	0.391129	99.101
Blocky clear calcite spar WG 28.8	0.787	0.947371	97.336	98.70941	0.097	0.085652	0.294	0.257567	98.514
Blocky clear calcite spar WG 28.8	0.602	0.72248	97.96		0	0	0.27	0.235825	98.832
Blocky clear calcite spar WG 28.8	0.443	0.521652	100.02	99.22104	0.031	0.026777	0.269	0.230529	100.76
Blocky clear calcite spar WG 28.8	0.758	0.893469	99.417	98.72133	0.059	0.051013	0.388	0.332843	100.62
Blocky clear calcite spar WG 28.8	1.062	1.252295	98.825	98.1723	0.062	0.053628	0.608	0.521775	100.56
Blocky clear calcite spar WG 28.8	0.912	1.102804	96.698	98.50558	0	0	0.445	0.391616	98.055
Blocky clear calcite spar WG 28.8	0.497	0.595376	98.274	99.17764	0.003	0.002636	0.233	0.203137	99.038
Blocky clear calcite spar WG 28.8	0.635	0.76641	97.202	98.83309	0.087	0.077024	0.351	0.308313	98.297
Blocky clear calcite spar WG 28.8	1.02	1.209628	98.827	98.73411	0.024	0.020878	0.041	0.035386	99.912
Blocky clear calcite spar WG 28.8	0.716	0.83725	100.36	98.86508	0.014	0.012009	0.298	0.253604	101.44
Blocky clear calcite spar WG 28.8	0.923	1.091639	99.126	98.76542	0	0	0.159	0.136858	100.22
Blocky clear calcite spar WG 28.8	1.163	1.389304	97.654	98.27604	0.156	0.136699	0.212	0.184311	99.205
Blocky clear calcite spar WG 28.8	0.893	1.07478	97.353	98.70914	0.052	0.045908	0.188	0.164673	98.494
Blocky clear calcite spar WG 28.8	1.025	1.217891	98.294	98.39008	0.045	0.039221	0.408	0.352811	99.772
Blocky clear calcite spar WG 28.8	0.807	0.972786	97.17	98.67701	0.024	0.021222	0.375	0.328982	98.376
Blocky clear calcite spar WG 28.8	0.908	1.086492	97.854	98.64135	0.048	0.042131	0.261	0.227289	99.075
Blocky clear calcite spar WG 28.8	0.927	1.118057	96.92	98.47762	0.007	0.006193	0.452	0.396753	98.308
Blocky clear calcite spar WG 28.8	0.495	0.593468	98.07	99.0532	0.074	0.06508	0.328	0.286196	98.97
Blocky clear calcite spar WG 28.8	0.688	0.82119	98.278	98.82147	0.047	0.04115	0.364	0.316194	99.377

Blocky clear calcite spar WG 28.8	0.566	0.679414	97.985	99.08726	0.01	0.008805	0.257	0.224517	98.818
Blocky clear calcite spar WG 28.8	0.786	0.938362	98.194	98.75811	0.044	0.038532	0.305	0.264999	99.329
Blocky clear calcite spar WG 28.8	0.942	1.133382	97.164	98.48512	0.034	0.030007	0.392	0.343248	98.544
Blocky clear calcite spar WG 28.8	0.653	0.785954	97.583	98.94589	0.017	0.015009	0.289	0.25315	98.542
Blocky clear calcite spar WG 28.8	0.519	0.620335	98.525	99.20763	0	0	0.186	0.161796	99.245
Blocky clear calcite spar WG 28.8	0.515	0.618701	97.974	99.15726	0.03	0.026437	0.226	0.197597	98.745
Blocky clear calcite spar WG 28.8	0.876	1.048888	97.776	98.62734	0	0	0.348	0.30325	99.03
Blocky clear calcite spar WG 28.8	0.813	0.977332	97.378	98.61713	0.067	0.059081	0.396	0.346453	98.654
Blocky clear calcite spar WG 28.8	0.917	1.100089	97.372	98.40847	0.111	0.097679	0.451	0.39376	98.851
Blocky clear calcite spar WG 28.8	0.919	1.109767	96.78	98.45587	0.03	0.026574	0.464	0.407785	98.193
Blocky clear calcite spar WG 28.8	0.721	0.867249	97.508	98.80718	0.027	0.023823	0.329	0.288006	98.605
Blocky clear calcite spar WG 28.8	0.481	0.570693	99.138	99.09176	0.027	0.023499	0.348	0.300493	100.01
Blocky clear calcite spar WG 28.8	0.52	0.623324	98.204	99.1699	0.003	0.002638	0.234	0.204138	98.961
Blocky clear calcite spar WG 28.8	0.599	0.714282	98.473	98.92357	0.037	0.032364	0.38	0.329779	99.489
Blocky clear calcite spar WG 28.8	0.602	0.71292	99.158	98.92628	0.044	0.038222	0.368	0.317168	100.18
Blocky clear calcite spar WG 28.8	0.823	0.988267	97.407	98.53813	0.034	0.029948	0.459	0.401129	98.785
Blocky clear calcite spar WG 28.8	0.647	0.780218	97.394	98.94273	0	0	0.289	0.253634	98.364
Blocky clear calcite spar WG 28.8	0.91	1.080746	98.342	98.39228	0.087	0.075792	0.522	0.45118	99.861
Blocky clear calcite spar WG 28.8	0.731		98.114	98.68162	0.04	0.035031	0.471	0.409245	99.358

Table: Electron Microprobe Analysis of Planar Dolomite									
Sample Id/Sample No.	MgCO ₃ wt%	MgCO ₃ mol%	CaCO ₃ wt%	CaCO ₃ mol%	MnCO ₃ wt%	MnCO ₃ mol%	FeCO ₃ wt%	FeCO ₃ mol%	Total wt%
Plan. dolo, core WG 28.8	39.781	44.578	55.977	52.844	0.054	0.044	3.107	2.534	98.92
Grain 1, rim	38.436	43.229	57.34	54.329	0.105	0.087	2.877	2.355	98.76
Grain1, rim	36.891	41.772	57.978	55.305	0.078	0.065	3.468	2.858	98.42
Pla. dolo. grain 2 core	37.115	42.157	57.635	55.151	0.088	0.073	3.168	2.619	98.01
Grain 2, rim	37.877	42.674	57.721	54.785	0.131	0.108	2.967	2.433	98.7
Grain 2, rim	37.802	42.4	58.612	55.383	0.159	0.131	2.555	2.086	99.13
Pla.dolo. grain 3 core	38.425	43.009	56.659	53.427	0.014	0.011	4.361	3.552	99.46
Grain 3, rim	37.615	42.513	57.444	54.695	0.051	0.042	3.343	2.75	98.45
Grain 3, rim	38.964	43.642	57.012	53.795	0.088	0.072	3.056	2.491	99.12
Grain 4, core	39.718	44.388	56.085	52.804	0.101	0.083	3.351	2.726	99.26
Grain 4, rim	38.234	43.103	56.848	53.989	0.051	0.042	3.493	2.866	98.63
Grain 4, rim	36.455	41.246	57.43	54.74	0.127	0.105	4.746	3.908	98.76
Grain 4, rim	37.765	42.82	56.2	53.683	0.139	0.116	4.097	3.381	98.2
Grain 4, rim	34.709	39.397	60.474	57.827	0.047	0.039	3.313	2.737	98.54
Dolo. inclu. in cal.spar	41.381	46.455	53.859	50.937	0	0	3.192	2.608	98.43
Same grain	40.111	45.057	54.768	51.828	0.093	0.077	3.717	3.039	98.69
Pla. dolo grain 5 WG 17.8	37.862	42.174	59.293	55.64	0.061	0.05	2.635	2.136	99.85
Grain 5	37.238	41.876	58.515	55.435	0.09	0.074	3.195	2.615	99.04
Grain 5	41.191	45.675	57.18	53.415	0.065	0.053	1.062	0.857	99.5
Grain 6, core	41.299	45.791	56.614	52.882	0.119	0.097	1.525	1.231	99.56
Grain 6, core	39.991	44.868	56.615	53.511	0.064	0.053	1.921	1.569	98.59
Grain 7, core	40.706	45.44	55.968	52.633	0.071	0.058	2.3	1.869	99.045
Grain 7, close to rim	38.175	42.812	58.101	54.892	0.064	0.053	2.748	2.243	99.088

Grain 7, rim	38.095	42.952	56.544	53.709	0.107	0.088	3.961	3.25	98.707
Grain 7, rim	33.784	38.23	62.837	59.903	0.034	0.028	2.233	1.839	98.891
Grain 8, core	40.675	45.074	58.071	54.213	0	0	0.884	0.713	99.63
Grain 8, core	42.295	45.95	57.14	52.298	0.108	0.086	2.107	1.666	101.65
Grain 8, rim	37.357	42.074	56.553	53.658	0.051	0.042	5.156	4.226	99.117
Grain 8, rim	38.862	43.614	55.748	52.708	0.041	0.034	4.462	3.644	99.113
Grain 9, core	41.918	45.937	56.753	52.395	0.095	0.076	1.996	1.592	100.76
Grain 9, close to rim	38.789	42.789	59.007	54.836	0.081	0.066	2.876	2.309	100.75
Grain 9, close to rim	42.43	46.586	55.943	51.745	0.085	0.068	2.004	1.601	100.46
Grain 9, rim	38.435	42.955	56.484	53.181	0.135	0.111	4.615	3.754	99.669
Grain 10, core	42.327	46.485	56.195	51.991	0.135	0.109	1.771	1.415	100.43
Grain 10, core	42.532	46.424	56.768	52.2	0.054	0.043	1.677	1.332	101.03
Grain 10, close to rim	40.016	44.09	58.244	54.063	0.122	0.099	2.18	1.748	100.56
Grain 10, close to rim	41.579	46.198	55.36	51.818	0.068	0.055	2.385	1.929	99.392
Grain 11, core	41.967	45.978	56.475	52.124	0.105	0.084	2.275	1.814	100.83
Grain 11, close to rim	41.059	44.983	57.206	52.799	0.058	0.047	2.723	2.171	101.05
Grain 11, close to rim	40.994	44.97	57.382	53.03	0.085	0.068	2.42	1.932	100.92
NL planar dolomite NF 17.	39.24	44.031	56.642	53.544	0.105	0.086	2.863	2.338	98.85
NL planar dolomite	40.753	45.343	57.39	53.793	0.005	0.004	1.062	0.86	99.21
NL planar dolomite	40.738	45.228	57.354	53.643	0.027	0.022	1.37	1.107	99.489
NL planar dolomite	41.331	46.3	55.938	52.79	0.02	0.016	1.096	0.894	98.385
NL planar dolomite	38.65	43.22	56.746	53.458	0.214	0.176	3.867	3.147	99.477
NL planar dolomite	40.774	45.438	56.801	53.325	0.032	0.026	1.493	1.211	99.1
NL planar dolomite	40.033	44.718	56.139	52.829	0.066	0.054	2.951	2.399	99.189
NL planar dolomite	40.351	45.245	55.564	52.487	0.048	0.039	2.73	2.228	98.693

NL planar dolomite	39.874	44.474	56.44	53.032	0.088	0.072	2.984	2.422	99.386
NL planar dolomite	40.359	45.4	55.074	52.191	0.09	0.074	2.852	2.335	98.375
NL planar dolomite	39.794	44.582	55.946	52.802	0.134	0.11	3.074	2.506	98.948
NL planar dolomite	39.589	43.987	57.811	54.112	0.031	0.025	2.32	1.876	99.751
NL planar dolomite	40.087	44.888	55.619	52.468	0.151	0.124	3.092	2.52	98.949
Pla. dolo. grain 12, core	37.222	42.073	57.946	55.178	0.062	0.051	3.279	2.697	98.509
Grain 12, rim	36.981	41.749	57.954	55.118	0.111	0.092	3.702	3.042	98.748
Grain 12	37.98	42.809	57.603	54.697	0.083	0.069	2.957	2.426	98.623
Grain 13, core	38.728	43.158	58.412	54.837	0.071	0.058	2.401	1.947	99.612
Grain 13, rim	37.394	42.363	56.939	54.342	0.113	0.094	3.883	3.201	98.337
Grain 14, rim	33.46	37.998	60.088	57.487	0.114	0.095	5.348	4.42	99.031
Grain 14, rim	34.726	39.033	61.28	58.027	0.118	0.097	3.475	2.843	99.599
Grain 15, core	37.414	41.903	58.554	55.247	0.163	0.134	3.333	2.717	99.464
Grain 15, rim	37.909	42.559	57.591	54.468	0.069	0.057	3.57	2.917	99.139
Grain 16	32.153	36.524	63.771	61.026	0	0	2.964	2.45	98.888
Grain 16	39.156	44.228	54.935	52.274	0.201	0.167	4.052	3.331	98.344
Grain 17, core	36.999	42.006	56.406	53.95	0.204	0.17	4.689	3.874	98.298
Dolo. inclu. in cal. spar WG	37.734	42.325	58.36	55.146	0.017	0.014	3.081	2.515	99.216
same grain	37.656	41.737	58.345	54.479	0.139	0.113	4.551	3.671	100.69
same grain	36.847	41.489	57.121	54.183	0.118	0.097	5.162	4.23	99.293
Grain 18, core	37.085	41.648	58.415	55.267	0.132	0.109	3.641	2.976	99.305

Table: Electron Microprobe Analysis of Saddle dolomite									
Sample Id/Sample No.	MgCO ₃ wt%	MgCO ₃ mol%	CaCO ₃ wt%	CaCO ₃ mol%	MnCO ₃ wt%	MnCO ₃ mol%	FeCO ₃ wt%	FeCO ₃ mol%	Total wt%
Saddle dolomite, GS 20 m	37.646	42.344	56.097	53.156	0.123	0.101	5.373	4.398	99.239
Saddle dolomite, GS 20 m	38.9	43.73	55.9	52.94	0.06	0.049	4.01	3.281	98.8
Saddle dolomite, GS 20 m	37.934	42.901	55.528	52.904	0.045	0.037	5.052	4.158	98.559
Saddle dolomite, GS 20 m	38.331	42.963	55.679	52.574	0.124	0.102	5.346	4.361	99.48
Saddle dolomite, GS 20 m	38.282	43.242	55.788	53.088	0.079	0.065	4.385	3.605	98.534
Saddle dolomite, GS 20 m	38.137	42.926	56.075	53.171	0.071	0.059	4.693	3.844	98.976
Saddle dolomite, GS 20 m	37.956	42.75	55.943	53.082	0.098	0.081	4.986	4.087	98.983
Saddle dolomite, GS 20 m	38.464	42.99	56.178	52.896	0.076	0.062	4.981	4.052	99.699
Saddle dolomite, GS 20 m	37.906	42.33	56.864	53.495	0.105	0.086	5.031	4.089	99.906
Saddle dolomite, GS 20 m	39.114	44.027	55.728	52.844	0.068	0.056	3.751	3.073	98.661
Saddle dolomite, GS 20 m	39.229	43.751	55.777	52.406	0.094	0.077	4.64	3.766	99.74
Saddle dolomite, GS 20 m	37.945	42.395	56.591	53.265	0.081	0.066	5.256	4.274	99.873
Saddle dolomite, GS 20 m	38.086	42.533	56.754	53.395	0.1	0.082	4.909	3.99	99.849
Saddle dolomite, GS 20 m	38.8	43.548	55.8	52.76	0.05	0.041	4.47	3.651	99.2
Saddle dolomite, GS 20 m	39.413	44.394	55.836	52.984	0.07	0.058	3.128	2.564	98.447
Saddle dolomite, GS 20 m	39.292	44.298	55.7	52.903	0.095	0.079	3.316	2.721	98.403
Saddle dolomite, GS 20 m	38.85	43.911	55.952	53.277	0.089	0.074	3.328	2.738	98.219
Saddle dolomite, GS 20 m	38.643	43.571	55.892	53.091	0.041	0.034	4.026	3.304	98.602
Saddle dolomite, GS 20 m	38.952	43.586	56.646	53.398	0.15	0.123	3.552	2.893	99.3
Saddle dolomite, GS 20 m	39.159	44.203	55.583	52.857	0.048	0.04	3.531	2.901	98.321
Saddle dolomite, GS 20 m	39.2	43.96	56	52.906	0.05	0.041	3.79	3.093	99.1
Saddle dolomite, GS 20 m	38.807	43.533	56.593	53.483	0.061	0.05	3.594	2.934	99.055
Saddle dolomite, GS 20 m	38.157	42.637	57.016	53.672	0.091	0.075	4.447	3.616	99.711

Saddle dolomite, GS 20 m	37.811	42.811	55.686	53.116	0.061	0.051	4.882	4.023	98.44
Saddle dolomite, GS 20 m	39.491	44.244	55.322	52.215	0.073	0.06	4.27	3.482	99.156
Saddle dolomite, GS 20 m	37.867	42.774	55.884	53.18	0.129	0.107	4.791	3.939	98.671
Saddle dolomite, GS 20 m	38.7	43.111	57	53.492	0.1	0.082	4.09	3.316	99.8
Saddle dolomite, GS 20 m	39.496	44.058	57.034	53.598	0.068	0.056	2.818	2.288	99.416
Saddle dolomite, GS 20 m	39.393	44.393	56.068	53.229	0.078	0.064	2.821	2.314	98.36
Saddle dolomite, GS 20 m	40.19	44.691	57.051	53.444	0.081	0.066	2.223	1.799	99.545
Saddle dolomite, GS 20 m	39.361	44.132	57.1	53.934	0.031	0.025	2.339	1.909	98.831
Saddle dolomite, GS 20 m	39.049	43.838	57.324	54.215	0.076	0.063	2.307	1.885	98.756
Saddle dolomite, GS 20 m	38.36	43.111	55.735	52.769	0.08	0.066	4.957	4.054	99.132
Saddle dolomite, GS 20 m	38.1	42.801	56.3	53.282	0.1	0.082	4.69	3.834	99.2
Saddle dolomite, GS 20 m	38.095	42.704	56.522	53.378	0.113	0.093	4.689	3.825	99.419
Saddle dolomite, GS 20 m	39.647	44.435	56.235	53.096	0.057	0.047	2.97	2.423	98.909
Saddle dolomite, GS 20 m	37.941	42.615	55.861	52.858	0.139	0.115	5.398	4.413	99.339
Saddle dolomite, GS 20 m	37.232	42.043	56.013	53.285	0.11	0.091	5.574	4.581	98.929
Saddle dolomite, GS 20 m	37.518	42.462	55.716	53.122	0.068	0.056	5.293	4.36	98.595
Saddle dolomite GS 22.7m	37.24	41.589	58.125	54.685	0.104	0.085	4.48	3.641	99.949
Saddle dolomite GS 22.7m	38.6	43.252	56.6	53.428	0.14	0.115	3.93	3.205	99.3
Saddle dolomite GS 22.7m	36.969	41.475	57.548	54.39	0.108	0.089	4.955	4.046	99.58
Saddle dolomite GS 22.7m	38.245	43.033	55.891	52.979	0.084	0.069	4.785	3.918	99.005
Saddle dolomite GS 22.7m	37.859	42.225	56.91	53.472	0.095	0.078	5.205	4.225	100.069
Saddle dolomite GS 22.7m	37.017	41.81	56.733	53.983	0.047	0.039	5.07	4.168	98.867
Saddle dolomite GS 22.7m	39.688	44.354	56.429	53.127	0.056	0.046	3.04	2.473	99.213
Saddle dolomite GS 22.7m	37.152	41.825	56.955	54.016	0.116	0.096	4.96	4.064	99.183
Saddle dolomite GS 22.7m	37.4	41.606	57.6	53.981	0.1	0.082	5.35	4.331	100

Saddle dolomite GS 22.7m	37.131	42.079	55.727	53.202	0.072	0.06	5.649	4.659	98.579
Saddle dolomite GS 22.7m	37.761	42.862	55.008	52.601	0.059	0.049	5.433	4.488	98.261
Saddle dolomite GS 22.7m	37.71	42.482	56.061	53.204	0.07	0.058	5.191	4.256	99.032
Saddle dolomite GS 22.7m	38.561	43.617	54.715	52.138	0.099	0.082	5.056	4.162	98.431
Saddle dolomite WG 17.0m	40.567	45.456	55.956	52.82	0.009	0.007	2.105	1.717	98.637
Saddle dolomite WG 17.0m	40.505	45.52	55.639	52.676	0.127	0.105	2.077	1.699	98.348
Saddle dolomite WG 17.0m	38.011	42.962	57.683	54.924	0.031	0.026	2.538	2.088	98.263
Saddle dolomite WG 17.0m	39.201	43.862	56.512	53.269	0.073	0.06	3.449	2.809	99.235
Saddle dolomite WG 17.0m	41.871	46.629	54.872	51.48	0.08	0.065	2.252	1.825	99.075
Saddle dolomite WG 17.0m	38.022	42.802	57.532	54.561	0.024	0.02	3.195	2.618	98.773
Saddle dolomite WG 17.0m	38.455	43.45	54.839	52.199	0.131	0.109	5.159	4.242	98.584
Saddle dolomite WG 17.0m	38.946	43.869	55.734	52.888	0.102	0.084	3.854	3.159	98.636
Saddle dolomite WG 17.0m	36.843	41.412	58.249	55.157	0.134	0.11	4.059	3.32	99.285
Saddle dolomite WG 17.0m	37.497	42.37	57.757	54.98	0.065	0.054	3.157	2.596	98.476
Saddle dolomite WG 17.0m	39.986	45.054	55.779	52.946	0.057	0.047	2.382	1.953	98.204
Saddle dolomite WG 17.0m	37.01	41.69	56.601	53.713	0.112	0.093	5.494	4.504	99.217
Saddle dolomite WG 17.0m	37.982	43.062	55.34	52.856	0.092	0.077	4.855	4.006	98.269
Saddle dolomite WG 17.0m	36.741	41.682	56.226	53.737	0.094	0.078	5.454	4.503	98.515
Saddle dolomite WG 17.0m	38.811	43.517	56.111	53.002	0.08	0.066	4.186	3.416	99.188
Saddle dolomite WG 17.0m	40.554	45.435	55.88	52.742	0.043	0.035	2.193	1.788	98.67
Saddle dolomite WG 17.0m	41.104	46.064	55.514	52.41	0.084	0.069	1.786	1.457	98.488
Saddle dolomite WG 17.0m	31.167	34.927	66.984	63.238	0.076	0.062	2.173	1.772	100.4
Saddle dolomite WG 17.0m	39.759	44.442	56.991	53.666	0.081	0.066	2.244	1.825	99.075
Saddle dolomite WG 17.0m	39.028	43.915	55.845	52.937	0.062	0.051	3.782	3.097	98.717
Saddle dolomite WG 17.0m	39.683	44.411	56.339	53.117	0.079	0.065	2.955	2.407	99.056

Saddle dolomite WG 17.0m	40.354	44.835	56.937	53.292	0.101	0.082	2.214	1.79	99.606
Saddle dolomite WG 17.0m	40.167	44.993	56.192	53.026	0.093	0.076	2.337	1.905	98.829
Saddle dolomite WG 17.0m	38.972	43.556	56.967	53.636	0.119	0.098	3.333	2.711	99.391
Saddle dolomite WG 17.0m	37.503	41.719	59.342	55.612	0.042	0.034	3.254	2.634	100.141
Saddle dolomite WG 17.0m	38.971	43.397	57.198	53.658	0.091	0.074	3.542	2.871	99.802
Saddle dolomite WG 17.0m	38.428	42.904	56.684	53.315	0.118	0.097	4.535	3.685	99.765
Saddle dolomite WG 17.0m	31.054	34.97	64.401	61.096	0.121	0.1	4.679	3.835	100.255
Saddle dolomite WG 17.0m	37.584	42.446	55.781	53.071	0.097	0.08	5.356	4.402	98.818
Saddle dolomite WG 17.0m	38.342	42.86	56.003	52.739	0.097	0.08	5.312	4.321	99.754
Saddle dolomite WG 17.0m	37.194	41.923	57.342	54.449	0.082	0.068	4.34	3.56	98.958
Saddle dolomite WG 17.0m	36.571	41.116	59.016	55.896	0.069	0.057	3.582	2.931	99.238
Saddle dolomite WG 17.0m	38.444	43.206	55.986	53.007	0.057	0.047	4.572	3.74	99.059
Saddle dolomite WG 17.0m	39.68	44.498	54.752	51.726	0.062	0.051	4.563	3.724	99.057
Saddle dolomite Gs 20.0 m	38.217	42.345	57.209	53.402	0.123	0.1	5.15	4.153	100.699
Saddle dolomite Gs 20.0 m	37.852	42.12	56.873	53.314	0.058	0.047	5.58	4.519	100.363
Saddle dolomite Gs 20.0 m	37.436	41.772	57.091	53.666	0.095	0.078	5.522	4.484	100.144
Saddle dolomite Gs 20.0 m	38.721	43.573	55.071	52.208	0.102	0.084	5.048	4.134	98.942
Saddle dolomite Gs 20.0 m	37.595	42.187	56.446	53.361	0.085	0.07	5.366	4.382	99.492
Saddle dolomite Gs 20.0 m	35.954	40.375	58.646	55.481	0.078	0.064	4.991	4.079	99.669
Saddle dolomite Gs 20.0 m	37.129	42.185	55.729	53.341	0.078	0.065	5.332	4.409	98.268
Saddle dolomite Gs 20.0 m	39.776	44.283	55.456	52.013	0.072	0.059	4.499	3.645	99.803
Saddle dolomite Gs 20.0 m	36.97	41.508	56.583	53.52	0.101	0.083	5.983	4.889	99.637
Saddle dolomite Gs 20.0 m	37.77	42.494	56.312	53.373	0.082	0.068	4.966	4.066	99.13
Saddle dolomite, J4	32.72	37.427	57.165	55.086	0.356	0.299	8.634	7.188	98.875
Saddle dolomite, J4	34.139	39.001	56.654	54.525	0.49	0.411	7.292	6.063	98.575

Saddle dolomite, J4	34.57	39.387	55.873	53.629	0.428	0.358	7.991	6.626	98.862
Saddle dolomite, J4	34.348	39.155	56.915	54.657	0.34	0.284	7.116	5.904	98.719
Saddle dolomite, J4	33	37.587	58.9	56.517	0.3	0.251	6.81	5.645	99
Saddle dolomite, J4	34.945	39.356	57.113	54.188	0.48	0.397	7.392	6.059	99.93
Saddle dolomite, J4	33.617	38.506	56.39	54.414	0.544	0.457	7.944	6.622	98.495
Saddle dolomite, J4	33.65	37.978	57.873	55.026	0.747	0.618	7.764	6.377	100.034
Saddle dolomite, J4	34.307	38.848	57.636	54.981	0.299	0.248	7.187	5.923	99.429
Saddle dolomite, J4	34.864	39.441	56.811	54.143	0.358	0.297	7.431	6.118	99.464
Saddle dolomite, J4	34.768	39.147	57.428	54.473	0.247	0.204	7.538	6.177	99.981
Saddle dolomite, J4	33.4	38.015	57.3	54.942	0.43	0.359	8.07	6.685	99.1
Saddle dolomite, J4	32.361	36.944	59.217	56.952	0.341	0.286	7.003	5.818	98.922
Saddle dolomite, J4	34.858	39.489	55.714	53.172	0.433	0.36	8.465	6.979	99.47
Saddle dolomite, J4	33.706	38.306	57.08	54.649	0.372	0.31	8.142	6.734	99.3
Saddle dolomite, J4	34.837	39.444	56.4	53.797	0.341	0.283	7.858	6.475	99.436
Saddle dolomite, J4	34.398	38.83	57.283	54.476	0.372	0.308	7.773	6.386	99.826
Saddle dolomite, J4	34.2	38.521	57.6	54.656	0.35	0.289	7.97	6.533	100
Saddle dolomite, J4	34.17	38.915	56.425	54.136	0.415	0.347	7.966	6.603	98.976
Saddle dolomite, J4	33.046	37.58	57.628	55.21	0.643	0.536	8.063	6.673	99.38
Saddle dolomite, J4	33.597	38.152	57.539	55.046	0.817	0.681	7.407	6.122	99.36
Saddle dolomite, J4	33.839	38.497	57.344	54.958	0.314	0.262	7.589	6.283	99.086
Saddle dolomite, J4	33.877	38.505	57.345	54.91	0.348	0.29	7.609	6.294	99.179
Saddle dolomite, J4	33.698	38.061	58.006	55.193	0.339	0.281	7.865	6.465	99.908
Saddle dolomite, J4	34.853	39.257	55.854	52.999	0.469	0.387	8.974	7.356	100.15
Saddle dolomite, J4	32.382	36.825	59.775	57.266	0.304	0.254	6.833	5.655	99.294
Saddle dolomite, J4	34.549	39.262	56.89	54.465	0.314	0.262	7.268	6.011	99.021

Saddle dolomite, J4	33.09	37.973	55.992	54.131	0.328	0.276	9.123	7.619	98.533
Saddle dolomite, J4	34.588	38.936	57.52	54.549	0.345	0.285	7.605	6.23	100.058
Saddle dolomite, J4	33.526	38.338	56.493	54.423	0.414	0.347	8.282	6.892	98.715
Saddle dolomite, J4	32.445	37.134	59.018	56.905	0.279	0.234	6.874	5.726	98.616
Saddle dolomite, J4	34.275	39.139	56.51	54.363	0.361	0.302	7.455	6.196	98.601
Saddle dolomite, J4	34.265	38.962	56.598	54.217	0.5	0.417	7.738	6.404	99.101
Saddle dolomite, J4	34.718	39.177	57.015	54.201	0.397	0.329	7.663	6.293	99.793
Saddle dolomite, J4	34.212	38.849	56.739	54.278	0.394	0.328	7.919	6.544	99.264
Saddle dolomite, J4	34.534	39.283	56.785	54.417	0.313	0.261	7.295	6.039	98.927
Saddle dolomite, J4	34.199	38.879	57.308	54.886	0.324	0.27	7.209	5.965	99.04
Saddle dolomite, J4	34.137	38.353	58.192	55.078	0.346	0.285	7.686	6.284	100.361
Saddle dolomite, J4	33.957	38.872	56.679	54.66	0.376	0.316	7.384	6.152	98.396
Saddle dolomite, J4	33.795	38.432	56.85	54.464	0.317	0.264	8.264	6.84	99.226
Saddle dolomite, J4	34.413	38.955	57.114	54.465	0.354	0.294	7.63	6.286	99.511
Saddle dolomite, J4	34.83	39.23	57.197	54.272	0.503	0.416	7.42	6.082	99.95
Saddle dolomite, J4	34.166	38.903	57.139	54.81	0.327	0.273	7.258	6.014	98.89
Saddle dolomite, J4	34.189	39.148	56.652	54.649	0.349	0.293	7.092	5.91	98.282
Saddle dolomite, J4	33.868	38.34	57.792	55.115	0.355	0.295	7.586	6.25	99.601
Saddle dolomite, J4	32.649	37.281	57.594	55.403	0.376	0.315	8.424	7.001	99.043
Saddle dolomite, J4	34.306	38.612	57.873	54.874	0.339	0.28	7.61	6.234	100.128
Saddle dolomite, J4	34.245	38.834	57.274	54.715	0.351	0.292	7.463	6.159	99.333
Saddle dolomite, NF 18.6 m	35.158	39.874	56.844	54.311	0.291	0.242	6.752	5.573	12.858
Saddle dolomite, NF 18.6 m	34.808	39.546	56.975	54.531	0.238	0.198	6.924	5.725	13.085
Saddle dolomite, NF 18.6 m	34.823	39.31	57.359	54.548	0.228	0.189	7.247	5.954	13.618
Saddle dolomite, NF 18.6 m	35.305	39.76	57.23	54.296	0.255	0.211	6.995	5.733	13.194

Saddle dolomite, NF 18.6 m	34.876	39.691	56.493	54.162	0.215	0.179	7.205	5.968	13.567
Saddle dolomite, NF 18.6 m	36.809	41.389	57.151	54.137	0.206	0.17	5.259	4.304	9.939
Saddle dolomite, NF 18.6 m	36.419	40.998	56.901	53.963	0.301	0.249	5.847	4.79	11.187
Saddle dolomite, NF 18.6 m	36.423	41.104	56.586	53.797	0.142	0.118	6.065	4.981	11.306
Saddle dolomite, NF 18.6 m	36.074	40.714	57.096	54.287	0.221	0.183	5.863	4.816	11.083
Saddle dolomite, NF 18.6 m	40.973	46	55.002	52.021	0.217	0.179	2.204	1.801	4.401
Saddle dolomite, NF 18.6 m	35.055	39.882	56.241	53.903	0.292	0.244	7.212	5.971	13.719
Saddle dolomite, NF 18.6 m	33.579	38.718	57.343	55.701	0.21	0.178	6.44	5.404	12.232
Saddle dolomite, NF 18.6 m	37.535	42.066	56.345	53.197	0.299	0.246	5.507	4.492	10.544
Saddle dolomite, NF 18.6 m	35.657	40.093	57.923	54.867	0.19	0.157	5.968	4.884	11.199
Saddle dolomite, NF 18.6 m	37.401	42.108	56.184	53.288	0.202	0.167	5.416	4.438	10.223
Saddle dolomite, NF 18.6 m	35.406	39.877	56.327	53.444	0.282	0.233	7.865	6.447	14.827
Saddle dolomite, NF 18.6 m	34.87	39.121	57.332	54.188	0.356	0.293	7.836	6.398	14.883
Saddle dolomite, NF 18.6 m	32.762	37.204	60.213	57.604	0.225	0.187	6.055	5.004	11.471

APPENDIX D

STABLE ISOTOPE DATA

Table: Isotopic analysis of blocky clear calcite spar			
Sample No:	Petrographic features	d 18O	d 13C
W.G. 31.8mab	Clear coarse calc.spar , intergranular pore space	-8.9	0.16
28.8 mab	Clear coarse calc.spars in oncoids	-9.1	0.27
12.1 mab	Clear calc.spar, intergranular pore space	-9.2	0.15
14.1 mab	Clear calc spar, intergranular porosity	-9.5	-0.1
17.8mab	Clear spar, pore central	-8.6	0.36
25 mab	Clear spar from girvanella oncoids	-9.2	0.38
W.G. 19.6m	Clear , coarse calcite spar, intergranular porosity	-8.6	0.01
	Intergranular, clear calc.spar	-9.5	-1.4
W.G. 33.8m	Intragranular, clear calc.spar, coarse	-9.5	0.1
W.G 30.2m	do	-9.7	-0.39
W.G 21.1m		-9.1	-0.92
W.G. 8.0m	Intergranular, clear calc.spar	-9.4	0.72
Date: 06/04/91			
W.G. 34.6m	Intragranular, clear, blocky calcite spar	-9.6	-0.03
W.G. 26.2m	do	-9.4	0.24
W.G. 27.6m	Intragranular clear blocky calcite spar	-9.3	0.1
W.G. 24.1m	Intergranular, clear blocky calcite spar	-9.6	0.15
W.G. 45.8m	do	-9.7	0.06
Date: 06-06-91			
GS 30.8m	Intragranular, clear, blocky calcite spar	-9.24	-0.04
W.G. 20.4m	Intragranular, clear, blocky calcite	-8.95	0.3
W.G. 15.2m	?	-9.9	-0.04

Table: Isotopic analysis of turbid calcite spar			
Sample No:	Petrographic features	d 18O	d 13C
14.1 mab	Cloudy calc spar	-7.5	0.303
W.G. 18.9m	Intergranular turbid calcite spar	-8.2	0.65
	Intergranular turbid calcite spar	-8.43	-0.16
G.S. 19.4		-7.8	0.22
G.S. 20.0mab	Intergranular, turbid calcite spar	-7.83	0.71
G.S. 21.6m	do	-7.7	-0.32
G.S. 25.6m	do	-7.8	0.36
G.S. 29.3	do	-8.5	0.65
G.S. 29.6m	do	-7.9	0.42
W.G. 14.0m	do	-7.27	0.46
W.G. 31.8m	do	-7.3	0.5
W.G. 31.8m	do	-7.1	0.48
GS 22.7m	do	-8.5	0.036
GS 25.6m	do	-8.5	0.35
W.G. 15.3m	do	-8.2	0.53
W.G. 12.1m	do	-8.6	0.012
GS 27.0m	Intergranular turbid calcite spar	-7.5	0.9
GS21m	Intergranular turbid calcite spar	-8.7	-0.82
N.F. 18.5m	do	-8.6	0.195
G.S. 18.6m	do	-9.05	-0.62
W.G. 21.1m		-9.1	-0.92
W.G. 11.2m	do	-8.9	0.22
W.G. 12.1mab	do	-8.8	-0.7

Table: Stable isotope values for Baroque dolomite (Type IV) and stylolite dolomite (Type III)				
Sample Id	Sample Description	d 18O at 25 C	d 13C at 25 C	
W.G. 17.0m	Baroque dolo, intragra.pore	-8.2	0.32	
G.S. 22.7mab	Baro. dolo. intragranular pore	-8.68	1.24	
G.S. 20.0mab	do	-7.3	1.41	
G.S. 18.6m	do	-8.68	0.73	
NF 18.5m	Baroque dolomite in intragran	-7.45	0.74	
W.G. 14.0m	do	-7.21	1.25	
GS 27.0m	do	-7.7	1.43	
NF 19.6m	do	-8.38	0.74	
W.G. 15.2m	Baro.dolomite	-7.59	0.86	
W.G. 17.0m	do	-7.32	1.46	
W.G. 17.8m	do	-7.59	1.42	
W.G. 15.3m	do	-8.1	1.58	
N.F. 19.0m	do	-6.68	0.82	
GS 20	Stylolite associated dolomite	-8.5	1.26	
NF 18.5m	do	-7.9	1.31	
Thm 47.7a	do	-7.5	0.52	
Thm 27.5	do	-7.8	0.33	
ThM 47.7	do	-8.4	0.91	
NF 19.5	do	-8.2	1.28	
Isotopic values of Cambrian Intraclasts				
Sample Id #	Description	d 18O	d 13C	
T-15 Chwy	Peloidal laminated clast	-8.6	0.02	
AA-4	do	-8.85	-1.45	
do	do	-8.7	-1.5	
H-13	do	-8.7	-1.03	
Z-1	do	-8.8	-0.96	
S-4	do	-8.3	-0.34	
do	do	-9	0.12	
X-5	do	8.8	-0.03	
H-6 Chwy	do	-8.12	-1.14	
do	do	-8.7	-0.5	

X-5 Chwy	do	-8.6	-0.5	
AA-7a	Calcareous siltstone	-8.7	-0.7	
M-3 Chwy	do	-8.6	-0.04	
T-2 Chwy	do	-8.7	-0.45	
I-3 Chwy	do	-9.7	-1.5	
P-4 Chwy	do	-8.5	-0.2	
	do	-8.6	-0.5	
A-3 Chwy	Micrite intraclasts	-7.9	-1.7	
A-4 Chwy	do	-8.8	-1.3	
E-5	do	-7.7	-1.01	
E-7 Chwy	do	-8.1	-0.3	
Thm 40.0	do	-7.5	-0.4	
Thm 40.0	do	-8.4	-1.1	
	do	-8.3	-0.8	
	do	-8	-1	
	do	-8.5	-1.1	
	do	-8.6	0.24	

Table: Carbon and oxygen isotopic values of ooids and fibrous cements					
Sample Id	d13C	d18O	Sample Id	d13C	d18O
Cambrian ooids	-0.1	-7.7	Cambrian fibrous cements	-0.6	-8.9
do	0.3	-7.8	do	-0.1	-9.4
do	-0.1	-7.9	do	-0.7	-9.5
do	0.2	-7.6	do	-0.2	-8.4
do	0	-8	do	-0.2	-8.2
do	0.2	-8.1	do	-0.87	-8.8
do	-0.3	-9.2			
do	-0.7	-10			
do	-0.4	-9.1			
do	-0.8	-10.2			
do	-0.4	-9			
do	-1.4	-8.9			
do	-1.1	-8.8			
do	-0.1	-8.8			
do	-1.3	-8.5			
do	-0.6	-9.1			
do	-0.2	-8.5			

VITA

Srinivasan Krishnan was born on May 10, 1962, in Hyderabad, India. He lived in Hyderabad with his parents, brother and a sister until July 1982. He graduated from High School in May 1979.

Srinivasan entered Osmania University in August 1979 and graduated with a B.S. (Hons) in Geology in May 1982. In July 1982, he entered the Indian Institute of Technology, Kharagpur, and graduated with a M.S. degree in Geology in July 1984. His M.S. thesis topic was on mineralogy and low grade metamorphism of Middle Proterozoic Cumbum Formation, Cuddapah Supergroup. Between February 1985 and August 1987, Srinivasan was employed as a geologist with the Oil and Natural Gas Commission, Bombay, India. Realizing that this was not where his interests lay, in September 1987, Srinivasan enrolled in the Doctoral Program at the University of Tennessee, Knoxville. From 1987 to 1993 he was employed by the Geology Department as a Graduate Teaching Assistant. His research was directed towards depositional environments, sequence stratigraphy, and diagenesis of Cambrian carbonates.

Srinivasan is a member of the Geological Society of America and the Society of Economic Paleontologists and Mineralogists.